

PHYSIOLOGICALLY RELEVANT SIT-TO-STAND  
MOVEMENT WITH OUTPUT FEEDBACK TRACKING



SAMINA RAFIQUE  
01-281142-001

A thesis submitted in fulfilment of the  
requirements for the award of the degree of  
Doctor of Philosophy (Electrical Engineering)

Department of Electrical Engineering

BAHRIA UNIVERSITY ISLAMABAD

JANUARY 2022

## APPROVAL FOR EXAMINATION

Scholar's Name: SAMINA RAFIQUE Registration No. 18781 Programme of Study: PhD Thesis Title: Physiologically Relevant Sit-to-Stand Movement with Output Feedback Tracking . It is to certify that the above scholar's thesis has been completed to my satisfaction and, to my belief, its standard is appropriate for submission for examination. I have also conducted plagiarism test on this thesis using HEC prescribed software and found similarity index \_\_\_\_\_% that is within the permissible limit set by HEC for PhD degree thesis. I have also found the thesis in a format recognized by the BU for the PhD thesis.

Principal Supervisor's Signature: \_\_\_\_\_

Dated: \_\_\_\_\_ Name: Dr Asif Mahmood Mughal

Co-supervisor's Signature: \_\_\_\_\_

Dated: \_\_\_\_\_ Name: Prof. Dr M Najam ul Islam

## AUTHOR'S DECLARATION

I, SAMINA RAFIQUE hereby state that my PhD thesis titled **“Physiologically Relevant Sit to Stand Movement with Output Feedback Tracking”** is my own work and has not been submitted previously by me for taking any degree from this university **Bahria University, Islamabad** or anywhere else in the country/world.

At any time if my statement is found to be incorrect even after my graduation, the University has the right to withdraw/cancel my PhD degree.

Name of scholar: SAMINA RAFIQUE

Date: \_\_\_\_\_

## **PLAGIARISM UNDERTAKING**

I, solemnly declare that research work presented in the thesis titled “Physiologically Relevant Sit to Stand Movement with Output Feedback Tracking”, is solely my research work with no significant contribution from any other person. Small contribution / help wherever taken has been duly acknowledged and that complete thesis has been written by me.

I understand the zero-tolerance policy of the HEC and Bahria University towards plagiarism. Therefore, I as an Author of the above titled thesis declare that no portion of my thesis has been plagiarized and any material used as reference is properly referred / cited.

I undertake that if I am found guilty of any formal plagiarism in the above titled thesis even after award of PhD degree, the university reserves the right to withdraw / revoke my PhD degree and that HEC and the University has the right to publish my name on the HEC / University website on which names of scholars are placed who submitted plagiarized thesis.

Scholar / Author's Sign: \_\_\_\_\_

Name of the Scholar: SAMINA RAFIQUE

## **DEDICATION**

This work is dedicated to my parents and parents in law.

My father always took pride in his children's academic achievements. My mother taught us to make seeking education our priority. My father-in-law used to fondly ask, how much my Ph.D. work had been done? He would say "Get the highest education, my child, you will be the first lady to get a doctoral degree in our family".

Their encouragement added more motivation in my endeavor, without which this uphill task would have been impossible.

## ACKNOWLEDGMENT

I thank almighty Allah to help me in my pursuit of Ph.D. and throughout my life. My belief in Him made things easy for me: I knew if I could not do my Ph.D., it would mean that it was not good for me.

I owe my thanks to many individuals who helped me complete my work:

First of all, many thanks to my supervisor Dr. Asif M Mughal, under whose able guidance I did this research. The Co-supervisor of this research, Dr. Muhammad Najam always supported me and gave valuable guidance in the technical issues of Ph.D.

My colleagues at my workplace Air University always extended their moral support and technical guidance whenever I needed ones; Umair Aziz always extended his help to solve technical problems that I faced during thesis formatting. My special thanks go to Ehtisham-ul-Hassan, Aleena Akhlaq and Aleena Mazhar who helped me avail access to the biomechanics lab at Riphah University.

My experimental work at Riphah International University helped authenticate my theoretical work. HoD Biomedical Engineering Dr. M. Shafique, faculty member Hamza Toor, student volunteers Bilal and Momin did a wonderful job in conducting motion and force capture experiments on subjects. Without their support, I could have never been able to utilize sophisticated instruments and complex data acquisition systems.

Lastly, it is my family; my elder sister Dr. Bushra and the youngest Humera Rafique, who always gave me moral and technical support respectively. My husband Wing Commander Jamil and my children, who always took pride in my seeking higher education, despite the cost of neglecting them.

## ABSTRACT

This research work proposes a modeling framework to simulate joints and head position trajectories as control variables during STS. Besides this, a modeling scheme for CNS's inference mechanism to estimate appropriate joint angles and the torques to perform the required motion is also presented. Clinical studies suggest that CNS controls a motion and maintains the balance by gathering multisensory data. CNS develops short term motion control strategies, called fast dynamics, and long-term strategies called slow dynamics. Slow dynamics include learning the appropriate motion patterns. For any voluntary motion, CNS anticipates set patterns of inputs from multisensory systems, and compares them with patterns built in / learnt over long period of time, as slow dynamics. The concept of slow dynamics, is the motivation to develop a modeling and simulation framework, for the clinical hypothesis, that besides numerous other factors, CNS controls STS motion, by tracking pre-learned kinematic trajectories of joints and/or head position. The solution of this research problem is achieved through following steps: 1) STS motion data from young, able-bodied subjects are collected using infra-red cameras and passive reflective markers. A force platform is used to gather Ground Reaction Force (GRF) data during STS. 2) A biomechanical modeling and simulation framework to synthesize and control human-like STS using joint/head position trajectories is proposed, which comprises an analytical four-segment rigid body human biomechanical model, various controllers to model CNS as STS motion controller and the STS patterns learnt by CNS as reference trajectories/control variables. 3) Finally, the proposed modeling scheme is mapped on real subjects so that the synthesized motion may be compared with real humans' STS motion. A comparison between experimental measurements and simulation results is used to validate motion synthesis frameworks. For low-level control linear robust controllers worked well. The task-level control was achieved by Adaptive Neuro-Fuzzy Inference System (ANFIS) based controller, although the ANFIS operation remains limited to feed forward control only. Cartesian control presents complete framework for task-level control but needs fine tuning for more realistic STS motion. The main achievements of this research work are 1) the development of STS motion and force dataset of healthy young adults. This

dataset can be used as a reference to provide a comparison with some pathological STS. 2) The validation of a human model that was extensively used for analysis of STS over quite some time. 3) Customization of human biomechanical model on real subjects using weighing coefficient method 4) CNS modeling as robust controller, ANFIS and Cartesian controller using full/reduced order measurements 5) Task-space-training algorithm to train/customize ANFIS system. Accurate modeling and understanding of human motion have significant scope in the fields of rehabilitation, humanoid robotics and virtual characters' motion planning based on high-level task control schemes. In the future, we aim to study STS motion control based on brain signals using real subjects and compare our human-CNS modeling scheme used for the synthesis of the same motion.



## TABLE OF CONTENTS

APPROVAL FOR EXAMINATION .....	ii
AUTHOR’S DECLARATION .....	iii
PLAGIARISM UNDERTAKING .....	iv
DEDICATION .....	v
ACKNOWLEDGMENT .....	vi
ABSTRACT .....	vii
TABLE OF CONTENTS .....	ix
LIST OF TABLES .....	xviii
LIST OF FIGURES .....	xix
LIST OF SYMBOLS .....	xxv
CHAPTER 1 .....	1
INTRODUCTION .....	1
1.1        Sit-to-stand (STS) Motion .....	1
1.2        The Research Gap .....	1
1.3        The Research Problem .....	2
1.4        Research Objectives .....	2
1.5        Methodology Adopted .....	3
1.5.1        Joint measurements feedback control .....	3
1.5.2        Head position tracking using ANFIS control .....	4

1.5.3	Head position tracking using Cartesian Control .....	4
1.6	Significance and Outcomes of this Research .....	5
1.7	Thesis Outline .....	5
CHAPTER 2 .....		7
LITERATURE REVIEW .....		7
2.1	Human Motion in General.....	7
2.1.1	Human movement: A historical perspective.....	7
2.1.2	Human movement from a biomechanical perspective.....	7
2.1.3	Human motion control from a biomechanical perspective .....	8
2.1.4	Computer simulation as an analysis tool .....	9
2.1.5	Applications of human motion analysis.....	11
2.1.6	Techniques of human motion data acquisition .....	17
2.2	STS Motion .....	21
2.2.1	Significance of STS .....	21
2.2.2	Applications of STS analysis studies.....	21
2.2.3	STS variables and hypotheses.....	22
2.2.4	Components of STS motion simulation.....	24
PART I.....		29
CHAPTER 3 .....		30
ANALYTICAL HUMAN BIOMECHANICAL MODEL.....		30
3.1	Physical Parameters.....	31

3.2	Mathematical Model .....	32
3.3	SimMechanics Model.....	35
3.3.1	SimMechanics environment.....	35
3.3.2	SimMechanics blocks .....	36
3.4	Linear Human Biomechanical Model .....	37
3.4.1	Linearization of the model .....	38
3.4.2	Open-loop stability analysis.....	39
3.5	Summary .....	41
CHAPTER 4 .....		42
EXPERIMENTAL VALIDATION OF HUMAN BIOMECHANICAL MODEL USING MOTION AND FORCE CAPTURE.....		42
4.1	Methodology .....	43
4.1.1	Workflow .....	43
4.1.2	Motion and force capture .....	44
4.1.3	Motion data analysis .....	48
4.1.4	Anthropometric conversion .....	52
4.1.5	Human biomechanical model .....	52
4.1.6	STS motion synthesis.....	53
4.2	Results .....	54
4.3	Discussion .....	57
4.4	Summary .....	59

PART II.....	61
CHAPTER 5 .....	62
STS MOTION SYNTHESIS USING ROBUST CONTROL .....	62
5.1 Methodology .....	63
5.2 Full State Measurement Scheme .....	63
5.2.1 Linearized model for full state .....	63
5.2.2 LQR Compensator .....	64
5.3 Reduced State Measurement Scheme .....	66
5.3.1 Linearized model for reduced measurement.....	67
5.3.2 LQG robust compensator .....	67
5.3.3 $\mathcal{H}^\infty$ controller.....	69
5.4 Trajectory Generation .....	71
5.5 STS Motion Synthesis in SimMechanics .....	72
5.5.1 LQR scheme.....	72
5.5.2 LQG scheme .....	76
5.5.3 $\mathcal{H}^\infty$ scheme .....	78
5.6 Discussion .....	81
5.6.1 LQR compensation .....	81
5.6.2 LQG compensation .....	82
5.6.3 $\mathcal{H}^\infty$ compensation.....	83
5.7 Summary .....	83

CHAPTER 6 .....	84
NUERO-FUZZY CONTROL OF STS MOTION USING HEAD POSITION TRACKING.....	84
6.1 Methodology .....	85
6.1.1 Workflow .....	85
6.1.2 Analytical modeling.....	85
6.1.3 Modeling validation on experimental data .....	86
6.2 Analytical Modeling Framework .....	86
6.2.1 The general human biomechanical model .....	86
6.2.2 Forward kinematics (FK) analysis .....	86
6.2.3 Inverse kinematics (IK) analysis.....	88
6.2.4 Kinematic constraints of the human biomechanical model .....	88
6.3 Determination of Head Position Subspace.....	89
6.4 Joint Angle Estimation Scheme .....	89
6.4.1 Task-space training (TST) algorithm.....	90
6.5 Development of the ANFIS Controllers.....	91
6.5.1 Structure of ANFIS .....	91
6.5.2 Training and optimizing ANFIS controllers .....	95
6.5.3 Testing the trained ANFIS controllers.....	96
6.5.4 Features of ANFIS controllers .....	97
6.5.5 Stability of ANFIS training.....	98

6.6	Simulation of STS Motion .....	100
6.6.1	Head position trajectory generation .....	102
6.6.2	General human biomechanical model and general ANFIS control 103	
6.6.3	Custom human biomechanical models and general ANFIS control 104	
6.6.4	Custom human biomechanical models and custom ANFIS control 104	
6.7	Discussion .....	108
6.8	Summary .....	109
CHAPTER 7 .....		111
CARTESIAN CONTROL OF SIT-TO-STAND MOTION USING HEAD POSITION FEEDBACK .....		111
7.1	Methodology .....	112
7.1.1	Workflow .....	112
7.1.2	Analytical modeling.....	112
7.1.3	Modeling validation on experimental data .....	113
7.2	Analytical Modeling Framework .....	113
7.2.1	CNS modeling: STS controller design.....	113
7.2.2	Cartesian controller for STS .....	117
7.2.3	Stability of the Cartesian control .....	118
7.3	Simulation of STS Motion .....	120

7.3.1	Simulation using the analytical scheme .....	120
7.3.2	Simulation using the custom biomechanical model.....	126
7.4	Discussion .....	131
7.5	Summary .....	133
CHAPTER 8 .....		134
CONCLUSIONS & FUTURE DIRECTIONS .....		134
8.1	Biomechanical Model Validation.....	134
8.2	Joint Position and Velocity Feedback .....	135
8.3	Joint Position Feedback.....	135
8.4	Head Position Feedback .....	135
8.4.1	Neuro-fuzzy inference and control .....	136
8.4.2	Robotic control.....	137
8.5	Assumptions and Limitations.....	137
8.6	Future Outlook .....	138
References.....		139
PART III .....		149
Appendices.....		149
APPENDIX A. Ethics Committee Certificate .....		150
APPENDIX B. Human Anthropometry.....		151
B.1	Weighing Coefficient Method [56] .....	151
B.2	Segment dimensions ( <i><b>l</b></i> ).....	151

B.3 Segment mass ( $m$ ) and CoM ( $k$ ).....	151
B.4 Mass moment of Inertia ( $I$ ) .....	152
APPENDIX C. Motion & Force Capture Operation .....	154
C.1 Experiment Apparatus .....	154
C.2 Procedure .....	154
C.3 Data Acquisition & Motive Screen .....	156
APPENDIX D. Introduction to MoCap Toolbox .....	157
D.1 Reading & Plotting the MoCap Data.....	157
D.2 Defining the Segments.....	158
D.3 Animation in Joint Space.....	159
APPENDIX E. Introduction to SimMechanics/Simscape .....	160
E.1 Modeling Biomechanical Systems: Lower leg model.....	160
E.2 Animation visualization.....	164
APPENDIX F. Introduction to ANFIS .....	165
F.1 Fuzzy Inference System (FIS) .....	165
F.2 Adaptive Neuro-Fuzzy Inference System (ANFIS) .....	165
F.2.1 Example: Ankle Motion Control.....	165
F.3 Training and Test Data for ANFIS .....	166
APPENDIX G. Linearization of Non-Linear Model [67] .....	169
G.1 Operating Point Selection.....	169
G.2 MATLAB command.....	169



G.3 SimMechanics Linear Analysis tool.....	170
APPENDIX H. Force Augmentation Devices for STS .....	172
H.1 Exoskeletons for soldiers.....	172
H.2 Motion assistance and rehabilitation devices .....	173
H.3 Physiotherapy exercises and equipment.....	173
APPENDIX I: LIST OF PUBLICATIONS.....	174

## LIST OF TABLES

Table 3.1. Body segment parameters of analytical human biomechanical model.....	31
Table 4.1. Surface plot that defines inference of ANFIS.....	44
Table 4.2. BSP data based on total body mass and Height/length.....	52
Table 6.1. Parameters of ANFIS controllers.....	98
Table 6.2. A quantitative comparison of RMS errors between actual and simulated trajectories.....	107
Table B. 1. Anthropometric conversion table based on subject's height and mass.....	152
Table B. 2. Subjects' physical parameter data.....	153

## LIST OF FIGURES

Figure 3.1. 2D four segment STS mode. ....	30
Figure 3.2. Human biomechanical model in SimMechanics .....	37
Figure 3.3 Model is defined in standing position [0, 0, 0] (left) and sitting position [0, - $\pi/2$ , $\pi/2$ ] is the initial condition .....	37
Figure 4.1. The workflow of experimental and analytical techniques.....	43
Figure 4.2. STS data capture setup: a subject with markers on segments and feet on a force plate (left), marker-based model (center) and joint based model (right) extracted from motion capture data .....	45
Figure 4.3. From left to right; calibration square, calibration wand, infrared camera by OptiTrack .....	46
Figure 4.4. Force data were captured by 2-axis 4-beam Pasco force platform.....	47
Figure 4.5. Three phases of STS animation reconstructed from motion capture using marker data.....	49
Figure 4.6. Ensemble average trajectories of head position. Curves in dashed lines represent $\pm 1$ Standard Deviation.....	49
Figure 4.7. Three phases of STS animation reconstructed from motion capture using marker data.....	50
Figure 4.8. Trajectories of joint angles from all subjects using motion capture during STS transfer .....	51
Figure 4.9. The ensemble average of joint angles from all subjects using motion capture. Curves in dashed lines represent $\pm 1$ SD .....	51
Figure 4.10. The 4-segment human biomechanical model in the sagittal plane.....	53

Figure 4.11. STS motion synthesis framework in SimMechanics.....	54
Figure 4.12. Average head position trajectories from motion capture ( $X_{exp}$ , $Y_{exp}$ ) and simulation ( $X_{exp}$ , $Y_{exp}$ ).....	55
Figure 4.13. Average experimental and simulated ankle, knee and hip joint trajectories. ....	55
Figure 4.14. Ground reaction torque $M_z$ and support moment $M_s$ (sum of joint torques) .....	56
Figure 4.15. The force plate shows experimental bodyweight $F_w$ (bold line) that correlates closely ( $R=0.94$ ) to vertical ground reaction force $F_y$ (dashed line) obtained from simulation.....	57
Figure 4.16. Phases of STS from motion capture. Trajectories of joints are also shown (top), simulated STS motion in SimMechanics environment (bottom).....	59
Figure 5.1. The Human STS motion control mechanism is based on the LQR scheme. $X_d$ is the reference input comprising ankle, knee and hip joint position trajectories..	66
Figure 5.2. The Human STS motion control mechanism is based on the LQG scheme. ....	68
Figure 5.3. Human STS motion control mechanism based on $\mathcal{H}^\infty$ scheme. The compensator is determined in (5.21).....	70
Figure 5.4. Experimental joint angle trajectories measured from motion capture.....	71
Figure 5.5. Analytically generated reference joint angle trajectories to be tracked. ...	72
Figure 5.6. STS motion synthesis framework in SimMechanics. The CNS modeled as LQR compensator is shown in the blue rectangle .....	72
Figure 5.7. Joint angular position estimates by LQE observer (top), measured joint positions (center) and error between the reference and actual values (bottom) .....	73

Figure 5.8. Joint angular velocity estimates by LQR observer (left), measured joint positions (center) and error between the reference and actual values (right) .....	74
Figure 5.9. Torque inputs to joint generated by LQR controller .....	75
Figure 5.10. Control action of LQR without feedback delays and measurement noise .....	75
Figure 5.11. STS motion synthesis framework in SimMechanics. The CNS modeled as LQG compensator is shown in the blue rectangle .....	76
Figure 5.12. Joint angular position estimated (left), measurements (right) and error between the reference and actual values using LQG / Kalman observer scheme .....	77
Figure 5.13. Joint velocity estimates using LQG / Kalman observer .....	78
Figure 5.14. Torque inputs to joint actuators using LQG control.....	78
Figure 5.15. STS motion synthesis framework in SimMechanics. The CNS modeled as $\mathcal{H}^\infty$ compensator is shown in the blue rectangle .....	79
Figure 5.16. Joint angular position estimates (left), measurements (center) and error between the reference and actual values using $\mathcal{H}^\infty$ control.....	80
Figure 5.17. Joint velocity estimates using $\mathcal{H}^\infty$ .....	80
Figure 5.18. Torque inputs to joint actuators using $\mathcal{H}^\infty$ control.....	81
Figure 6.1. The workflow of experimental and analytical techniques.....	85
Figure 6.2. Three DoF biomechanical human biomechanical model is defined in the body frame. {S}, {T} and {H} represent shank, thigh and HAT frames for segments $l_1, l_2$ and $l_3$ .....	87
Figure 6.3. Head position subspaces with joint-angle and link-length constraints; general (dots) and during STS (circles) .....	89
Figure 6.4. Three ANFIS controllers generate ankle, knee and hip joint angle commands .....	90

Figure 6.5. Schematic of ANFIS <sub>n</sub> : 2 inputs X, Y, 2k-input MFs, j-output MFs and one output $\theta_n$ .....	91
Figure 6.6. Initial MFs on X (same on Y) for ANFIS1 before training.....	92
Figure 6.7. Two inputs, 10 MF ANFIS1 with 25 rules.....	93
Figure 6.8. MFs on Y after training (12 epochs) .....	94
Figure 6.9. Learning curves of ANFIS on different numbers of membership function .....	96
Figure 6.10. Learning curves for ANFIS controllers for training data and validation dataset. ....	96
Figure 6.11. Errors of test data for ANFIS controllers .....	97
Figure 6.12. Surface plots of <i>ANFIS1</i> , <i>ANFIS2</i> and <i>ANFIS3</i> for three joint angles..	97
Figure 6.13. Neuro-fuzzy control-based STS motion synthesis framework in SimMechanics.....	100
Figure 6.14. Experimentally generated head position trajectories.....	102
Figure 6.15. Analytically generated head position trajectories.....	103
Figure 6.16. Joint angles generated by general ANFIS controller using general head trajectory .....	104
Figure 6.17. Ensemble average trajectories of head position from simulations using custom ANFIS controlled simulations. Dashed lines represent $\pm 1SD$ , showing intra-subject variations .....	105
Figure 6.18. Ensemble average trajectories of joint angles using custom ANFIS controlled simulations. Dashed lines represent $\pm 1SD$ , showing intra-subject variations .....	106
Figure 6.19. The error of head position between experimental and simulation trajectories using general (solid line) and custom (dashed line) ANFIS control.....	106

Figure 6.20. The error of joint position measurements between experimental and simulation trajectories using general (solid line) and custom (dashed line) ANFIS control .....	107
Figure 7.1. The workflow of the STS motion control scheme.....	112
Figure 7.2. STS control scheme to emulate CNS .....	117
Figure 7.3. STS control scheme implemented in SimMechanics .....	120
Figure 7.4. Comparison of reference and measured head position trajectories .....	121
Figure 7.5. Ankle, knee and hip joint angle trajectories measured during STS .....	122
Figure 7.6. The actual joint positions measured from STS motion by actual humans .....	122
Figure 7.7. Head orientation reference generated analytically and measured from simulation.....	123
Figure 7.8. Force command generated by Cartesian control law .....	123
Figure 7.9, Torque commands generated by the controller for ankle, knee and hip joints .....	124
Figure 7.10. Ground reaction forces under the feet of the analytical human biomechanical model .....	125
Figure 7.11. Kinetic analysis of STS simulation; ground reaction torque and the sum of joint torques .....	125
Figure 7.12. Average reference and measured head position trajectories from simulations .....	126
Figure 7.13. Comparison of ensemble average head position trajectories from motion capture experiments and simulations. ....	127
Figure 7.14. Comparison of average experimental joint trajectories with estimated and simulated trajectories. ....	128

Figure 7.15. Reference head orientation trajectory obtained from the average of experimental and head orientation measurements from simulations.....	129
Figure 7.16. Average ground reaction force curve FW, measured by the force platform, showing the trajectory of body weight variation during STS by the subjects. Fy shows the same variable measured during subject-specific simulations. ....	129
Figure 7.17. Joint torque command by motion controller for ankle, knee and hip....	130
Figure 7.18. Average ground reaction torque $Mz$ and support moment $Ms$ (sum of joint torques).....	131
Figure C. 1. Four Flex 3 cameras set up to capture STS motion	154
Figure C. 2. Calibration square is used to establish a reference frame.....	155
Figure C. 3. A calibration wand is used to tune camera measurements .....	155
Figure C. 4. Motive environment showing markers movement .....	156
Figure D. 1. Marker positions while the subject is sitting	157
Figure D. 2. Marker connected as segments.....	158
Figure D. 3. Markers at terminals of each segment.....	159
Figure D. 4. Animation of STS motion. Note middle marker on HAT is dis aligned due to garment artifact .....	159
Figure F. 1. SimMechanics model of shank-ankle-foot with ANFIS controller .....	166
Figure F. 2. Two input and one output representation of Sugeno type ANFIS.....	167
Figure F. 3. Surface plot that defines inference of ANFIS .....	167
Figure H. 1. Knee exoskeleton for force augmentation of soldiers.....	172
Figure H. 2. Light weight force augmentation device to prevent toilet related falls .	173
Figure H. 3. Robotic based STS physiotherapy .....	173



## LIST OF SYMBOLS

2D	Two dimensional
ANFIS	Adaptive Neuro-fuzzy Inference System
ANN	Artificial Neural Network
BSP	Body Segment Parameters
CNS	Central Nervous System
CoG	Center of Gravity
CoM	Center of Mass
Cop	Center of Pressure
DoF	Degree of Freedom
EMG	Electro Mayo Gram
FK	Forward Kinematics
FL	Fuzzy Logic
GRF	Ground Reaction Force
HAT	Head Arm Trunk
IK	Inverse Kinematics
LQG	Linear Quadratic Regulator

MF	Membership Function
MoCap	Motion Capture toolbox
$M_s$	Support moment
$M_z$	Ground reaction torque
R	Correlation factor
rad	Radians
RMS	Root Mean Square
SD	Standard Deviation
STS	Sit To Stand
TST	Task Space Training
WC	Weighing Coefficient

# CHAPTER 1

## INTRODUCTION

### 1.1 Sit-to-stand (STS) Motion

Sit-to-stand is a motion that every individual executes numerous times a day. It is the preamble to many other movements that are part of activities of daily living like walking or stair climbing. With disease or aging, like other human body movements, STS also deteriorates. An individual's physical independence is ensured as long as he is capable to perform at least STS. With more percentage of population reaching old age every year throughout the world, it is now more important to give more attention on understanding the STS motion mechanism, so that problems related to the execution of STS could be better understood and their solutions could be suggested.

### 1.2 The Research Gap

Despite a large volume of research available on STS motion, numerous gaps can be identified among these studies. Some of these are:

- 1) Determination of STS variables has been predominantly done in clinical environment and still there is a lack of simulation schemes to translate experimental settings into simulation framework.
- 2) Specifically for the motion capture, there is lack of protocols to conduct experiments and collect motion and force data.

3) Usually, the experiments are conducted for an arbitrary set of variables which make it very difficult to derive relevance among various studies [1] and reach a concrete result on how much a variable contributes to a certain motion.

4) Success of any theoretical modeling scheme relies heavily on validation of its assumptions. It is therefore required that a biomechanical simulation framework must be validated through experimental findings.

### **1.3 The Research Problem**

There is clinical evidence that human motion control and maintenance of balance by CNS rely on inputs from vision, proprioception, tactile/somatosensory and vestibular systems. It is yet to be proved but still there is a section of researchers [2] that believes and hypothesizes that the multisensory integration, combined with motion control undergo both quick and slow alterations which are termed as fast and slow dynamics in CNS respectively. For any voluntary motion, CNS anticipates set patterns of inputs from multisensory systems. The anticipated pattern of signals is a function of slow dynamics in CNS, which is due to long term processes of learning a motion pattern or changes in motion strategy due to aging or disease.

Keeping this hypothesis in view we formulate our problem of synthesizing STS motion using head position trajectory as a reference pre-learned by CNS due to its slow dynamics related to STS motion execution strategy.

In this study, we intend to evaluate the clinical hypothesis that besides numerous other factors, the Central Nervous System (CNS) controls STS motion by tracking a pre-learned head position trajectory.

### **1.4 Research Objectives**

The main objective of this research is to propose a modeling and simulation framework to synthesize and control STS motion using only head position trajectory as

a reference to be tracked. To find the solution of this problem, we have set forth a set of objectives that if achieved, will contribute to the relevant knowledge base:

- 1) To collect motion and force data from young, able bodied subjects for STS.
- 2) To propose biomechanical framework, comprising human-CNS models to synthesize and control physiologically relevant STS motion based on the joint/head position feedback to CNS.
- 3) To map the modeling and control scheme on real subjects so that the synthesized motion may be compared with real humans' STS motion.

## **1.5 Methodology Adopted**

Based on the clinical evidence that the head position measured by the multisensory system contributes to motion control, this study we will suggest a biomechanical human-CNS modeling and control framework for sit-to-stand motion synthesis. Motivated by the evidence for a task-oriented encoding of motion by the central nervous system, we propose a framework to synthesize and control sit-to-stand motion using only head position trajectory in the high-level task-control environment. The task must be achieved in a physiologically relevant way i.e., the motion must be human like as well as the forces involved in this motion, like, joint torques and ground reaction forces must be similar to those found in actual humans while performing STS motion.

### **1.5.1 Joint measurements feedback control**

To start with STS motion is generated using robust linear controllers, using joint position and velocity measurements. A generalized four-segment biomechanical model from literature is used to model the human anatomical system for voluntary movement. Different control schemes are then used to execute STS using full as well as reduced

state feedback with the help of the estimation technique. Details of this work are available in chapter 4.

### **1.5.2 Head position tracking using ANFIS control**

Later we work out our main research problem and we synthesize STS motion using only head position feedback to CNS/controller. We design a generalized analytical framework comprising a human biomechanical model and a motion controller to emulate CNS. We introduce the task-space training algorithm for the ANFIS training. The ANFIS controller is optimized in the number of membership functions (MF) and training cycles (epochs) to avoid over-fitting. Next, we develop custom human biomechanical models based on anthropometric data of real subjects. Using the weighting coefficient method, we estimate Body Segment Parameters (BSP). The subject-specific body segment parameter values are used (a) to scale the human biomechanical model for real subjects and (b) in task-space training to train custom ANFIS controllers.

### **1.5.3 Head position tracking using Cartesian Control**

The second strategy to control STS motion using the head position is carried out by using a robotic approach for the synthesis of STS motion. The robotic control will be achieved by modeling the CNS to control STS in two steps: using the head position as a reference Estimator part of the controller will infer joint angles that correspond to head position using inverse kinematics. This step is termed as low-level task generation. The second role of CNS is the motor execution function. In this phase, the STS motion specific head position trajectory assumes the role of slow dynamics pattern embedded in CNS for STS motion. The motor execution is done through the Cartesian Controller subsystem that generates torque commands to the joints. We reconstruct the dynamic motion through the control of simulated custom human-CNS models to follow the captured head position trajectories in real-time. We perform kinematic, kinetic analyses and comparison of experimental and simulated motions.

## 1.6 Significance and Outcomes of this Research

The following objectives have been achieved through this research

1) Motion and force data of STS in the sagittal plane is recorded. The subjects were healthy and young adults with no pathology in their STS transfer. The dataset thus achieved can be used as a reference of normal STS motion for the comparison with some other group of subjects with different age groups and/ pathology.

2) The experimental data is used to validate a human biomechanical model that was developed analytically and was used extensively for STS motion synthesis by a series of researchers.

3) The biomechanical framework to synthesize and control physiologically relevant STS motion based on joint angular positions, velocities and only head position feedback is presented, thereby accomplishing the STS motion for given conditions, in a control theoretic setting using biomechanical modeling and computer simulation tools.

4) A framework of scaling human biomechanical model and CNS to any real subject using only height and mass of the subject is presented. The framework is based on the Weighing Coefficient method of anthropometry for human biomechanical model scaling.

5) This work proposes the Task-Space-Training algorithm to tune the ANFIS system to model subject-specific CNS using only height and body mass of the subject.

## 1.7 Thesis Outline

The thesis is organized as follows:

The current chapter 1 describes PhD research problem and its background, followed by literature review on the topic in chapter 2.

The research work in this thesis is divided into three parts: Part I comprises chapter 3 and 4 and give a detailed description of human biomechanical model used.

In chapter 3, the basic human-biomechanical model used for the synthesis and control of STS motion is described. An open-loop stability analysis is also provided.

Chapter 4 presents the human biomechanical model validation scheme which is based on motion and force capture of STS motion on real subjects. Human biomechanical model customization for real subjects using the BSP is also presented here.

Part II comprises CNS as STS motion controller modeling schemes. Chapter 5 covers the CNS modeling scheme both for full order as well as the reduced-order measurement of joint position and velocities. This chapter covers various schemes employed to achieve low-level control (using joint position tracking). Various robust controllers to model CNS such as Linear Quadratic Regulator (LQR), Linear Quadratic Gaussian (LQG) and  $\mathcal{H}_\infty$  are used.

Chapters 6 and 7 present modeling and evaluation framework for the clinical hypothesis that head position trajectory feedback to CNS plays a role in synthesis and control of STS motion: Chapter 6 presents a CNS modeling scheme based on a neuro-fuzzy inference system for estimation of appropriate joint angles corresponding to head position trajectory during STS. Chapter 7 presents CNS modeled as an STS Controller, comprising an Estimator of joint angles and a Cartesian controller to generate torque commands to the joints. In the last, we present a brief conclusion and future directions for the presented work. Part III provides additional material in the form of appendices that give the reader an introduction to the experimental setup of motion and force capture, software used for motion capture, motion synthesis and analysis and weighing coefficient formulae and dataset for model mapping.



## **CHAPTER 2**

### **LITERATURE REVIEW**

#### **2.1 Human Motion in General**

##### **2.1.1 Human movement: A historical perspective**

Human movement results from a highly complex and coordinated interplay between joints, bones, ligaments and muscles within the human body which are all controlled by the central nervous system. Muscles generate pulling forces by contracting which results in moments at joints. Besides the joint movements, the musculoskeletal system must carry out these movements that ensure the static and dynamic stability of the body since gravitational and other forces are continuously affecting the required motion. The interaction of forces within the biological systems as well as with their surroundings received attention from early scholars like Aristotle, Leonardo da Vinci (1452-1519), Galileo Galilei (1564-1642), Johannes Kepler (1571-1630), Rene Descartes (1596-1650), and Isaac Newton, and this list goes on to the researchers of the present day. Their efforts to understand the effect of these mechanical interactions has been evolved into form a discipline of research called biomechanics [3].

##### **2.1.2 Human movement from a biomechanical perspective**

The human motion has gone through a long evolutionary process and now it seems that human capabilities to generate finer movements have improved a lot. To predict how a body will move in response to a force is important to be estimated so that movements can be optimized. This knowledge is directly linked with the design and development of devices in every field like sports, ergonomics, orthosis and industries [4]. The study of motion in biological systems is called biomechanics. The word

'biomechanics' is a combination of the words 'biology' and 'mechanics' where the application of the laws of physics and the laws of mechanics, on biological systems, are studied. Motion biomechanics is the science of motions of the neuro-musculoskeletal system that focuses on the role of joints, sensors, bones, muscles and the central and peripheral nervous system [5]. Similarly, any injury to, or lesion in any of the individual elements of the musculoskeletal system will bring degradation in motion and instability in posture. Contrary to this, correction and modification in the mechanical environment can help prevent injury, remove the abnormality and devise new techniques for healing and rehabilitation. Therefore, motion analysis gives a strong basis for studying the causes of motion disorder related diseases and making strategies for their prevention [3].

Musculoskeletal systems are usually articulated and hence are modeled as multi-segment machines. In such systems, including the human body there are more joints and muscles than are necessary for performing our daily motor tasks. The end effector can approach the target using different combinations of joint angles. This situation is called redundancy. It is an interesting fact that redundancy provides an alternate solution to a movement task in case an injury or disease to the musculoskeletal system makes it difficult or impossible to achieve the target in a normal way. Redundancy however makes it difficult to determine the internal forces noninvasively [3].

### **2.1.3 Human motion control from a biomechanical perspective**

Humans can very well perform various physical activities, like standing, holding objects, walking, running, throwing as well as more fine motor functions as writing, sewing, etc. [5]. The behavioral richness exhibited in natural human motion is a result of both biomechanical and neurological parts. A better understanding of all involved factors is a must to understanding the mechanism of human motion as well as constructing a framework for generating this motion. Basic constituents of the human motor system include biomechanical plants and CNS [6]. To create a dynamic simulation of some human motion a three-step process is adapted: First, the analytically developed skeletal model is customized for a subject by scaling it to the experimentally

measured size of the subject. Next based on inverse kinematics analysis the values of generalized coordinates for the model that closely matches the experimentally measured kinematics of the subject are calculated. Muscle torques are calculated then to implement the control and come up with an optimal set of actuation strategies for the forward dynamic simulation that closely matches the experimental results [7].

#### **2.1.4 Computer simulation as an analysis tool**

To investigate a clinical hypothesis that some variable contributes as a feedback element in the control mechanism of motion, computer simulation is a powerful tool. Human motion is synthesized and investigated in a simulation environment using a human-CNS model. Computer-based methods in biomechanics are based upon a human anatomical model and the role of CNS is simulated by a controller [6]. Computer simulations identify and optimize new movements as an athletic training tool to reduce injury risk and enhance efficiency. The optimization is achieved by establishing a valid relationship between kinematics (posture), physiological kinetics like muscle forces, and ground reaction forces. These elements have proven their relevance in human motion synthesis and control and have been observed in clinical experiments but the information these experiments provide is always limited and fails to reach concrete results. Moreover, these experiments cannot be conducted to see the effects of change in some variables. It is where the power of simulation comes in action: Using a motion synthesis model comprising a human biomechanical model and a controller to simulate CNS a motion generation platform is established. Depending upon the situation this platform can simulate normal motion or can be modified to generate pathological movement by adding a model of pathology in the human anatomical model. Next optimization techniques are applied that provide solutions to counter the negative effects of these pathologies. For example, patients with knee ortho-arthritis (OA) feel difficulty standing from the sitting position. A comparison of simulations between healthy and diseased peoples' STS provides valuable information regarding the change in strategy that a knee OA patient adapts to cope with this difficulty. Different hip and knee flexing and activation of thigh muscles help these patients to carry out this activity. Individual elements like muscles and joint forces are simulated to generate motion and

their effect on posture is studied. Similarly, by generating some required movement or posture in simulation resulting or required forces can be estimated. Since some of these forces result from muscles, a rehabilitation exercise can be customized for the patient to train a weak muscle or train a different posture to cope up with difficulty in movement. Simulations also allow us to establish cause-and-effect relationships giving insights into muscle function. The most powerful feature of simulations is the ability to perform “what if” studies to test hypotheses, predict functional outcomes, and identify emergent behaviors [7].

Simulations of motion provide biomechanical analysis as well as the power of motion synthesis. For an existing motion, captured using measurement and recoding techniques, simulation of reconstructed motion serves as an analysis tool; what body angles result from what muscle forces? How much ground reaction force is generated for a certain body posture? How data from a multitude of body sensors are contributing to the smooth execution of a particular motion? Is addition or omission of certain sensory data affecting speed, posture or balance? How muscle and ground reaction force vary when a certain set of sensory function is missing or is made inefficient for the experimental setting? Motion synthesis simulation, on the other hand, utilizes motion information to construct a dynamic virtual scenario. In [8] the researchers first studied basic patterns of human motion by a musculoskeletal model in motion. Later a comparison was conducted between gaits generated by two models: one with a normal gait and another with a disordered gait.

Modeling human body motion, however, is not an easy task owing to the multifaceted nature of this work. Indeed, this requires the understanding of internal/external biological and physical principles that govern human movement and coordination, as well as, keeping in mind the physical constraints of the overall system to provide the motion mechanism a realistic representation with high-fidelity. Due to the highly complex nature of the human body and the forces from the environment that interact with it, despite over 30 years of research in biomechanics, results are mitigated [4].

Computer-based motion analysis plays almost the same role as an ergonomist, a physician, a trainer or any other specialist that objectively and quickly evaluates the

motion by observing and then evaluating it using his knowledge about the relevant field. Once the data is captured the higher-level processing of this data can be carried out for human activity recognition, motion reconstruction, pose estimation, event detection, a biomechanical study of motion, etc. Computer simulation and analysis of human motion provide many advantages over experiments: simulations are free of risk, a smaller number of prototypes are required to reach the final design which reduces effort, cost and expense. While going through simulations a researcher comes up with a result, algorithm or optimization technique that can serve as a training tool. Simulations can solve complex engineering problems and can speed up and automate experimentally based decision-making. Human motion simulation is used to analyze walking dynamics, simulate surgical procedures, and analyze the joint loads and to design medical devices [9].

### **2.1.5 Applications of human motion analysis**

Human motion analysis and simulation have a multitude of relevant applications that have a great social and economic impact. Human motion analysis is the basis of procedures adopted in a large number of domains e.g. sports, rehabilitation, robotics, surveillance, gesture-based user interfaces, etc. [9]. The human motion analysis, as well as the computer simulation of several human capabilities, have shown to be essential in many different types of applications, including:

#### **2.1.5.1 Clinical perspective: Diagnosis and rehabilitation**

Traditionally human motion used to be studied by physiologists in clinical settings. Both normal and diseased subjects were observed and studied to achieve a better understanding of human motion. This would lead to developing an understanding of neuromuscular impairments that affect motion, followed by developing a scientific basis for treatment [9]. With the advancement in biomechanics and computing tools now clinical biomechanics-based computer models and simulations of the musculoskeletal system give a better and scientific understanding of mechanisms behind human motion, both normal and pathological which becomes the foundation of

a better understanding of the human motion and its underlying dynamics. This leads to developing more effective methods based on scientific laws for treatment e.g. tendon transfers and physical therapy [8]. The most commonly observed human motion in clinical settings has been a clinical gait analysis. Even today a physician or a therapist who is not equipped with motion and force measurement equipment uses visual observation to check the quality of gait pattern. This is the simplest and also the most informal way to analyze it. This method however does not lead to a systematic analysis and detailed documentation of an observation that required modern measurement and analysis tools. Combining advanced measurement technology and biomechanical modeling, human gait can now be studied in both quantitative and dynamic terms of the body and its limbs during motion [9].

Human motion analysis proves to be a powerful tool to assess the deviations from normal movement. The analyses quantify altered kinematic, kinetic or Electromyography (EMG) patterns with reference to normal neuro-musculoskeletal conditions. This technique leads to diagnose a disorder more specifically and help classify a patient in relevant pathology groups such as those with Cerebral Palsy (CP), stroke, knee osteoarthritis (OA), diabetes mellitus (DM), and spinal cord injury (SCI). A review of pathological motion analysis and its impacts on treatment strategies have been discussed in [3]. The study shows one of the most successful applications of clinical gait analysis is the surgical planning in CP. The study was conducted on 70 CP patients. After computer-based gait analysis, 89% of the original treatment plans were revised and 39% of the previously recommended procedures were not done.

A large volume of research has been conducted on the effects of the severity of knee OA on the compensatory STS [10] as well as gait patterns and to establish the effect of these gait changes to reduce loading on the diseased knee. The comparison between normal and knee OA groups' gait revealed that the diseased group had increased pelvic anterior tilt, swing-pelvis list, decreased standing knee abduction, as well as a decreased standing hip flexor and knee extensor moments. The severe group also demonstrated increased hip abduction, knee extension and ankle plantar flexion. These results suggest a physiotherapy strategy for the training of the knee and hip muscles and pelvic control for rehabilitating patients with mild to severe knee OA. The same study [3] discusses the role of motion analysis in clinical settings: A group of

patients with anterior cruciate ligament deficiency (ACL D) was engaged in a task of obstacle crossing. Since the ACL has both structural and proprioceptive functions so ACL D is characterized by posture instability, a lower muscle function, dysfunctional or poor somatosensory feedback of the knee. Obstacle-crossing helps assess both the structural and proprioceptive functions of the ACL. Normally a safe and successful obstacle-crossing requires stability of the body which depends both on the stability of posture as well as a motor action that ensures foot clearance. The stability of posture is largely a function of the joint while foot clearance is termed as the sensory function of the joints. An ACL D patient who suffers from both stability and sensory feedback shortcomings typically fails to complete the obstacle-clearing target satisfactorily. The motion analysis of ACL D patients helps classify patients who fall in a subgroup: those who no longer suffer from structural instability after rehabilitation but still suffer from residual impaired sensory feedback of the affected joint. Therefore, detailed analysis and study of the ACL D subjects during obstacle-crossing would help establish a more complete picture of the integration and interaction of the structural and sensory functions of the ACL during functional activity. These examples demonstrate the use of motion analysis in evaluating the pathology of the neuro-musculoskeletal system and assessing treatment. The analysis results are also helpful for improving the management of relevant patient populations [3].

#### **2.1.5.2 Estimation of unobservable quantities**

Several techniques are available for measuring 3D joint kinematics. Among these most techniques that provide accurate results are invasive and hence are not a preferred strategy for data collection. Noninvasive methods on the other hand lack accuracy. With the development of theoretical and experimental methods to improve accuracy and reliability, human motion analysis has become a useful investigative and diagnostic tool to estimate those parameters using data collected non-invasively. Computer simulation relies on mathematical models that serve as a tool to simulate motion. The inverse dynamics of mathematical models is used in conjunction with noninvasive experimental measurements to calculate non-measurable internal forces. Most often the measurable values of quantities in human motion analysis are recorded

with the help of skin markers and the motion capture systems. External forces applied to the actual musculoskeletal system can be measured by force plates. With the 3D trajectories of skin markers, the GRFs and Center of Pressure (CoP) measured using force plates, the unmeasurable inter-segmental forces and joint moments are inferred from Newton's equations of motion. This approach is called the inverse dynamics analysis [3]. The inverse dynamic analysis is a strong tool for the validation of the human biomechanical model and has been extensively used in the literature [10]–[15].

### **2.1.5.3 Sport sciences**

Human motion analysis and improvement techniques are now being extensively used in sports coaching [16], [17]. Sports biomechanics research mainly focuses on performance enhancement, injury prevention and safety in sports. Motion analysis helps analyze the cause of injuries, the safe extent of force application, improvement in sports training by optimizing sporting moves and analyzing their pros and cons even before an athlete practices them. The training strategies are mainly based upon the determination of joint loadings in the legs during exercises and estimating effects on the speed with different pedal rates, step lengths and step heights. The study of the joint kinematics and the CoP movements help determine various postures that lead to an efficient and safe move during sports [3].

A popular methodology of sports training is based on simulations using computed muscle torques. These strategies help control and identify new movements that are safer and that reduce ligament injury risk especially in braking and sidestepping movements. Braking movements are common in racket games like tennis and squash. Sidestepping movements are made during a change of direction while running and are frequent in basketball and soccer. The motion analysis and simulation techniques help determine kinematic changes that reduce peak valgus knee moments during the weight-acceptance phase of an unanticipated sidestep. Since the kinematic changes influencing peak valgus knee moments during an unanticipated sidestep are not well understood the researchers in [7] have used different primary kinematic strategies to reduce peak valgus knee moments.



Biomechanical analysis of movements helps athletes and their coaches to observe and compare their techniques with a particular professional athlete so that they can eventually improve their performances. Simulation of some sport move help assessment and extent of injury that can be avoided in real life scenario [9].

Computer simulations not only provide help to individual sportsmen but are very popular in presenting real-world baseball data to support real batting practice in a virtual world [8].

#### **2.1.5.4 Robotics and orthosis**

Synthesis of human-like motion finds its application in physical settings; the robotics community seeks a high-level control framework for robotic systems [6]. An emerging field of bipedal [18], [19] and humanoid robots [18], [20], [21] is also linked with this type of study.

Research in human/animal locomotion and gait analysis also helps to design and control prosthetics and implants (like crutches), diagnosis and rehabilitation processes [22]–[24] and equipment's design. Knowledge of the mechanical and control behavior of the musculoskeletal system is used in designing assistive devices like prostheses, orthoses and neuro-prostheses in case that parts of the neuro-musculoskeletal system fail [5].

Human motion analysis helps understand the accurate evaluation of critical joint motion measurements both from normal and pathological subjects. This comparison enables the designer of orthoses, such as functional knee braces and lateral-wedged insoles, and the design and development of fall-prevention strategies during obstacle crossing to come up with a design that is reliable and less likely to fail while being used [3].

### **2.1.5.5 Computer vision, surveillance and animation**

Synthesis of human-like motion gives a strong foundation to the science of computer animation as well: In computer graphics, virtual characters now can generate a multitude of realistic and situation related movements that are more autonomous and detailed. Given a high-level task, the virtual characters produce human-like motions since the motion-related low-level control is automatically generated [6].

Another application is virtual reality. In this scenario, the actual human motion is captured using skin markers and infer-red cameras and this motion data is used to animate virtual characters which later become part of an overall mixed reality environment [8].

Humans are capable of generating infinitely many expressions and physical motions. To instantly generate the desired motion from such a large domain of all movements is a great challenge in virtual human simulation. In [25], the novel emotion affected motion classification and anatomical motion classification are presented. The authors propose an anatomical approach for this purpose. They also present novel motion capture and parameterization methods like a Hierarchical Translations and Rotations (HTR) file format. This approach is based upon a compact motion database and using architecture for the real-time generation of new motions is also proposed [25].

Computer simulation in the perspective of computer vision help identify objects in image sequences. This strategy helps to track their motion automatically. Using artificial intelligence and computer vision techniques human gesture and body language can be understood. In automated surveillance systems such motion analyses setup can identify and classify human actions and even human intentions. The identified gestures are used to control something or take some decision. Besides security another major goal of this field of research is to develop intuitive human-machine interfaces that lead to reducing the need for input devices such as joysticks or keyboards. Thus, allowing users to give instructions to the computer mainly through gestures, poses or facial expressions. The possible domains of gesture recognition-based devices include gaming and entertainment, sign language recognition, movement assessment, senior

home monitoring, device remote control, and human-robot interaction, to name a few [9].

#### **2.1.5.6 Ergonomic design**

Traditionally a design engineer comes up with a design although unsure how eventually the device will perform. This leads to the necessity of redesign which leads to an increase in effort and cost. Motion analysis helps provide an insight into flaws and shortcomings in a proposed design before it is finally manufactured. An ergonomic efficient design means that the item is safe and convenient for the user and will ensure fatigue and injury avoidance despite prolonged use. Ergonomic designs are more important in applications like prostheses, sports equipment, workspaces and cars [9]. For an ergonomic design, the captured human motion can be used to create safe environments, products and devices in practically all areas and even study the human posture while stepping into the car. The output data of the models (either motion trajectories or joint angles of critical body segments) can be used by human biomechanical modeling software tools to drive digital human biomechanical models, providing data on potential injury risk and postural analysis [8].

#### **2.1.6 Techniques of human motion data acquisition**

There are two broad categories of techniques used for capturing the motion data i.e., optical and non-optical. Non-optical systems are the sensor-based systems, like the inertial, magnetic and mechanical motion capture systems. These systems are intrusive in nature and remarkably affect the performance of any systems that are coupled to it.

In the early 1990s, the first piezo-resistive sensors were used in conjunction with digital mobile monitors that were used for movement analysis. These inertial sensors needed proper calibration to give accurate and reliable measurements using gravity and movement. Inertial sensors therefore not only can measure the movement but also the orientation with reference to gravity. Due to a very smaller size, these inertial sensors seemed ideal to fix to the human body hence they are considered better

substitute as compared to the complex and expensive equipment required in the gait lab. Gyroscopes are also used to measure angular velocity. The combination of three accelerometers and three gyroscopes is used as a fixed body sensor for motion capture is used in [26].

A study [27] based on inertial measurement systems reports that STS motion-captured was very accurate and free from drifts. Reference [28] gives an overview of 17 motion capture systems used in sports applications. Among all these methods marker-based motion capture system was reported as the accurate one, despite its limitations in terms of cost, the need for a controlled environment, high sensitivity to noise, line of sight capture, etc. Research is underway to device marker-based systems that cost less and are independent of specialized motion capture equipment. In [29] Microsoft Kinetic, a low-cost motion sensor was used with markers to rectify inaccuracies inherent in the Kinetic motion sensor. To address the issue of missing marker positions due to occlusion or skin and garment artifact [30] suggested a data-driven piece-wise linear modeling technique to estimate missing data. Motion capture has an application in the animation industry as well. But the extraction of the skeleton from marker data results in loss of information about the body surface. Reference [31] proposed a parametric human body model, extracted from a system of a sparse set of markers. The model helped retain information of both pose and posture of the body during the motion.

Optical-based systems comprise small circular shape devices called markers. Markers can be active, i.e., which radiate light like Light Emitting Diodes (LED) or they can be passive, which reflect light from some other source. Usually, the markers are made in spherical shapes so that light incident from any angle may be reflected to and detected by the camera. Depending upon the application, these markers are available in different sizes; those used for the detection of lips and face skin movement are smaller and shaped like buttons. Besides markers, the system comprises a set of infra-red cameras. The minimum number of cameras needed for the transformation of 3D imaging from 2D motion capture is 3. But it is application specific as well. Human motion analysis is typically carried out in an experimental setup called gait lab. The subject whose motion is to be captured attaches markers on specific body parts using adhesive tape or Velcro. These systems utilize data captured from one or more image

sensors (e.g., video cameras) to triangulate the 3D position of a subject. This equipment is highly sensitive to noise and needs frequent calibration. Besides highly controlled laboratory conditions must be ensured. The light source illuminating the marker is mounted on the cameras. There are many systems available commercially that offer a data capturing technique without using markers. These systems are capable to generate accurate data by tracking surface features identified dynamically for each particular subject. These systems, also known as optical-based marker-less systems have the advantage of being non-intrusive [9].

#### **2.1.6.1 Experimental setup and protocols**

STS including other human motions is observed in an experiment setup called gait lab. This is a space specifically instrumented and used to measure human movement under standardized and supervised conditions. A traditional clinical gait lab is equipped with camera systems, force plates and EMG to analyze the biomechanics of movement. Camera systems either use passive retro-reflective markers or active markers (LEDs) placed on landmark locations on the subject. Several cameras are calibrated to measure the displacement of these markers in space over time [26].

In a study on experimental research on STS [32] it is found that 27 out of the 39 studies made use of a combination of force plate(s) and a motion analysis system for data capture. Only 10 out of 39 made use of EMG analysis. The number of trials made for STS movements per subject ranged from 1 to 15. There were 7 studies among the total of the 39 in which a single trial was used for statistical analysis. The number of subjects ranged from 2 to 51 in these experiments.

For another study [33], the researcher recruited 12 male subjects in their twenties without any impairments. The quantities measured were CoP and EMG to read muscle activity in different experimental conditions like variation in visual, vestibular, and tactile stimulations. The vision was stopped by closing the eyes, the vestibular sensation was disturbed by pouring cold water into one ear. The effect of tactile stimulation was introduced by the touch on the skin by another volunteer. To quantify the role of visual and proprioceptive sensory inputs the Sensory Organization Test (SOT) is conducted.

This test examines how subjects utilize combinations of that sensory feed-back to maintain an upright stance. To measure brain function in response to fast dynamics, Functional Near-Infrared Spectroscopic (fNIRS) imaging is used to identify the region(s) associated with sensory input processing during the change in the conditions of the SOT [33].

In [34] six healthy subjects, four females and two males with average age 27.7 years first gave informed consent to participate in the activity. The experiment was approved by the Human Subjects Review Committee before conducting the experiments. Motion data was captured by the VICON motion measurement and analysis system and two force platforms. The system consisted of six infrared video cameras mounted on tripods and arranged in a half-sphere on the left side of the subject. Video data were collected at a frequency of 120 Hz. Cameras were calibrated to the measurement volume using a calibration wand and calibration square. Spherical markers of 2 cm diameter were applied to the left side of the subject's body using self-adhesive Velcro. To capture force data two Bertec force plates were placed underneath each of the subject's feet. The force data were sampled by an analog to digital converter. The force data collection system was made synchronized to the camera system.

Some studies like [35] collected data from a single subject: An adult male aged 23, the height of 168 cm and a body mass of 68 kg, carried out several jumps and back somersaults. Force and motion data were recorded simultaneously. The ground reaction forces were measured using a Kistler 9281B force platform at the rate of 1000 samples/sec. The body motion was recorded at 50 Hz by 4 synchronized cameras. The global reference frame determined by the calibration square was attached to the center of the force platform. The positions of the 23 anatomical points were determined by markers to reconstruct the motion.

## **2.2 STS Motion**

### **2.2.1 Significance of STS**

STS movement is a skill that helps determine the functional level of a person [32]. The ability to rise from sitting to standing is critical to a person's quality of life, as it is linked with the functional independence of an individual. Studies on the hierarchy of disability indicate that problem in STS starts at a later stage than problems in walking commence. STS is a mechanically more demanding physical activity as the body has to work against gravity more than it does during walking [26]. For people having motion disorders due to disease or aging, sit-to-stand (STS) is the minimum of the motion that may keep them from being fully handicapped. The human factor involved in studying STS is therefore very high. STS activity and the problems associated with it have traditionally been termed as a phenomenon linked purely with old age. For this reason, the amount of STS research is very small as compared to work done on gait. Moreover, research on STS is done in recent times. Although it is a fact that the problem in STS is very often an old age-related phenomenon; since for the ages above 50 years, muscle mass reduces rapidly (almost 1-2% per year) that results in a reduction of muscle force. When one loses the ability to stand up it restricts the individual from performing other activities that are associated with moving around [26].

### **2.2.2 Applications of STS analysis studies**

Studies on STS are done in two broader perspectives; (a) for clinical applications where collection of normal/pathological STS motion data are used for diagnosis of disorder, development of motion assistance devices and making decision on treatment strategies. A biomedical engineer can model pathologies in human STS motion synthesis framework, and different strategies can be formulated in simulation environment, to reduce the effect of some anomaly, (b) the humanlike motion synthesis, which is implemented both in physical setting, like in robots as well as in virtual environment, like gesture recognition-based applications and virtual characters' motion.

### 2.2.3 STS variables and hypotheses

Like other physical movements, STS poses serious challenges to understand and replicate its complicated mechanism. STS movement takes place in coordination between physical components like bones, muscles and tendons etc. Moreover, the CNS generates movement commands following feedback from sensory organs about joint positions, velocities and torques besides information about the position and orientation of different parts of the body. The components and roles of different feedbacks to CNS in the STS movement is still not known completely and is an active area of research in biomechanics [36]. Interaction of the human body with its environment also plays a significant role in human motion, especially STS. This phenomenon was studied in [32] and it was found that chair seat height, use of armrests and foot position effect the ability to stand from sitting. A higher chair seat helps reduce the moments at the knee as well as at the hip. Using the armrests reduced the moment at the hip joint. This technique helped maintain the range of motion of the joints. Even feet position influences over maximum mean extension moments at the hip, when foot position is changed from anterior to posterior [32].

Kinematic variables associated with human physical parameters like joint positions, velocities, acceleration, Centre of Mass (CoM), Centre of Gravity (CoG), CoP and kinetic variables like GRF, joint torques and ground reaction torques play an important role as feedback elements to CNS in STS motion control.

In [37] the research was done to evaluate the roles of GRF, moments and CoP during STS. The results validated a modeling scheme that depended upon GRF and moments as variables of interest. There is clinical evidence that human motion control and maintenance of balance by CNS rely on inputs from vision, proprioception, tactile/somatosensory and vestibular systems. The multisensory integration, combined with motion control undergo both quick and slow alterations which are termed as fast and slow dynamics in CNS respectively. For any voluntary motion, CNS anticipates set patterns of inputs from multisensory systems. The anticipated pattern of signals is a function of slow dynamics in CNS, which is due to long term processes of learning a motion pattern or changes in motion strategy due to aging or disease [33].



A study in [38] evaluated the role of vision in STS by collecting various parameters like weight transfer time, rising index and CoG velocity sway during STS. Data were collected from volunteers, first with open eyes and then blindfolded. Results showed that there were significant differences between the two trials and suggested that visual perception played a role in balance control during STS.

Of all sensory inputs, head position and orientation are an area of researchers' interest. The vestibular system senses linear and angular head motions. The CNS uses this information for posture and gaze control [39]. Vestibular sense, in conjunction with neck proprioception, estimates body orientation [33]. The role of head position feedback to CNS in smooth execution of STS is studied in [34], where authors have provided the detailed experimental and physiological analyses that suggested the dependence of the STS movement on kinematic variables such as CoM and head position during the task. A person rises from a chair, then leans forward by putting his head position over the CoM point and then extends into a standing position. The head position trajectory is also considered pivotal to provide a basis for the endpoint hypothesis for STS movement stabilization, which shows that the entire task becomes simple by maneuvering the head to the endpoint of the trajectory. This phenomenon was simulated and studied in [40] by proposing the feedback control law based upon inverse kinematic actuation and validating with experimental results of kinetic variables.

The posture control needed to maintain a balanced STS is a very important and basic requirement in everyday activities. Since the body has to maintain balance despite gravity and other forces acting on the body, appropriate posture control is maintained with the combined effort of CNS, sensory and musculoskeletal system. Sensory inputs from proprioception, tactile and somatosensory inputs play an important role in controlling posture-regulating muscles in specifically in lower extremities and the overall body as a whole. The regulation mechanism of posture however is still not known completely and is an area of research in the field of biomechanics. Changes in multisensory inputs estimate quick changes in a posture called fast dynamics in the CNS. The human brain integrates sensory information to Figure out actual posture and compares it with the required posture to maintain the balance. The error between these two positions is used by CNS to generate appropriate torque commands to the muscles such that the error is minimized and the posture attains the balance. It is assumed by

researchers that CNS integrates multisensory information to calculate body state, like CoM and direction of motion. Despite inherent noise in sensory signals, CNS estimates meaningful information by using a 'weighted' sum depending upon the reliability of sensory information. Besides quick dynamics, CNS undergoes long-term alterations called slow dynamics due to aging and learning [33].

## **2.2.4 Components of STS motion simulation**

### **2.2.4.1 Human anatomical modeling**

Traditionally, the musculoskeletal system was modeled mathematically as a multi-link system with individualized model parameters, such as the length of each segment, the joint center positions, and the lines of action of the muscles and tendons. The success of any theoretical model relies heavily on the validation of its assumptions. Mathematical and biomechanical models of the human musculoskeletal system are used to understand and improve body movement mechanism. The first step in this strategy is the development of a human biomechanical model to replicate motion such that the role of various kinematic and kinetic variables, noise involved in the neurological feedback system and reaction forces generated from contact points of the body may be evaluated. The accuracy of results primarily depends upon the quality of the human biomechanical model. For motion analysis and development of a control scheme, usually, an analytical model based on general physical parameters is realized. Such models and control schemes are extensively available in the literature on motion analysis [40], [41] and the design of robotic devices [42]. Since the human STS is performed almost entirely in the sagittal plane [43], the models used to replicate this motion comprise a multi-level inverted pendulum, whose motion is governed by Euler-Lagrange equations. Musculoskeletal models also incorporate muscles that largely contribute to body motion [10], [11]. In [44] Maxim Raison et al, have utilized the 5-repetition-STs test technique to construct an inverse dynamic model. In [45] the human STS stable movement has been modeled by a four-link biomechanical model for various phases of STS. To simulate finer motions, however, detailed human anatomical models are required. The model proposed in [35] has 44 Degrees of Freedom (DoF) and

16 anatomical segments composed of 33 rigid bodies. Joint actuators model muscles that produce joint actuation. The presented model is used to generate finer motions like take-off to aerial trajectories and standing backward somersault. The kinetic analysis of these motions reveals joint moments and reaction forces. The geometrical model of the locomotor apparatus developed in [3] was validated by EMG and telemetered force data from two instrumented patients. Knowledge of accurate kinematics of natural human joints, including 3D rigid body and surface kinematics, is essential for the understanding of their function and is utilized in many clinical applications. For this purpose, an accurate measurement method for the kinematics of skeletal motion is needed which is discussed in this paper.

#### **2.2.4.2 Customization of models**

To analyze a motion mechanism more accurately, the simulated motion must be compared with actual human motion. For this purpose, custom biomechanical models are developed that are more useful in the design and tuning of customizable motion assistance and rehabilitation devices. Custom human biomechanical models are based upon BSP values. Reimer et al [46] have given an overview of methods available for the estimation of BSP. Weighing Coefficient (WC) based methods are convenient since they are based on empirical formulas and do not need expensive measurement apparatus, but the error in results can be up to 40%. Geometric approaches are more reliable (error less than 5%), but tedious, as the number of body part measurements can go even higher than 240. Medical imaging is also accurate (error<5%) but needs expensive equipment in addition to dangerous exposure to radiation. Among all these methods marker-based motion capture system was reported as the accurate one, despite its limitations in terms of cost, the need for a controlled environment, high sensitivity to noise, line of sight capture, etc.

#### **2.2.4.3 CNS modeling: The controllers**

CNS is the most sophisticated and complicated mechanism in the human body. Sensory signals from all the body are transported to the CNS where this data is

processed and in case a motion is to be generated motor signals are sent back to the required periphery. An average human CNS roughly comprises  $10^{11}$  interneurons. Each interneuron has almost 10000 connections with other interneurons to exchange and process information. The processing potential of a CNS can be understood by making a comparison with a huge parallel computer system that on average contains up to 128000 parallel chips! Contrary to this computer CNS processes information in parallel. Keeping in view this capacity of processing the modeling of CNS is always based on some oversimplified assumption and often simulating a single operation at a time [5]. Based on some specified tasks, CNS performs motor planning which culminates low-level control issued as a motor command to biomechanical plant. Some knowledge of biomechanical plant is also assumed to be encoded in CNS. One possible model which is the most commonly used to synthesize the motion is the joint space control [6]. It is possible to divide motion control into the task generation phase and a motor execution phase. This abstraction is more relevant to the design of engineered systems that augment physiological systems. Synthesis of human motion involves accurate reconstruction of movement sequences, modeling of musculoskeletal kinematics, dynamics and actuation of segment joints [47]. Task-based methods used in robotics may be leveraged to provide novel musculoskeletal modeling methods and physiologically accurate performance predictions. The advantage of robotic based effort models frequently utilizes quantities that are derivable purely from skeleton kinematics and that are not specific to muscle actuation. As already mentioned, in human-like motion synthesis frameworks, modeling of CNS is always very vague [6] and hence it is limited to serve some specific task only. To emulate CNS, some controller is used following the concept that there exist optimal controllers in human CNS [40]. Due to similarity with the human reasoning mechanism, ANFIS seems a natural choice for biomechanical motion simulation [14] and applications [48]. Unlike most of the conventional controllers, ANFIS is a model-free controller [49], [50]. It is the combination of two soft computing techniques, namely Artificial Neural Networks (ANN) and Fuzzy Logic (FL). An ANFIS is a Generalized Neural Network (GNN) that implements a Fuzzy Inference System (FIS) based on Sugeno type reasoning. ANFIS was proposed in [51] to compensate FL's shortcoming of learning mechanism and ANN's inability to translate linguistic fuzzy rules into an inference system. Controlling human motion assistance devices using ANFIS is frequently found in the literature.

Robotic manipulators for human-assist exoskeleton using the neural-fuzzy scheme in [48] described the suitability of ANFIS in the biomechanical control application. In [45] fuzzy modeling and fuzzy controller are employed to study the mechanics of the human musculoskeletal system during the STS movement. In [52] a Linear Matrix Inequalities (LMI) based control is used by a mixed  $\mathcal{H}_2/\mathcal{H}_\infty$  controller. STS motion control using reduced measurement is studied in [53]. The control scheme is based on Kalman estimation and the CNS has been modeled by an  $\mathcal{H}_\infty$  controller which works in the presence of neural delays and measurement noise. Postural stability in elderly people is studied in [54] where dis-balance leading to a fall is studied. The role of CNS to counter such incidents is postulated as a feed-forward controller. The iterative LQR controller for non-linear biological movements has been employed in [55].

#### **2.2.4.4 Model validation**

Models are necessary to transform the theories on motion control into testable and quantifiable hypotheses which can be subsequently validated through experiments [3]. Once a biomechanical model to reproduce human-like motion is developed, it must be validated against real human motion using kinematic and kinetic analysis techniques. The kinematics is the science of motion. All representations of motion like position, velocity and acceleration are measured in the kinematic analysis. Although accelerated motion always results from force, the kinematic analysis does not take force into account. In biomechanics, the kinematic analysis takes joint angular positions, velocities and translatory motions or trajectories of any body parts into the account. The data collected by the motion capture system is reconstructed and is subject to kinematic analysis. Very often motion capture data is made the basis of developing a human biomechanical model. This model is then used in the framework of motion synthesis. The synthesized motion is compared with actual motion and the kinematic analysis is done to check the similarity between the two datasets. This is the validation technique for a biomechanical model. Using some optimization technique, the error between kinematic variables is minimized to the lowest possible level and the final model is therefore validated.

On the other hand, the kinetics is the study of the motion and its causes. In experimental setups for motion capture kinetic measurements largely comprise the forces acting between the foot and the ground, which are commonly measured by an instrumented section of the floor known as a “force platform”[9]. Besides this arrangement, some invasive methods are rarely used for measuring joint torques and muscle activity. In [7], the researchers used musculoskeletal modeling and optimization to investigate the relationship between posture, muscle forces, and ground reaction forces. The researchers' goal was to determine if posture influences the muscles' capacity to generate ground reaction forces. Causes and effects of crouch position of posture were also studied and its advantages and disadvantage were established using kinematic and kinetic analyses. Crouch gait is generally considered to be disadvantageous for patients with cerebral palsy; however, a crouched posture may result in biomechanical advantages. A crouch posture helps achieve balance in a moving vehicle or acquire better agility to produce some sports move.

In [42] the proposed 6-link human biomechanical model was checked for its accuracy using references from experimental data. The relation of two kinetic variables; GRF and reaction moments were recorded from subjects and compared with the same forces resulting in simulations [56]. The regression plots of two variables endorsed similarity between them during the gait cycle. The validation of the modeling scheme through the experimental result is also done in [10]–[12], [47]. In [57] the researcher collected data of STS motion using infrared cameras and force plates and applied the data to a multi-segment biomechanical model for the analysis of the kinematic contribution of major body segments.

In [58] effect of disturbance on human quiet standing has been studied using a two-link (double inverted pendulum) model. The model is compared with actual subjects who were ear-muffled and blindfolded while counterbalancing a tilt in the platform they were standing on. Inter-joint dynamic interaction during quiet standing is also studied by [59] where the balancing of an inherently unstable standing position is examined by induced acceleration analysis.

**PART I**

**Human Biomechanical Modeling**

**&**

**Experimental Validation**

## CHAPTER 3

### ANALYTICAL HUMAN BIOMECHANICAL MODEL

This chapter gives details of the human biomechanical model used in this study which is a nonlinear four-segment rigid body model with 3 DoF for human STS motion analysis and synthesis, as shown in Figure 3.1. The key movements of joints and limbs during STS take place in the sagittal plane only, hence we limit our model to planar 2D motion.

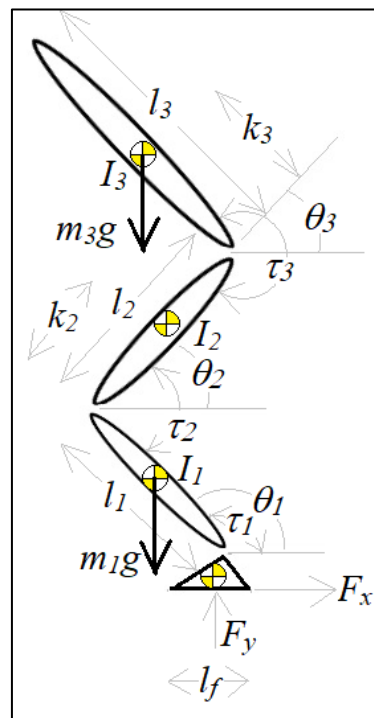


Figure 3.1. 2D four segment STS mode.

The model consists of four segments; foot is the fixed triangular base of support, the lower segment ( $l_1$ ) represents the shank, the middle segment ( $l_2$ ) represents the thigh and the upper segment represents the Head-Arm-Trunk (HAT) termed as a single segment ( $l_3$ ).



Since the model is defined in the sagittal plane, the symmetry about the vertical axis of the body is therefore implied. The foot is fixed on the ground hence no stepping action is allowed to maintain the balance. Both arms are wrapped across the chest and no swinging action of arms or push from the armrest is allowed during STS. All joints are revolute (hinge-like) and the model is an open-chain mechanism with three actuators at each joint.  $\theta_1$ ,  $\theta_2$  and  $\theta_3$  represent ankle, knee and hip joint positions respectively.

The model is based on physiological proportions as shown in Table 3.1. This model has been extensively used in studies for STS motion synthesis [12], [14], [15], [19], [37], [40], [41], [43], [45], [52], [53], [60]–[63] using various controllers and has been analyzed for different regions of stability.

### 3.1 Physical Parameters

Throughout this research we have used following physical parameters to model analytical human biomechanical model:

Table 3.1. Body segment parameters of analytical human biomechanical model

Segment	Mass in kg		Length in m		Moment of inertia in kg.m <sup>2</sup>		Center of gravity in m	
	Symbol	Value	Symbol	Value	Symbol	Value	Symbol	Value
Foot	$m_f$	1.91	$l_f$	0.27				
Shank	$m_1$	6.14	$l_1$	0.43	$I_1$	0.11	$k_1$	0.25
Thigh	$m_2$	13.20	$l_2$	0.43	$I_2$	0.26	$k_2$	0.25
HAT	$m_3$	44.75	$l_3$	0.84	$I_3$	7.53	$k_3$	0.31

### 3.2 Mathematical Model

The non-linear model for STS motion [40] is given by nonlinear matrix equation as

$$\vec{\tau} = \mathbf{D}(\theta)\vec{\ddot{\theta}} + \mathbf{H}(\theta, \dot{\theta})\vec{\dot{\theta}} + \vec{G}(\theta) \quad (3.1)$$

where  $\mathbf{D}(\theta)$  is the inertial component matrix of joint moments,  $\mathbf{H}(\theta, \dot{\theta})$  is the Coriolis component matrix and  $\vec{G}(\theta)$  is the gravitational component vector.  $\vec{\theta}$  is joint angle vector in body frame and  $\vec{\tau}$  is the joint torque vector. The model is derived using equations of motion based on Euler-Lagrange dynamics for multi-segmented open chain mechanism. Same dynamic model can be obtained using Newton-Euler equations. The complete algorithm for computing joint torques from motion of joints comprises two parts: first the link velocities and accelerations are iteratively computed for  $l_1$  to  $l_3$  using Newton-Euler equations for each link. Next forces and torques that propagate from  $l_3$  to foot are recursively computed. The general algorithm [64] for N+1 links is summarized as:

$$D_{ij} = \begin{cases} l_i[m_j k_j + l_j \sum_{p=j+1}^N m_p] \cos(\theta_i - \theta_j); & i < j \\ D_{ji}; & i > j \\ l_i + m_i k_i^2 + l_i^2 \sum_{p=i+1}^N m_p; & i = j \end{cases} \quad (3.2)$$

For human biomechanical model used in our study, the foot is fixed on ground and 3 links are interacting through 3 revolute joints, hence  $i=j=1,2,3$ .  $i < j$  corresponds to below diagonal entries and  $i > j$  are above the diagonal entries of D matrix. The  $i=j$  are diagonal values of D. The Coriolis and gravitational matrices are segregated from L given by:

$$\begin{aligned}
& (m_i k_i + l_i \sum_{p=i+1}^N m_p) [(g + \dot{Y}_1) \cos \theta_i - \dot{X}_1' \sin \theta_i] \\
& + m_i k_i + l_i \sum_{p=1}^{i-1} l_p \dot{\theta}_p^2 \sin (\theta_i - \theta_p) \\
L = & + l_i \sum_{p=i+1}^N m_p k_p \dot{\theta}_p^2 \sin (\theta_i - \theta_p) \\
& + l_i \sum_{p=i+1}^N \sum_{q=1}^{p-1} m_p k_q \dot{\theta}_q^2 \sin (\theta_i - \theta_q)
\end{aligned} \tag{3.3}$$

And output torque weighting matrix T is:

$$T = \begin{cases} 1 & j = i \\ -1 & j = i + 1 \\ 0 & \end{cases} \tag{3.4}$$

The equations obtained are

$$\begin{aligned}
\tau_1 - \tau_2 = & d_{11} \ddot{\theta}_1 + d_{12} [\ddot{\theta}_2 \cos(\theta_1 - \theta_2) + \dot{\theta}_2^2 \sin(\theta_1 - \theta_2)] \\
& + d_{13} [\ddot{\theta}_3 \cos(\theta_1 - \theta_3) + \dot{\theta}_3^2 \sin(\theta_1 - \theta_3)] \\
& + g f_1 \cos \theta_1
\end{aligned} \tag{3.5}$$

$$\begin{aligned}
\tau_2 - \tau_3 = & d_{22} \ddot{\theta}_2 + d_{12} [\cos(\theta_1 - \theta_2) \ddot{\theta}_1 \\
& - \sin(\theta_1 - \theta_2) \dot{\theta}_1^2] + d_{23} [\cos(\theta_2 - \theta_3) \ddot{\theta}_3 \\
& + \sin(\theta_2 - \theta_3) \dot{\theta}_3^2] + g f_2 \cos \theta_2
\end{aligned}$$

$$\begin{aligned}
\tau_3 = & d_{33} \ddot{\theta}_3 + d_{13} [\cos(\theta_1 - \theta_3) \ddot{\theta}_1 \\
& - \sin(\theta_1 - \theta_3) \dot{\theta}_1^2] + d_{23} [\cos(\theta_1 - \theta_3) \ddot{\theta}_3 \\
& - \sin(\theta_1 - \theta_3) \dot{\theta}_3^2] + g f_3 \cos \theta_3
\end{aligned}$$

The coefficients of  $\ddot{\theta}_i$  terms constitute inertial matrix  $D$ . Terms with coefficients  $\dot{\theta}_i^2$  represent Coriolis effect and those with  $\dot{\theta}_i \dot{\theta}_j$  belong to centrifugal force and are combined in Coriolis matrix  $H$ . All terms with gravitational constant  $g$  are gathered in matrix  $G$  as shown below:

$$\mathbf{D} = \begin{bmatrix} d_{11} & d_{12} \cos(\theta_1 - \theta_2) & d_{13} \cos(\theta_1 - \theta_3) \\ d_{12} \cos(\theta_1 - \theta_2) & d_{22} & d_{23} \cos(\theta_2 - \theta_3) \\ d_{13} \cos(\theta_1 - \theta_3) & d_{23} \cos(\theta_2 - \theta_3) & d_{33} \end{bmatrix} \quad (3.6)$$

$\mathbf{H}$

$$= \begin{bmatrix} 0 & d_{12} \dot{\theta}_2 \sin(\theta_1 - \theta_2) & d_{13} \dot{\theta}_3 \sin(\theta_1 - \theta_3) \\ d_{12} \dot{\theta}_1 \sin(\theta_1 - \theta_2) & 0 & d_{23} \dot{\theta}_3 \sin(\theta_2 - \theta_3) \\ d_{13} \dot{\theta}_1 \sin(\theta_1 - \theta_3) & d_{23} \dot{\theta}_3 \sin(\theta_2 - \theta_3) & 0 \end{bmatrix}$$

$$\vec{G} = g[f_1 \cos\theta_1 \ f_2 \cos\theta_2 \ f_3 \cos\theta_3]^T$$

where

$$d_{11} = m_1 k_1^2 + (m_2 + m_3) l_1^2 + I_1,$$

$$d_{22} = m_2 k_2^2 + m_3 l_2^2 + I_2,$$

$$d_{33} = m_3 k_3^2 + I_3,$$

$$d_{12} = f_2 l_1, d_{13} = f_3 l_1, d_{23} = f_3 l_2$$

$$f_1 = m_1 k_1 + (m_2 + m_3) l_1$$

$$f_2 = m_2 k_2 + m_3 l_2$$

$$f_3 = m_3 k_3$$

where all variables are as defined in Table 3.1. Equation (3.1) can be written as

$$\ddot{\theta} = \mathbf{D}^{-1}(\theta) [-\mathbf{H}(\theta, \dot{\theta}) \dot{\theta} - \mathbf{G}(\theta) + \vec{\tau}] \quad (3.7)$$

which represents a non-linear system of equations for a human biomechanical model in the sagittal plane.

Let's define the state vector  $\vec{x}$

$$\vec{x} = [\theta_1 \ \theta_2 \ \theta_3 \ \dot{\theta}_1 \ \dot{\theta}_2 \ \dot{\theta}_3]^T$$

where  $\theta_1 \ \theta_2 \ \theta_3$  are the ankle, knee and hip joint positions and  $\dot{\theta}_1 \ \dot{\theta}_2 \ \dot{\theta}_3$  are the respective joint's velocities. Writing in standard state-space notation

$$\vec{x} = [x_1 \ x_2 \ x_3 \ x_4 \ x_5 \ x_6]^T$$

Also, define

$$\vec{u} = \vec{\tau} = [\tau_1 - \tau_2, \tau_2 - \tau_3, \tau_3]$$

Non-linear state space equation is

$$\dot{x}_1 = x_4, \dot{x}_2 = x_5, \quad \dot{x}_3 = x_6 \quad (3.8)$$

$$\begin{bmatrix} \dot{x}_4 \\ \dot{x}_5 \\ \dot{x}_6 \end{bmatrix} = [\mathbf{D}]^{-1} \left[ -\mathbf{H} \begin{bmatrix} x_4 \\ x_5 \\ x_6 \end{bmatrix} - \mathbf{G} + \vec{\tau} \right]$$

### 3.3 SimMechanics Model

#### 3.3.1 SimMechanics environment

SimMechanics is a toolbox of SIMULINK/MATLAB to provide an environment of simulation of multi-body biomechanical models, robots, vehicle parts and even landing gears. The simulation environment offers convenience in model realization since the user has to implement the model without developing equations of motion. A multi-body system is realized using blocks available in the libraries representing bodies, joints, constraints, force elements and sensors/actuators.

SimMechanics automatically formulates and solves equations of motion using these components. Besides this, the environment helps develop control and test system-level performance. The toolbox is seamlessly compatible with MATLAB and Simulink hence the models can be parameterized using MATLAB variables and all features of SIMULINK can be used to obtain the final controlled system. Refer to Appendix E for a brief introduction to SimMechanics in the human biomechanical modeling perspective.

### 3.3.2 SimMechanics blocks

Using the SimMechanics environment the STS model of (3.8) has been implemented (see Figure 3.2) in terms of physical quantities involved (see Table 3.1). **Machine Env** block defines the simulation environment for the model. The stationary or reference point of the mechanical model is represented by the **Ground** block. The **Weld** block represents the immobile joint, which shows that the foot is in a fixed position. The four segments *i.e.*, foot, shank, thigh and HAT are defined as rigid **Body** blocks. Each segment is defined in terms of physical properties like mass, lengths, CoM and inertia tensor. Each block is also defined in terms of its position and orientation with respect to any other block or World frame. The four Body block parameters are defined individually such that the model is defined in body frame and standing position (see Figure 3.3 left). All Body blocks are connected through Joints blocks. Three joints *i.e.*, ankle, knee and hip are defined as revolute and their axis of rotation is  $z$ . Each joint is equipped with a **Sensor** block ( $J_i$ ) to measure angular positions ( $\theta_i$ ) and angular velocities ( $\dot{\theta}_i$ ). The initial position is determined by Initial Condition block (IC). Position at the ankle, knee and hip is  $[0, -\pi/2, \pi/2]$  rad respectively, to define sitting posture at the start of STS motion. See Figure 3.3 (right) for the initial position. Each joint is individually driven by an Actuator block ( $T_i$ ) which is regulated by control input ( $u_i$ ).

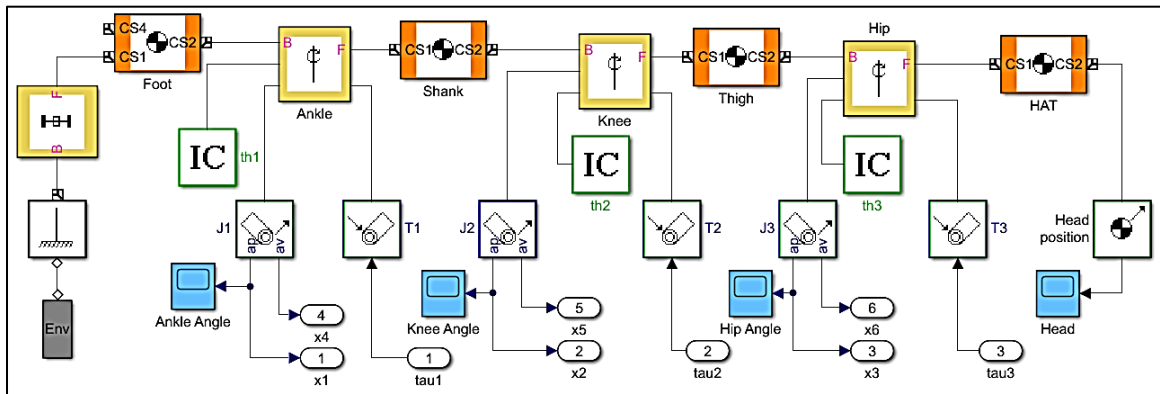


Figure 3.2. Human biomechanical model in SimMechanics

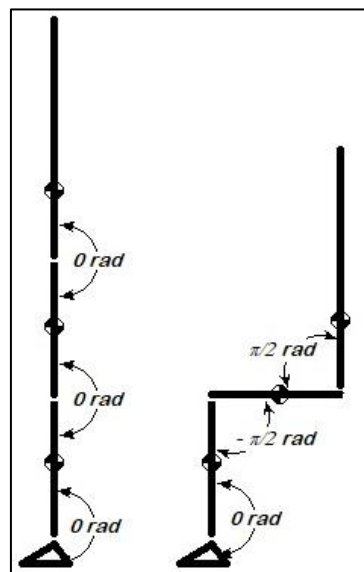


Figure 3.3 Model is defined in standing position  $[0, 0, 0]$  (left) and sitting position  $[0, -\pi/2, \pi/2]$  is the initial condition

### 3.4 Linear Human Biomechanical Model

To implement a linear control scheme in conjunction with the human biomechanical model implemented in SimMechanics as shown in Figure 3.2 we need to linearize the model so that a model-based linear controller could be implemented.

### 3.4.1 Linearization of the model

The model in SimMechanics is linearized using a linear analysis tool in SimMechanics. Let  $\theta_e$  represents the desired equilibrium position; then we can define the following state variables

$$\vec{\tilde{x}} = [\Delta\theta_1 \ \Delta\theta_2 \ \Delta\theta_3 \ \Delta\dot{\theta}_1 \ \Delta\dot{\theta}_2 \ \Delta\dot{\theta}_3]^T = [\Delta\theta_1, \Delta\theta_2, \Delta\theta_3, \Delta\dot{\theta}_1, \Delta\dot{\theta}_2, \Delta\dot{\theta}_3]^T$$

where  $\Delta\theta_i = \theta_i - \theta_e$ ,  $\vec{\tilde{\tau}} = \vec{\tau} - \vec{\tau}_e$  is the error between current and desired positions and torque respectively. State equation of linearized model is given by

$$\begin{bmatrix} \dot{x}_1 \\ \dot{x}_2 \\ \dot{x}_3 \end{bmatrix} = \begin{bmatrix} x_4 \\ x_5 \\ x_6 \end{bmatrix} \quad (3.9)$$

$$\begin{bmatrix} \dot{x}_4 \\ \dot{x}_5 \\ \dot{x}_6 \end{bmatrix} = \mathbf{D}^{-1} \left[ \frac{\partial \mathbf{G}}{\partial x} \begin{pmatrix} x_4 \\ x_5 \\ x_6 \end{pmatrix} + \vec{\tilde{\tau}} \right]$$

Refer to Appendix G for a short tutorial on this technique. The model is linearized at standing position. The state-space linear human biomechanical model obtained is:

$$\mathbf{A} = \begin{bmatrix} 0 & 0 & 0 & 1 & 0 & 0 \\ 0 & 0 & 0 & 0 & 1 & 0 \\ 0 & 0 & 0 & 0 & 0 & 1 \\ 26.0737 & -196.8976 & 3.1004 & 0 & 0 & 0 \\ -29.5050 & 428.1629 & -17.1673 & 0 & 0 & 0 \\ 3.5176 & -237.0909 & 31.0999 & 0 & 0 & 0 \end{bmatrix} \quad (3.10)$$

$$\mathbf{B} = \begin{bmatrix} 0 & 0 & 0 \\ 0 & 0 & 0 \\ 0 & 0 & 0 \\ 0.8592 & -1.7636 & 0.9272 \\ -1.7636 & 3.7774 & -2.1399 \\ 0.9272 & -2.1399 & 1.4413 \end{bmatrix}$$



$$C = I, \quad D = 0$$

### 3.4.2 Open-loop stability analysis

#### 3.4.2.1 Eigenvalues of the system matrix

From the linear state-space model of (3.10) stability analysis is done. The eigenvalues of the model are  $\pm 21.25$ ,  $\pm 5.10$  and  $\pm 2.75$ , which shows that system is open-loop unstable.

#### 3.4.2.2 Observability check

To design a feedback control scheme its observability must be checked through the rank of observability matrix  $\mathcal{O} = [C \ CA \ CA^2 \ \dots]^T$ . The matrix with numerical value is given as:

$$\mathcal{O} = 1 \times 10^7 \begin{bmatrix}
 0 & 0 & 0 & 0 & 0 & 0 \\
 0 & 0 & 0 & 0 & 0 & 0 \\
 0 & 0 & 0 & 0 & 0 & 0 \\
 0 & 0 & 0 & 0 & 0 & 0 \\
 0 & 0 & 0 & 0 & 0 & 0 \\
 0 & 0 & 0 & 0 & 0 & 0 \\
 0 & 0 & 0 & 0 & 0 & 0 \\
 0 & 0 & 0 & 0 & 0 & 0 \\
 0 & 0 & 0 & 0 & 0 & 0 \\
 0 & 0 & 0 & 0 & 0 & 0 \\
 0 & 0 & 0 & 0 & 0 & 0 \\
 0 & 0 & 0 & 0 & 0 & 0 \\
 0 & 0 & 0 & 0 & 0 & 0 \\
 0 & 0 & 0 & 0 & 0 & 0 \\
 0 & 0 & 0 & 0 & 0 & 0 \\
 0 & 0 & 0 & 0 & 0 & 0 \\
 0 & 0 & 0 & 0 & 0 & 0 \\
 0 & 0 & 0 & 0 & 0 & 0 \\
 0 & 0 & 0 & 0 & 0 & 0 \\
 0 & 0 & 0 & 0 & 0 & 0 \\
 0.0007 & -0.0090 & 0.0004 & 0 & 0 & 0 \\
 -0.0013 & 0.0193 & -0.0008 & 0 & 0 & 0 \\
 0.0007 & -0.0110 & 0.0005 & 0 & 0 & 0 \\
 0.0007 & -0.0090 & 0.0004 & 0 & 0 & 0 \\
 -0.0013 & 0.0193 & -0.0008 & 0 & 0 & 0 \\
 0.0007 & -0.0010 & 0.0005 & 0 & 0 & 0 \\
 0 & 0 & 0 & 0.0007 & -0.0090 & 0.0004 \\
 0 & 0 & 0 & -0.0013 & 0.0193 & -0.0008 \\
 0 & 0 & 0 & 0.0007 & -0.0110 & 0.0005 \\
 0 & 0 & 0 & 0.0007 & -0.0090 & 0.0004 \\
 0 & 0 & 0 & -0.0013 & 0.0193 & -0.0008 \\
 0 & 0 & 0 & 0.0007 & -0.0110 & 0.0005 \\
 0.2843 & -4.07320 & 0.1679 & 0 & 0 & 0 \\
 -0.6080 & 8.7264 & -0.3607 & 0 & 0 & 0 \\
 -0.34390 & -4.9532 & 0.2061 & 0 & 0 & 0
 \end{bmatrix}$$

The rank of this matrix is 6 which shows the matrix is full rank and hence the model is fully observable.

### 3.4.2.3 Controllability check

The model is then checked for its controllability. The rank of controllability matrix  $\mathcal{C} = [\mathbf{B} \ \mathbf{A}\mathbf{B} \ \mathbf{A}^2\mathbf{B} \ \dots]_{6 \times 18}$  is 6 which means the system is controllable. This matrix has numerical values as shown below:

$$\begin{aligned}
 & \mathbf{c} \\
 & = 1 \\
 & \times 10^5 \begin{bmatrix} 0 & 0 & 0 & 0 & 0 & 0 & 0 & 0 & 0 & 0.0037 & -0.0080 & 0.0045 & 0 & 0 & 0 & 1.6791 & -3.5970 & 2.0412 \\ 0 & 0 & 0 & 0 & 0 & 0 & 0 & 0 & 0 & -0.0080 & 0.0171 & -0.0097 & 0 & 0 & 0 & -3.5970 & 7.7062 & -4.3741 \\ 0 & 0 & 0 & 0 & 0 & 0 & 0 & 0 & 0 & 0.0045 & -0.0097 & 0.0056 & 0 & 0 & 0 & 2.0412 & -4.3742 & 2.4844 \\ 0 & 0 & 0 & 0 & 0 & 0 & 0.0037 & -0.0080 & 0.0045 & 0 & 0 & 0 & 1.6791 & -3.5970 & 2.0412 & 0 & 0 & 0 \\ 0 & 0 & 0 & 0 & 0 & 0 & -0.0080 & 0.0171 & -0.0097 & 0 & 0 & 0 & -3.5970 & 7.7062 & -4.3741 & 0 & 0 & 0 \\ 0 & 0 & 0 & 0 & 0 & 0 & 0.0045 & -0.0097 & 0.0056 & 0 & 0 & 0 & 2.0412 & -4.3742 & 2.4844 & 0 & 0 & 0 \end{bmatrix}
 \end{aligned}$$

The overall stability check reveals that although the system is open-loop unstable it is detectable as well as stabilizable. It means we can design a control mechanism for this model to synthesize STS motion using full or reduced order measurement feedback.

### 3.5 Summary

In this chapter, a four-segment human biomechanical model is introduced. The model is discussed in terms of equations of motions governing its dynamics, as well as its implementation in the SimMechanics environment in terms of its body segment parameters. Open-loop stability analysis of the linearized model is also presented. Next, this model is validated in experimental setting, using motion and force capture arrangement for data acquisition and analysis. Chapter 4 gives a detailed description of experiment, analysis and model validation.

## CHAPTER 4

### EXPERIMENTAL VALIDATION OF HUMAN BIOMECHANICAL MODEL USING MOTION AND FORCE CAPTURE

Sit to stand motion in the context of dynamic variables and their relation to the body segment parameters used for human biomechanical modeling is presented. The intent is to obtain a model that closely matches actual human movement profiles. To replicate the real motion, we collected STS motion and force data from 7 healthy subjects using reflective markers and multiple infra-red cameras based optical motion capture system and a 4-beam-2-axes force platform. We achieved following objectives from this study:

- 1) We collected kinematic and kinetic data of STS motion of healthy young subjects.
- 2) We realized a custom human biomechanical model in the sagittal plane as close as possible to the real human beings.
- 3) We scaled the analytical human biomechanical model of chapter 3 to the real subjects' BSP and used motion driven technique to simulate STS motion.

The motion and force capture-based modeling scheme has given results that show a reduction in the error expected from the weighing coefficient method of anthropometry.

The resulting model has been verified using kinematic and kinetic analyses of human STS motion. Since our experimental and simulation results closely match this validates our modeling scheme.

## 4.1 Methodology

### 4.1.1 Workflow

STS motion by 7 healthy subjects was recorded using 13 markers and 4 Flex-3 infra-red-cameras based motion-capture system. Force data were collected at the same time using a 2-axis 4-beam Pasco force plate. The data were used to construct motion and force profiles. A four-segment human biomechanical model with 3 DoF in the sagittal plane was developed in MATLAB's SimMechanics environment (Figure 3.2).

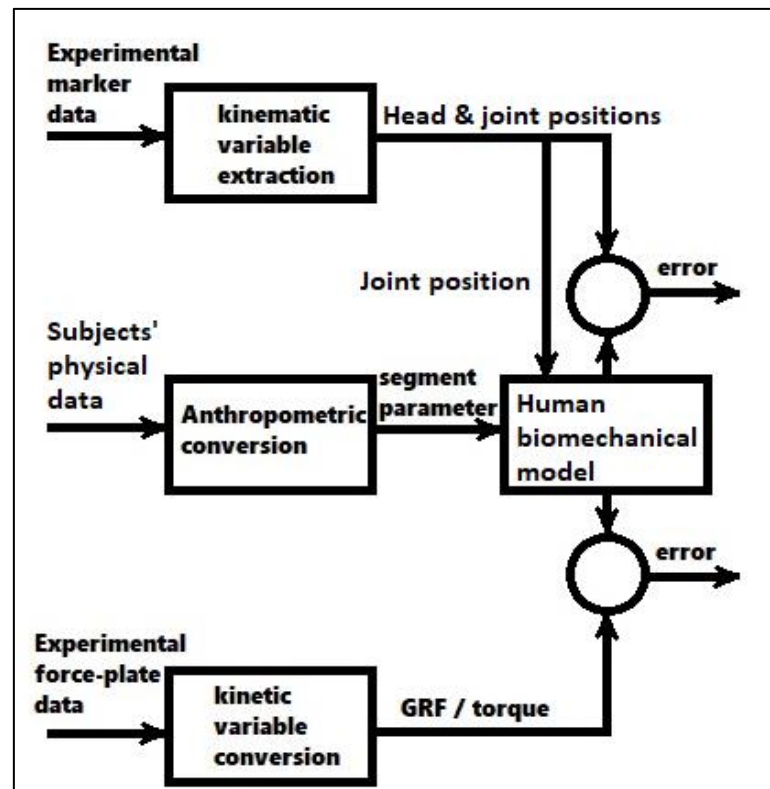


Figure 4.1. The workflow of experimental and analytical techniques

Each subject's physical (height and mass) data are converted into BSP using anthropometry. Refer to Appendix B for the anthropometry technique used in this study. BSP values are then used to customize the human biomechanical model. In motion driven technique the joint position commands are used to run the model. Head, joint positions, ground reaction forces and torques generated by the model are compared with real subjects' experimental data. Refer to [12] for a detailed description of this

study and the appendices C and D for hardware and software used in conducting the experiment and data acquisition.

## 4.1.2 Motion and force capture

### 4.1.2.1 Subjects for the STS experiment

Experimental data of sit to stand transfer were collected at the Biomechanics lab of Riphah International University. Seven healthy subjects (5 males and 2 females, age:  $22 \pm 0.81$  years, mass:  $72.58 \pm 11.61$  kg, height:  $1.70 \pm 0.04$  m) gave informed and prior consent to participate in the experiment. These subjects were chosen from individuals who were young and had no history of STS motion disorder. Table 4.1 shows the physical parameters of the participating volunteers. Refer to Appendix A for Ethics' Committee approval from the competent authority to conduct the experiment. As typical with motion capture experiments relatively small number of subjects is considered sufficient [23].

Table 4.1. Surface plot that defines inference of ANFIS

Subject ID	Gender	Age (year)	Mass (kg)	Height (m)
1	Male	21	76.55	1.69
2	Male	22	79.81	1.70
3	Male	21	50.05	1.69
4	Female	22	66.56	1.61
5	Female	22	84.91	1.67
6	Male	23	71.05	1.72
7	Male	23	79.10	1.78

#### 4.1.2.2 Experiment protocol

Initially, some mock experimentation was done to device a set of protocols regarding appropriate positioning of equipment, sampling frequency for data acquisition, number and position of markers on a subject's body and so on. Infra-red cameras are very sensitive to change in ambient light and slight disturbance in their positioning. Due to unavailability of skin-tight motion-capturing suit and Velcro bands, we faced additional difficulty in making all markers visible to cameras throughout the trials. Moreover, infra-red cameras may pick reflection from a shiny surface like doorknobs or zippers on garments. Each such item was identified and was covered with masking tape. The mock experimentation continued for some 1 week. Eventually, a set of protocol was finalized to conduct the actual experiments.

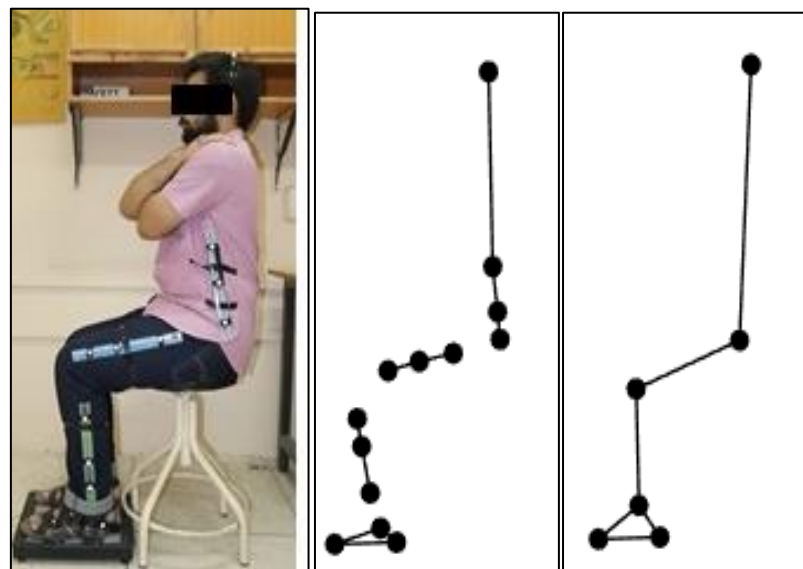


Figure 4.2. STS data capture setup: a subject with markers on segments and feet on a force plate (left), marker-based model (center) and joint based model (right) extracted from motion capture data

All the subjects used an armless chair 49 cm from the top surface of the force plate to complete STS transfer. A total of 13 spherical reflective markers were attached on the left side of each segment. 3 markers on foot, arranged on side of heel, toe and below ankle joint, to specify foot as a triangular base of support. 3 markers were affixed each on shank, thigh and trunk, using rigid plastic rulers, to counter garment artifact. The 13th marker was worn on top of the head, using a hairband.

For motion capture, we used four infra-red Flex-3 cameras by OptiTrack. The data were recorded at 100Hz using Optitrack Motive 2.0.1 data acquisition software. Force data too were collected using the Pasco force plate at 100 Hz, using Capstone software.

Each subject did at least 3 STS trials and all trials were done at once. During these trials the subject was seated in a chair, arms crossed across the chest so that head, arm and trunk could be treated as one segment. If arms are kept hanging during STS, their movement may add error to the STS dynamics for a model that incorporates both hands into a consolidated segment called head arm trunk or HAT. The two feet should be kept close so that both ankles should rotate about same axis. To start the trial, the subject was asked to 'stand up' at normal speed and then 'sit down' after 3 to 4 sec. Refer to Appendix C for more details regarding the motion and force capture setup arranged for this study.



Figure 4.3. From left to right; calibration square, calibration wand, infrared camera by OptiTrack





Figure 4.4. Force data were captured by 2-axis 4-beam Pasco force platform

#### 4.1.2.3 Equipment and calibration

There are no concrete rules available in the literature to help us determine the appropriate positions and number of markers as well as the optimum number and appropriate positioning of cameras for reliable motion capture. 3D motion capture is based upon 2D image processing by multiple cameras [29], [31]. To obtain the most reliable results, we, therefore, opted for multiple camera systems, along with spherical markers that ensure reliable data reconstruction by post-processing.

Data capture is a tedious job that needs calibration of cameras using ‘calibration wand’ and determination of frame of reference in the motion capture area using ‘calibration square’. Due to sensitivity to the light, temperature and any slight shift in the position of cameras, recalibration is frequently needed. To ensure accuracy, the force plate was checked for zero error before each trial.

Once motion data were captured, post processing is done. Each marker was manually numbered in the Motive Edit environment, first individually and then these markers were grouped into and named after segments. The segment labels too were assigned manually in Motive Edit mode for each trial. Motive exports motion capture data in *.tak* (specific for Motive) and *.c3d* (general format for motion capture) file formats. Kinematic analysis for this study was carried out by a motion capture software

MoCap [65], a freely available motion data analysis toolbox that works seamlessly with MATLAB. To get a brief introduction to the MoCap toolbox refer to Appendix D.

### **4.1.3 Motion data analysis**

#### **4.1.3.1 Data import, interpolation and normalization**

Motion data (.*c3d* format) were imported into the MATLAB's MoCap toolbox for analysis. This data were read into the MoCap environment and saved as a MATLAB variable. Using marker data, each trial of 7 subjects were simulated to check and recover any missing data using interpolation. MoCap uses linear interpolation to recover missing markers. Data from subject#5 were highly corrupted and hence were discarded. Using MoCap, markers can be assigned with numbers, so can be segments given names. All the motion data are used to reconstruct the motion of every subject and for every trial. The reconstructed animation is used to determine the start and end of the STS cycle. To normalize STS motion time by different subjects and during multiple trials, the STS motion profiles have been normalized as %STS Cycle.

#### **4.1.3.2 Analysis in marker space**

The markers are used to capture motion and define a segment and joint locations. The lone marker affixed on the head of the subject is used for accurate determination of height and to collect head position trajectory during STS. Marker data and joint data are used to animate STS transfer of all subjects. 3 frames from animation are shown in Figure 4.5 where different phases of STS motion can be seen. The motion has been reconstructed using markers connected to define segments. The trajectories of all marker are plotted in different colors to illustrate how various parts of the body move during STS.

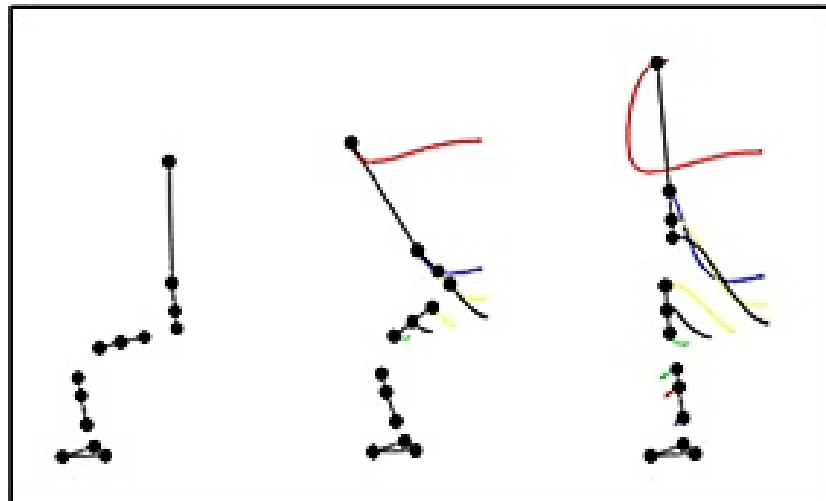


Figure 4.5. Three phases of STS animation reconstructed from motion capture using marker data

The ensemble average of all subjects' head position trajectories is shown in Figure 4.6. The trajectory is plotted in 2-dimensional Cartesian space.  $X_{ave}$  curve is the position trajectory to represent horizontal and  $Y_{ave}$  position trajectory shows the vertical component of the motion. The curves for  $\pm 1$  Standard Deviation (SD) are also plotted to depict intra-subject variation in head position trajectories.

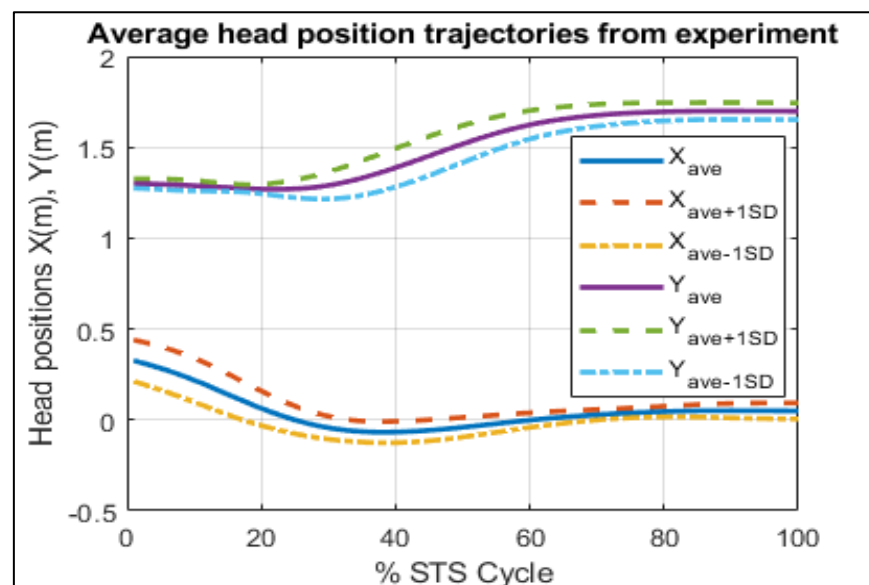


Figure 4.6. Ensemble average trajectories of head position. Curves in dashed lines represent  $\pm 1$  Standard Deviation

### 4.1.3.3 Analysis in joint space

MoCap gives provision to infer joints in the body from point of rotation between the two adjoining segments. Marker positions were used to infer joints and then angular positions of each joint in every frame was calculated. Figure 4.7 is the transformation of STS motion representation from markers' space to joint space. This representation of motion also displays the path of joints as separate trajectories during the STS motion.

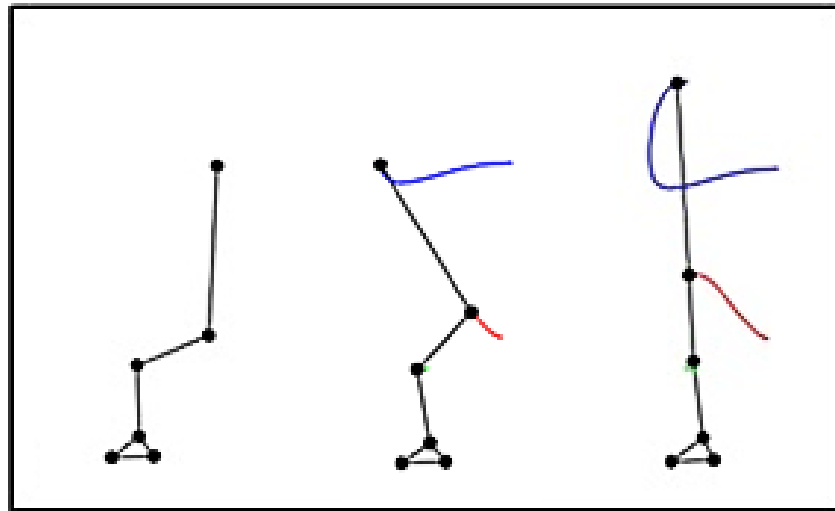


Figure 4.7. Three phases of STS animation reconstructed from motion capture using marker data

Ankle, knee and hip joint position trajectories of all subjects are reconstructed as shown in Figure 4.8. It can be seen from the Figure that even though joint angle profiles of STS motion of all subjects' single trials have been time normalized in percentage STS cycle, the curves show a lot of variation within the small group of subjects.

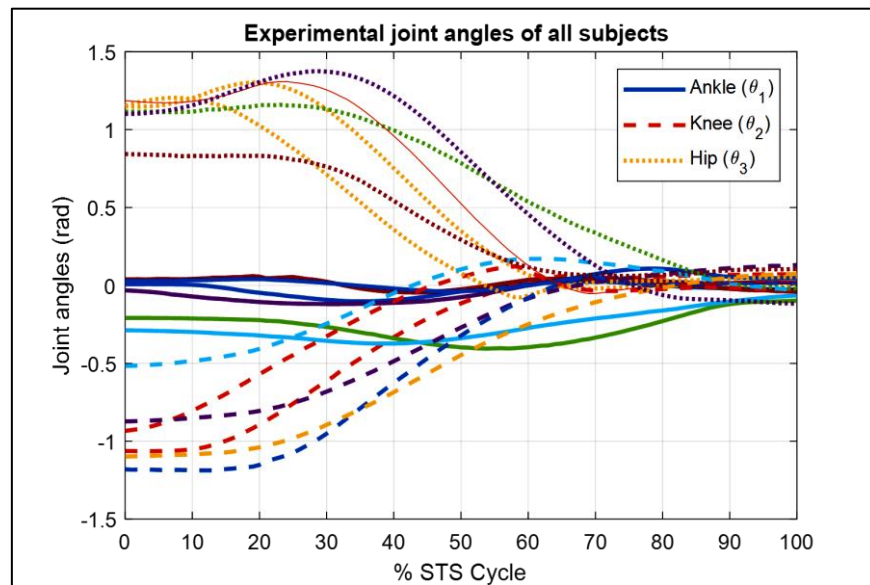


Figure 4.8. Trajectories of joint angles from all subjects using motion capture during STS transfer

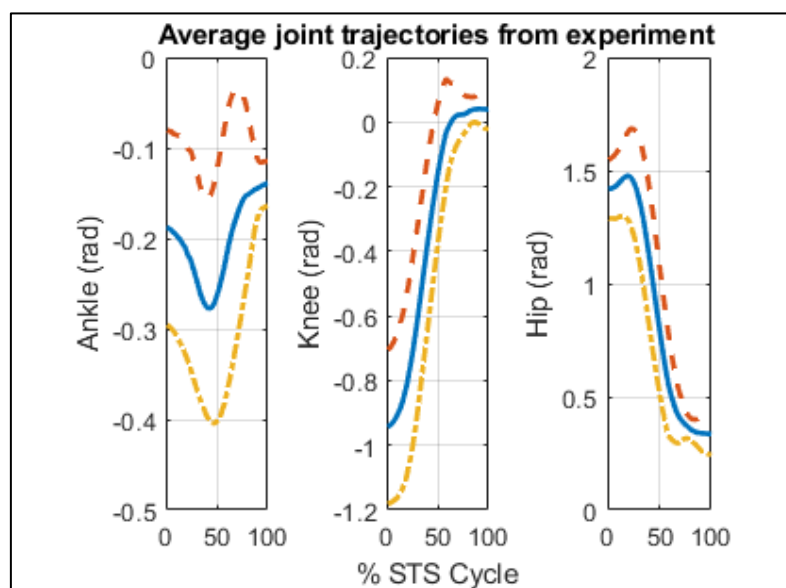


Figure 4.9. The ensemble average of joint angles from all subjects using motion capture. Curves in dashed lines represent  $\pm 1$  SD

To infer a trend of joint angle trajectories, an average value of joint angle profiles from all subjects was calculated and plotted as shown in Figure 4.9. The variation among the group is plotted as  $\pm 1$  Standard Deviation (SD) curves.

Table 4.2. BSP data based on total body mass and Height/length

Subj ID	Segment	Mass (kg)	Length/height (m)	Center of gravity (m) (measured from lower joint)	Moment of inertia (Kg. m <sup>2</sup> )
1	Feet	2.22	0.066	-	-
	Shanks	7.11	0.419	0.237	0.114
	Thighs	15.31	0.417	0.236	0.278
	HAT	51.90	0.801	0.299	8.199

#### 4.1.4 Anthropometric conversion

Among various methods available in the literature [46], we used the weighing coefficient method described in [56] and Appendix B, which is widely accepted among the research community. Weighing coefficient method is based on empirical formulas and does not need expensive measurement apparatus. For brevity, only one representative data out of a total of 7 subjects are presented in

Table 4.2. For complete data of BSP of all the 7 subjects see Table B. 2 in Appendix B.

#### 4.1.5 Human biomechanical model

The analytical part of our study mainly comprises the development of a four-segment human biomechanical model to simulate STS motion in the sagittal plane. The biomechanical model as shown in Figure 4.10 is realized in SimMechanics (see Figure 3.2) using only BSP; *i.e.*, lengths, masses, CoG and moment of inertia of foot, shank, thigh and HAT. The model is defined in body frame, where  $\theta_1$  stands for ankle,  $\theta_2$  for knee and  $\theta_3$  for hip joint positions. Hence the 2D model has 3 DoF, due to three revolute joints. The same model has been used in earlier studies [41], [53], [61] using an analytical scheme only and BSP values borrowed from [40], [43].

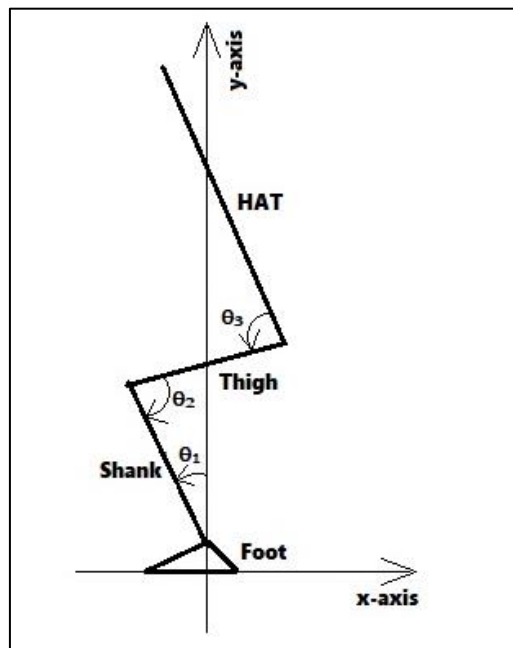


Figure 4.10. The 4-segment human biomechanical model in the sagittal plane

#### 4.1.6 STS motion synthesis

The motion synthesis scheme as shown in Figure 4.1 is implemented in MATLAB SimMechanics environment as shown in Figure 4.11. The human biomechanical model of Figure 3.2 has been incorporated with joint position-based motor control. The motion control command is generated by the block ‘angle’ that provides joint angle trajectory commands inferred from motion capture data of individual subjects. In SimMechanics, the position command must accompany the velocity and acceleration of the joint position trajectories, which is achieved by derivative blocks  $\frac{du}{dt}$  as shown in Figure 4.11. Force and motion sensors as well as scope blocks are used to measure and plot various kinematic and kinetic variables during the simulation.

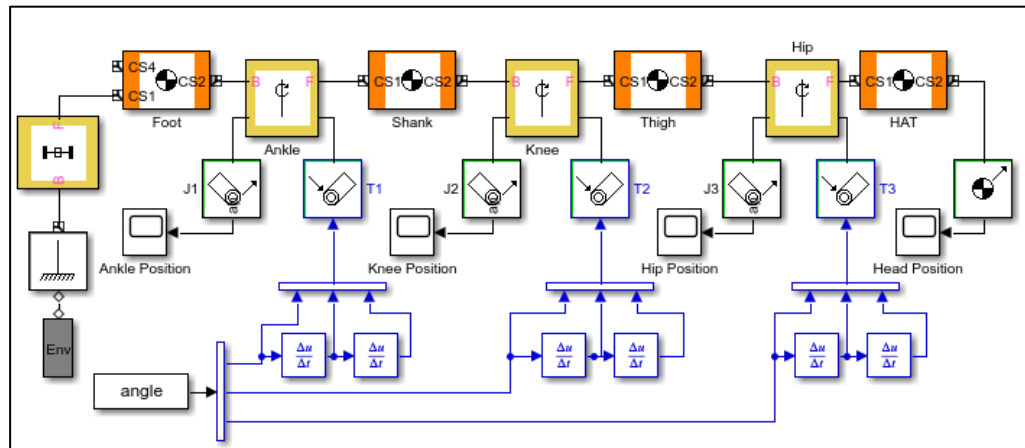


Figure 4.11. STS motion synthesis framework in SimMechanics

## 4.2 Results

The ensemble average of all motion and force data obtained from the experiment and simulations is calculated, compared and plotted. Head position in Cartesian space ( $X_{exp}$ ,  $Y_{exp}$ ) and joint angular position trajectories in joint space were recovered from motion capture data. Each of the customized human biomechanical models was simulated for STS transfer using the simulation scheme of Figure 4.11. Subject-specific joint position trajectories were used to run a subject-specific/customized human biomechanical model to simulate STS motion performed by a specific subject. From simulated motion head and joint positions were measured. In Figure 4.12 ensemble average head position trajectories from motion capture data are plotted as ( $X_{exp}$ ,  $Y_{exp}$ ) to depict horizontal and vertical components of experimental motion trajectory in Cartesian space. The head position measurements from simulations are plotted as ( $X_{sim}$ ,  $Y_{sim}$ ). The two sets of curves are analyzed for similarity. A correlation of  $R=0.74$  horizontal component of head motion and  $R=0.98$  for the vertical component was found.



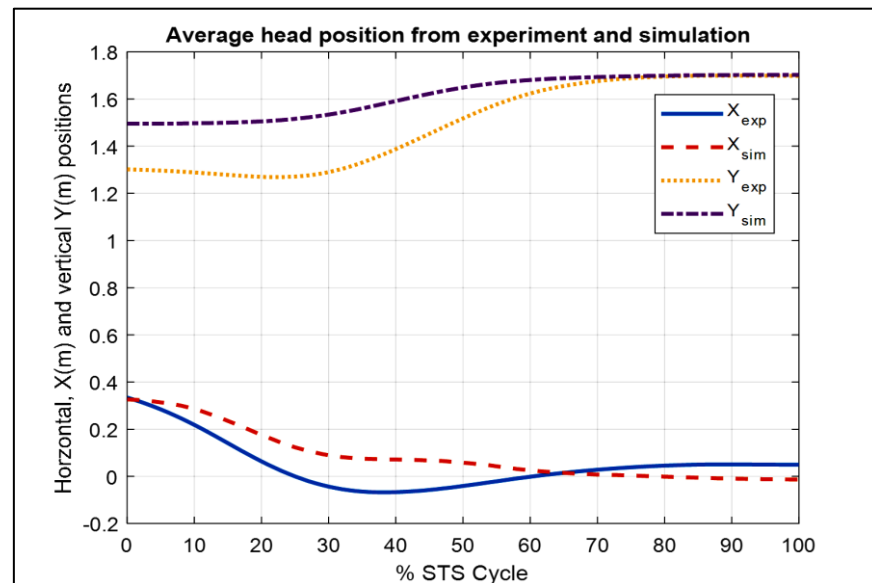


Figure 4.12. Average head position trajectories from motion capture ( $X_{exp}$ ,  $Y_{exp}$ ) and simulation ( $X_{exp}$ ,  $Y_{exp}$ ).

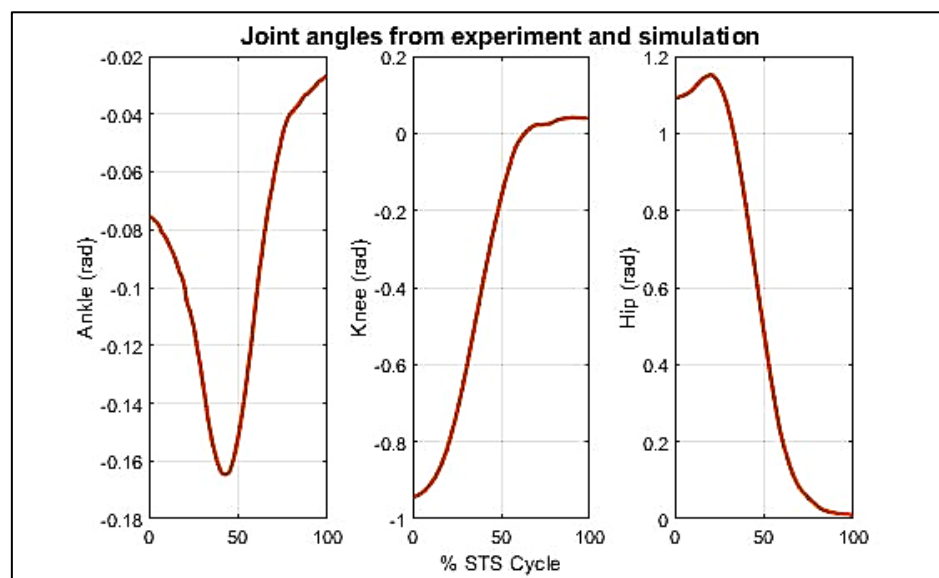


Figure 4.13. Average experimental and simulated ankle, knee and hip joint trajectories.

The joint angles are measured from simulations and plotted in Figure 4.13. Each of the three plots comprises joint angle profiles both from experiment and simulation. Joint angle trajectories are perfectly followed by the model in simulations so much so that both curves are almost overlapping and the correlation of  $R=0.99$  for all 3 angle sets is achieved.

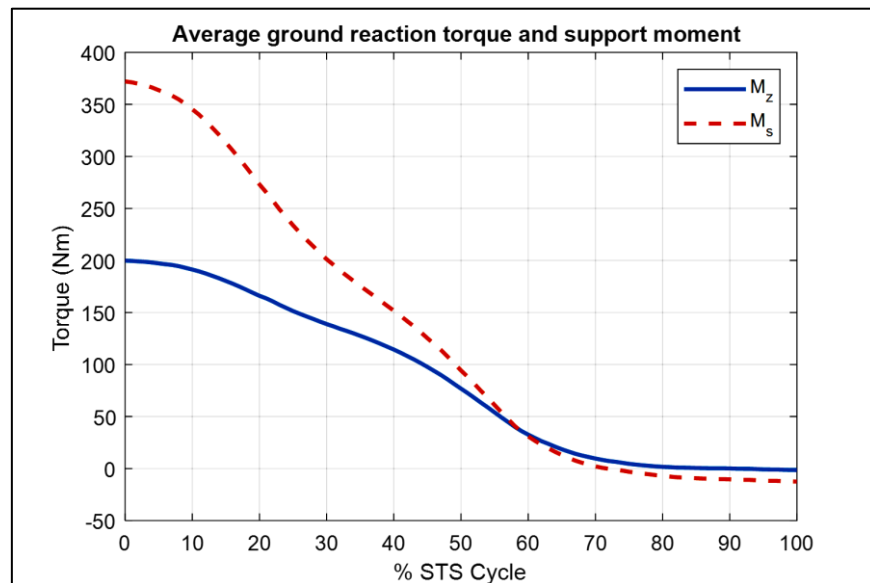


Figure 4.14. Ground reaction torque  $M_z$  and support moment  $M_s$  (sum of joint torques)

The plots of kinetic variables are presented below.  $M_z$  is the ground reaction torque measured under the feet during STS motion. The support moment,  $M_s$  is the sum of three joint torques calculated through inverse dynamics. The plots are shown in Figure 4.14. Comparison of ground reaction torque and the sum of joints' torque is considered correlated and is used for analysis and validation of a modeling and control scheme through simulation. In this study the correlation between the two torques is very high;  $R=0.98$ .

In Figure 4.15, an average of vertical ground reaction force,  $F_w$ , which is the average of body weights of all subjects measured by force plate during the STS trial has been plotted. The same force  $F_y$ , measured from simulations, is plotted in the same Figure. It can be seen from the plot that simulated motion shows a ground reaction force profile that closely matches the experimental GRF measured by the force platform. The two trajectories follow a similar trend and the kinetic analysis shows a correlation of  $R=0.94$  between them.

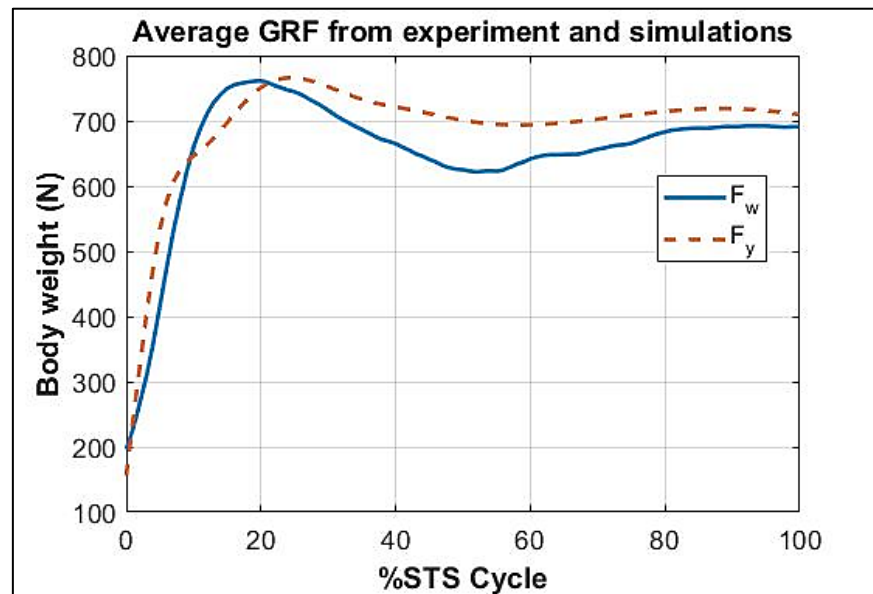


Figure 4.15. The force plate shows experimental bodyweight  $F_w$  (bold line) that correlates closely ( $R=0.94$ ) to vertical ground reaction force  $F_y$  (dashed line) obtained from simulation

### 4.3 Discussion

The marker-based motion capture technique is used to obtain a four-segment human biomechanical model capable to simulate STS motion in the sagittal plane. For all trials of STS carried by each of the seven subjects, motion and force data were collected simultaneously at 100 Hz. The OptiTrack cameras' data acquisition system operates on Motive 2.0.1 and the marker data were exported into the standard format of *.c3d* files. This format is compatible with the MoCap toolbox and gives full visualization and analysis power of MATLAB. Figure 4.2 shows the markers affixed on the subjects' left side and segment information recorded using infer-red cameras. Marker data are then used to obtain joint based 4 segment model in the sagittal plane. Out of seven subjects, one of the subject's data for all 3 STS trials were corrupted and hence were rejected. Figure 4.6 shows the ensemble average of head position trajectories from experimental data of all subjects. The intra-subject variation is also obvious in Figure 4.6 and is expressed in terms of standard deviation in conjunction with averages. Figure 4.7 shows STS motion phases in joint space. Figure 4.8 shows ankle, knee and hip joint trajectories recovered from motion capture data of all the subjects. Owing to different segment lengths and individual STS motion patterns, the

three sets of joint angles show much diversity. The height and body-mass of all the subjects are converted into BPS values using weighing coefficient anthropometry (See Appendix B for the technique used). Based on these values a 4-segment model is realized in SimMechanics. The model is customized for each of the subjects and the joint motion data of the same subject are used to simulate STS motion.

As a standard procedure, ensemble average plots of all experimental and simulated results have been presented. Figure 4.12 shows head position trajectories in the Cartesian plane, both from experimental data (from the marker on top of the head) and from simulation done by customized human biomechanical models.  $X_{sim}$  and  $Y_{sim}$  are average head trajectories of simulated motions based on scaled human biomechanical models. These models produce STS motion using joint motion commands of their respective subjects. The error between the two curves is mainly attributed to the fact that motion commands are generated for joints and no head position error is used for controlling the motion. Another reason can be the accumulated error of garment artifact and BPS conversion error used in the modeling. The tracking can be improved by applying subject-specific initial conditions in simulations and using specialized motion capture suits. Figure 4.13 shows an excellent match of experimental and simulated joint positions, to the extent that the set of all the three angles are completely overlapping, giving a correlation of 0.99. Figure 4.14 shows a close correlation (0.98) between ground reaction moment  $M_z$  and the support moment  $M_s$ , which is the sum of three joint torques. Figure 4.15 shows force exerted by body weight during STS changes. At the start of the STS cycle, the 200N value shows the weight of feet, shanks and partially of thighs, while seated. With the seat off, the weight on the force plate increases and so does the vertical component of the ground reaction force. The two forces match closely (correlation 0.94) and settle to the final value of the subjects' average weight. Our kinetic analysis is based on techniques available in the literature [11], [13] where correlating all posture variations with corresponding GRF, ground reaction moments and support moment is used as model validation technique. The close match in experimental and simulated motions gives evidence to the reliability of our modeling scheme. Figure 4.16 (top) depicts snaps from the animation of experimental STS. Four phases of STS have been shown and respective trajectories of joints during the motion can also be seen. In Figure 4.16 (bottom) the STS motion

phases from simulation, based on the customized human biomechanical model in SimMechanics can be seen. The two Figures show close resemblance, which is an indication of the reliability of motion and force capture methods and eventually the modeling technique we have used.

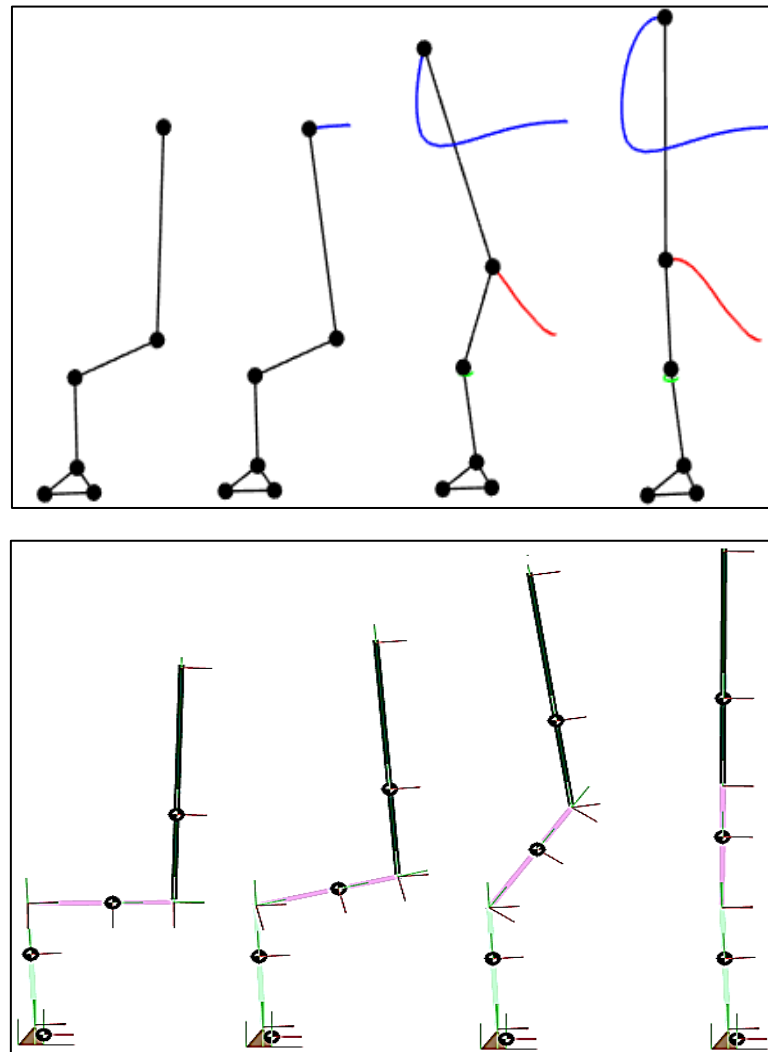


Figure 4.16. Phases of STS from motion capture. Trajectories of joints are also shown (top), simulated STS motion in SimMechanics environment (bottom)

## 4.4 Summary

In this chapter, we have presented STS motion synthesis based on the position driven motion control scheme. We developed motion and force capture protocols for STS captured in the sagittal plane. Using the physical parameters of the subjects, we estimated their body segment parameters, using the weighing coefficient method of

anthropometry. The BSP is used to scale the human biomechanical model to each of the subjects. The motion data are used to control STS motion. Joint angles, head positions, GRF and joint torques are used to compare simulated motions with experimental STS to validate the human biomechanical modeling scheme. The validated model is next used to synthesize STS motion with low-level control scheme, implemented by three different robust controllers. Chapter 5 gives the details.

## **PART II**

# **CNS Modeled as Controller for STS Motion Synthesis**

## CHAPTER 5

### STS MOTION SYNTHESIS USING ROBUST CONTROL

We now present three schemes to synthesize STS motion using the analytical human biomechanical model of chapter 2 and various robust controllers to model the CNS. The nonlinear state-space model of (3.8) is based upon 6 states; three states composed of joint angle positions and rest three are joint angular velocities. We model measurement noise and neurological feedback delays in sensory data to CNS in our scheme to replicate real-life physiological constraints.

Three control schemes are as follows: first, we use full order LQR compensator, the second one is based on Kalman observer using LQG design and the third scheme utilizes  $\mathcal{H}_\infty$  control law for STS motion using ankle, knee and hip position trajectories as reference. LQR scheme utilizes full state measurements. The LQR control is used to recover states from noise and to provide a robust control against feedback delays. Next, we present a reduced-order measurement scheme, where all the three joint position measurements are subject to sensor noise. The observer reconstructs joint position profiles recovered from noise and estimates joint angular velocity profiles so that a full state feedback controller may be employed. We later improve our results using the  $\mathcal{H}_\infty$  scheme for reduced ordered measurement-based control law.

The system tracks joint position trajectories to carryout natural and physiologically relevant STS motion. The motion obtained is smooth and close to human STS in angular profiles. The contribution of one kinematic variable i.e., joint positions in carrying out STS task in collaboration with CNS modeled as a control law implementation seems evident. This supports the clinical hypothesis that the human CNS carries out body movements by utilizing feedbacks of joint positions besides other variables.



## 5.1 Methodology

The human biomechanical model used for human-like STS motion synthesis is shown in Figure 3.1. In Figure 3.2, this model is implemented in SimMechanics. Ankle, knee and hip position trajectories are used as the references to be tracked. To develop a model-based linear control law like LQR, LQG and linear  $\mathcal{H}_\infty$ , the human biomechanical model must be linearized so that it could be incorporated in the control law. The control scheme is formulated in minimization of error between reference to be tracked and actual measured position. Robust control scheme thus gives mathematical justification of trajectory tracking. The measurements feedback to CNS (controller) are subject to neural delays and measurement noise. These factors give rise to unmodeled dynamics that are catered for using these robust controllers.

## 5.2 Full State Measurement Scheme

The three joint positions and velocities comprise the state vector  $\vec{x}$ . The measurements of joint positions and velocities using sensors are always contaminated with noise. Typical value of this noise is around  $10^{-10}$  watt [17]. Also, the neurofeedback to CNS is subject to time delay; 10 m sec, 15 m sec and 30 m sec delays for hip, knee and ankle joint positions respectively [37]. Both noise and time delays have been incorporated in the modeling and control scheme.

### 5.2.1 Linearized model for full state

The non-linear model for STS motion [43] is given by (3.1) and (3.8). Linearizing in the upright standing position, the initial condition of state  $\vec{x}$  for ankle, knee, hip joint positions and velocities respectively is given by:

$$\vec{x}_0 = [0 \ 0 \ 0 \ 0 \ 0 \ 0]^T \text{ and } \vec{u}_0 = [0 \ 0 \ 0]^T$$

and  $\vec{u}_0$  is the initial condition of control input. See Appendix G for details on linearization techniques and operating point selection.

Linearized state space model is

$$\vec{\dot{x}} = \mathbf{A}\vec{x} + \mathbf{B}\vec{u}|_{\vec{x}_0, \vec{u}_0} \quad (5.1)$$

$$\mathbf{A} = \begin{bmatrix} 0 & 0 & 0 & 1 & 0 & 0 \\ 0 & 0 & 0 & 0 & 1 & 0 \\ 0 & 0 & 0 & 0 & 0 & 1 \\ 26.0737 & -196.8976 & 3.1004 & 0 & 0 & 0 \\ -29.5050 & 428.1629 & -17.1673 & 0 & 0 & 0 \\ 3.5176 & -237.0909 & 31.0999 & 0 & 0 & 0 \end{bmatrix} \quad (5.2)$$

$$\mathbf{B} = \begin{bmatrix} 0 & 0 & 0 \\ 0 & 0 & 0 \\ 0 & 0 & 0 \\ 0.8592 & -1.7636 & 0.9272 \\ -1.7636 & 3.7774 & -2.1399 \\ 0.9272 & -2.1399 & 1.4413 \end{bmatrix}$$

$$\mathbf{C} = \mathbf{I}, \mathbf{D} = \mathbf{0}$$

## 5.2.2 LQR Compensator

The compensator comprises an estimator to reconstruct noise-free states and a controller to generate torque commands to the joints so that the human biomechanical model may track input reference trajectories through control action of LQR.

### 5.2.2.1 LQR Controller

LQR control scheme seeks minimization of quadratic cost function given by

$$J = \int_{t_0}^{t_f} (\vec{x}^T \mathbf{Q} \vec{x} + \vec{u}^T \mathbf{R} \vec{u}) dt \quad (5.3)$$

An LQR controller provides great flexibility of tuning the gains individually [66] using elements of state weighting matrix  $\mathbf{Q} \succcurlyeq \mathbf{0}$  and control weighting matrix  $\mathbf{R} \succ$

$\mathbf{0}$  , with  $\mathbf{Q} = \text{diag}(0.001, 0.005, 0.002)$  and  $\mathbf{R} = \text{diag}(90, 2.7 \times 10^5, 1000, 600, 1000, 800)$ . The term  $\vec{x}^T \mathbf{Q} \vec{x}$  represents penalty on states for deviating from origin and term  $\vec{u}^T \mathbf{R} \vec{u}$  represents cost on control. Controller thus obtained is robust and optimum. LQR control law is designed by solving the Riccati equation

$$\mathbf{P}\mathbf{A} + \mathbf{A}^T\mathbf{P} - \mathbf{P}\mathbf{B}\mathbf{R}^{-1}\mathbf{P} + \mathbf{Q} = \mathbf{0} \quad (5.4)$$

for  $\mathbf{P}$ . The controller gain  $\mathbf{G}$  is then determined using relation

$$\mathbf{G} = -\mathbf{R}^{-1}\mathbf{B}^T\mathbf{P} \quad (5.5)$$

The control law to be designed is

$$\vec{u} = -\mathbf{G}\vec{\hat{x}} \quad (5.6)$$

where  $\vec{\hat{x}}$  is the state vector estimated by the Linear Quadratic Estimator. Control output  $\vec{u}$  comprises the passive torques used to run three actuators at the joints.

### 5.2.2.2 Linear Quadratic Estimator

An estimator reconstructs the noise buried states that cannot be otherwise used for feedback control in this condition. The dynamic equation for the estimator is

$$\dot{\vec{\hat{x}}} = \mathbf{A}\vec{\hat{x}} + [\mathbf{B} \ \mathbf{K}] \begin{bmatrix} \vec{u} \\ \vec{e} \end{bmatrix} \quad (5.7)$$

where  $\vec{\hat{x}}$  is the estimate of state derivative,  $\vec{e}$  is the error between measured state  $\vec{x}$  and reference input  $\vec{X}_d$ . The linearized model of the plant  $[\mathbf{A}, \mathbf{B}, \mathbf{C}, \mathbf{D}]$  is used to design the estimator gain  $\mathbf{K}$  and controller gain  $\mathbf{G}$ . The estimator model is given by  $[\mathbf{A}_0, [\mathbf{B}_0 \ \mathbf{K}_0], \mathbf{C}_0, \mathbf{D}_0]$  , where  $\mathbf{A}_0 = \mathbf{A}, \mathbf{B}_0 = \mathbf{B}, \mathbf{C}_0 = \mathbf{I}_{6 \times 6}$  and  $\mathbf{D}_0 = \mathbf{0}_{6 \times 9}$ .  $\mathbf{K}$  is

designed by tuning matrices  $R_0 = \text{diag}(0.7, 0.35, 0.27, 0.7, 0.8, 1)$  and  $Q_0 = 1.5 \times Q$ .

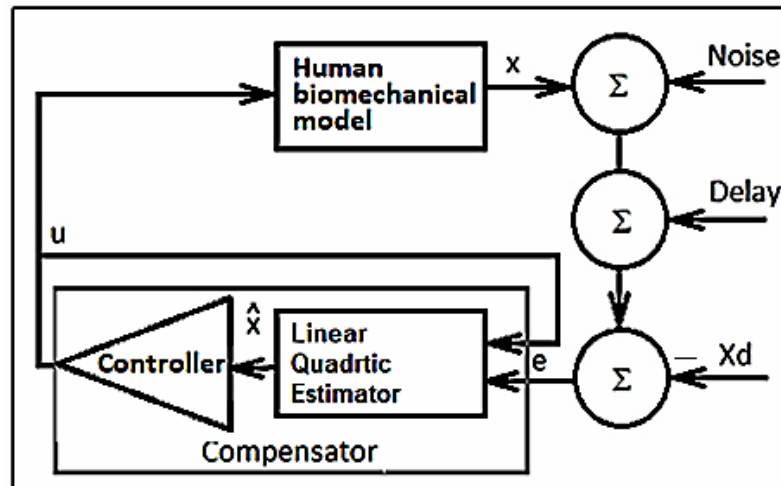


Figure 5.1. The Human STS motion control mechanism is based on the LQR scheme.  $X_d$  is the reference input comprising ankle, knee and hip joint position trajectories.

### 5.2.2.3 Close-loop stability analysis

The close-loop system is the combination of two subsystems in tandem; one close-loop system comprises human biomechanical model (plant) to be controlled by LQR controller  $G$ . The state matrix of this subsystem is given by  $A-BG$  and its eigenvalues are  $-690.49 \pm 131.17i$ ,  $-15.32$ ,  $-65.94$ ,  $-45.60$  and  $-37.89$ . The other subsystem comprising LQE with gain  $K$ . The state matrix of this subsystem is  $A-KC$ , and its eigenvalues are  $-3399.5$ ,  $-152.4$ ,  $-14.5$ ,  $-6.6$ ,  $-1.3$  and  $-1.0$ . The overall system hence become 12<sup>th</sup> order. Since all the eigenvalues are in left-half plane hence the system is close-loop stable.

## 5.3 Reduced State Measurement Scheme

To reduce the output measurements, no joint velocities are measured in the scheme discussed below. Since the system is observable (see section 3.5.2.2.) the full state vector is therefore reconstructed by an observer. The joint position measurements

are contaminated with noise. The control scheme incorporates measurement noise modeled by random white noise as shown in Figure 5.2.

### 5.3.1 Linearized model for reduced measurement

For reduced-order measurements, an observer in addition to the controller is required. To employ an LQG or an  $\mathcal{H}_\infty$  controller, first, the model is linearized at standing position; with state-space model  $\mathbf{A}_{6 \times 6}$ ,  $\mathbf{B}_{6 \times 3}$ ,  $\mathbf{C}_{3 \times 6}$  and  $\mathbf{D}_{3 \times 3}$ .

### 5.3.2 LQG robust compensator

Considering the measurement and process noise, the state-space model of plant modifies to

$$\dot{\vec{x}} = \mathbf{A}\vec{x} + \mathbf{B}\vec{u} + \mathbf{\Gamma}\vec{\xi} \quad (5.8)$$

$$\vec{y} = \mathbf{C}\vec{x} + \mathbf{D}\vec{u} + \vec{\varphi}$$

where  $\vec{\xi}$  is process and  $\vec{\varphi}$  is measurement random white noise with covariance  $\mathbf{\Xi}$  and  $\mathbf{\Psi}$  respectively.  $\mathbf{\Gamma}$  is the process noise matrix [67]. The Kalman gain is given by

$$\mathbf{K}_f = \mathbf{P}_f \mathbf{C}^T \mathbf{\Psi}^{-1} \quad (5.9)$$

where  $\mathbf{P}_f$  is found by the solution of algebraic Riccati equation

$$\mathbf{P}_f \mathbf{A}^T + \mathbf{A} \mathbf{P}_f - \mathbf{P}_f \mathbf{C}^T \mathbf{\Psi}^{-1} \mathbf{C} \mathbf{P}_f + \mathbf{\Gamma} \mathbf{\Xi} \mathbf{\Gamma}^T = \mathbf{0} \quad (5.10)$$

The estimated state  $\vec{\hat{x}}$  then replaces original state  $\vec{x}$  such that it is used to generate optimal control signal

$$\vec{u}^* = -\mathbf{K}_c \vec{\hat{x}} \quad (5.11)$$

where  $\mathbf{K}_c$  is the optimal state feedback controller which optimizes the cost

$$J = \lim_{t_f \rightarrow \infty} E \left\{ \int_0^{t_f} [\vec{\hat{x}}^T \vec{u}^T] \begin{bmatrix} \mathbf{Q} & \mathbf{N}_c \\ \mathbf{N}_c^T & \mathbf{R} \end{bmatrix} \begin{bmatrix} \vec{\hat{x}} \\ \vec{u} \end{bmatrix} dt \right\} \quad (5.12)$$

where  $\mathbf{Q} = \mathbf{Q}^T \succcurlyeq \mathbf{0}$  is a positive semidefinite state weighting matrix and  $\mathbf{R} = \mathbf{R}^T > 0$  is a positive definite control input weighting matrix with values  $\mathbf{Q} = \text{diag}(7 \times 10^5, 3 \times 10^6, 4000, 2000, 3000, 6000)$  and  $\mathbf{R} = \text{diag}(0.005, 0.005, 0.005)$ . Block matrix  $\mathbf{N}_c$  is typically a zero matrix. The overall compensator in compact form is given by

$$\mathbf{G}_c(s) = \left[ \begin{array}{c|c} \mathbf{A} - \mathbf{K}_f \mathbf{C} - \mathbf{B} \mathbf{K}_c + \mathbf{K}_f \mathbf{D} \mathbf{K}_c & \mathbf{K}_f \\ \hline \mathbf{K}_c & \mathbf{0} \end{array} \right] \quad (5.13)$$

Control input  $\vec{u}$  comprises passive torques and is used to run three actuators at the joints. LQG compensator is employed as shown in Figure 5.2.

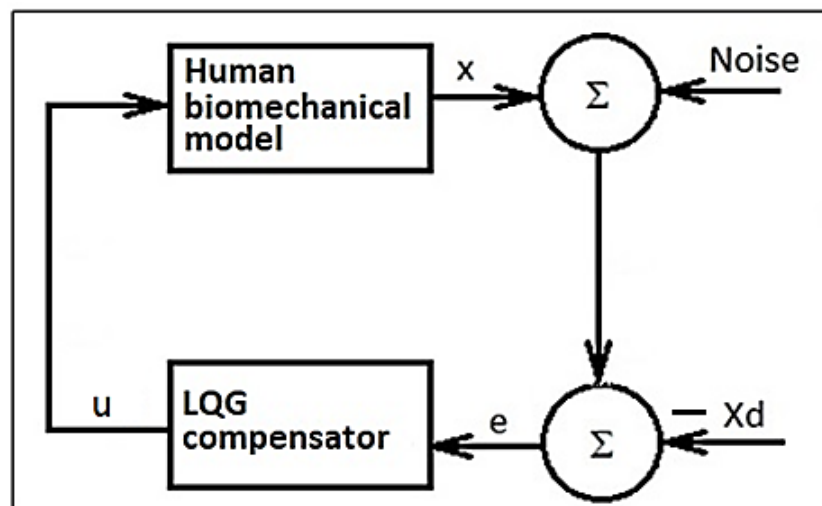


Figure 5.2. The Human STS motion control mechanism is based on the LQG scheme.

### 5.3.2.1 Close loop stability analysis

The Kalman observer provides estimates of whole state vector. The state matrix of this close loop system is given by  $(A - K_f C)$  with eigenvalues -21.2943, -21.2142, -2.3190, -5.4715, -3.3359 and -4.6708. The state matrix of close-loop system is given by  $(A - BK_c)$ . The eigenvalues of this system are -902.3, -211.9, -29.3, -0.8, -8.8 and -8.8. Since all eigenvalues are in left half plane, close loop system is stable.

### 5.3.3 $\mathcal{H}_\infty$ controller

The structure of the  $\mathcal{H}_\infty$  control problem [62] is given by

$$\dot{\vec{x}}(t) = A\vec{x}(t) + B_w\vec{w}(t) + B\vec{u}(t) \quad (5.14)$$

where  $B_w$  is the external disturbance covariance matrix. Process noise  $\vec{v}(t)$  and measurement noise  $\vec{z}(t)$  comprise  $\vec{w}(t)$ , which are assumed stationary white noise. The regulated and measured outputs are given by

$$\vec{y}(t) = C_y\vec{x}(t) + D_{yw}\vec{w}(t) + D_{yu}\vec{u}(t) \quad (5.15)$$

$$\vec{m}(t) = C_m\vec{x}(t) + D_{mw}\vec{w}(t) + D_{mu}\vec{u}(t) \quad (5.16)$$

respectively, where  $C_y$  is the weighting matrix for quantities to be optimized and  $C_m$  is the measurement matrix.  $D_{yw}$  and  $D_{mu}$  are zero matrices.  $D_{mw}$  and  $D_{yu}$  are the weights for process noise  $\vec{v}$  and input  $\vec{u}$  respectively. Steady-state solution of the problem is found by solving algebraic Riccati equations if a positive semi-definite solution exists for the linear model

$$XA + A^T X - X(BB^T - \gamma^{-2}B_w B_w^T)X + C_y^T C_y = 0 \quad (5.17)$$

$$YA + A^T Y - Y(C_m^T C_m - \gamma^{-2} C_y^T C_y)Y + B_w B_w^T = 0 \quad (5.18)$$

where  $X$  and  $Y$  are the solutions of Riccati equations and  $\gamma$  is the minimum bound on input disturbance and estimation error. The minimum bound for the linear model is determined by spectral radii of the above equations and is given by

$$\lambda_{max}(XY) = \rho(XY) < \gamma^2 \quad (5.19)$$

Using solutions  $X$  and  $Y$  to design an optimal controller, first state matrix  $A_c$  of controller  $K_\infty$  is determined:

$$A_c = A + \gamma^{-2} B_w B_w^T X - B B^T X - [I - \gamma^{-2} Y X]^{-1} Y C_m^T C_m \quad (5.20)$$

$$K_\infty = \begin{bmatrix} A_c & [I - \gamma^{-2} Y X]^{-1} Y C_m^T \\ -B^T X & 0 \end{bmatrix} \quad (5.21)$$

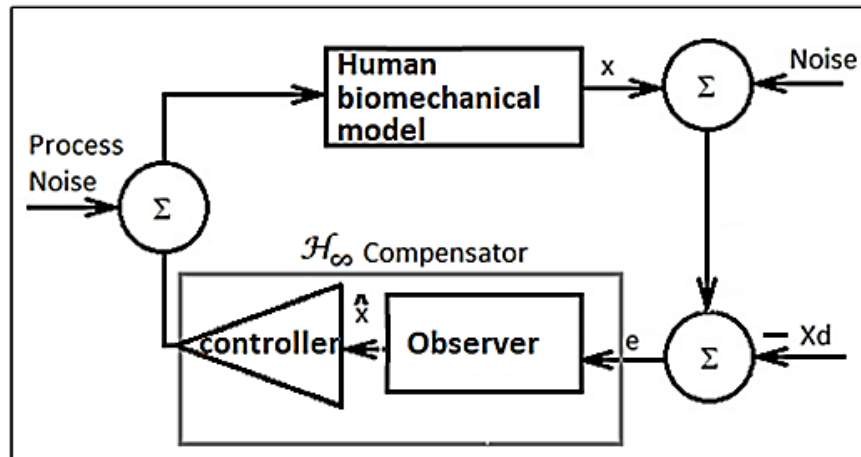


Figure 5.3. Human STS motion control mechanism based on  $\mathcal{H}_\infty$  scheme. The compensator is determined in (5.21)



### 5.3.3.1 Close loop stability analysis

For  $K_\infty$  robust controller employed as compensator, with state-space representation  $K_\infty = [A_c, B_c, C_c, D_c]$ . The state matrix of close-loop system is given by  $A + B C_c$ . The eigenvalues of this system are -1836.2, -291.2, -18.2, -4.6, -2.6 and -3.2. The observer state matrix is given by  $(A - B_c C_m)$ , whose eigenvalues are -21.4480, -6.5331  $\pm$  4.8153i, -5.0426, -0.7220 and -1.1994. Since all eigenvalues are in left half plane, close loop system is stable.

## 5.4 Trajectory Generation

Joint angle trajectories from motion capture data of one subject are shown in Figure 5.4.

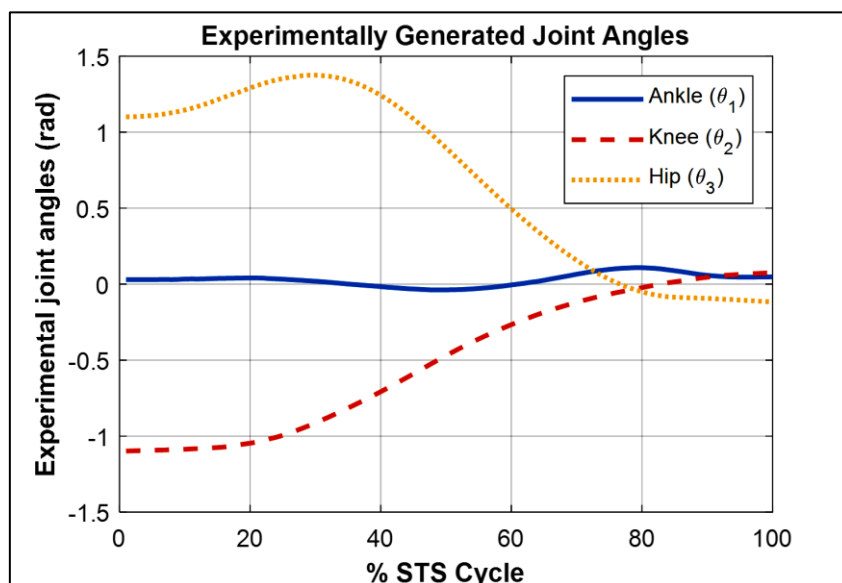


Figure 5.4. Experimental joint angle trajectories measured from motion capture

Similar joint angle profiles as shown in Figure 5.5 are generated analytically using scheme from [61]. In our scheme, joint angles are defined in the body frame using modifications to the basic technique presented in [68]. No velocity references have been provided for tracking. Trajectories in Figure 5.5 are the desired angle profiles at ankle, knee and hip.

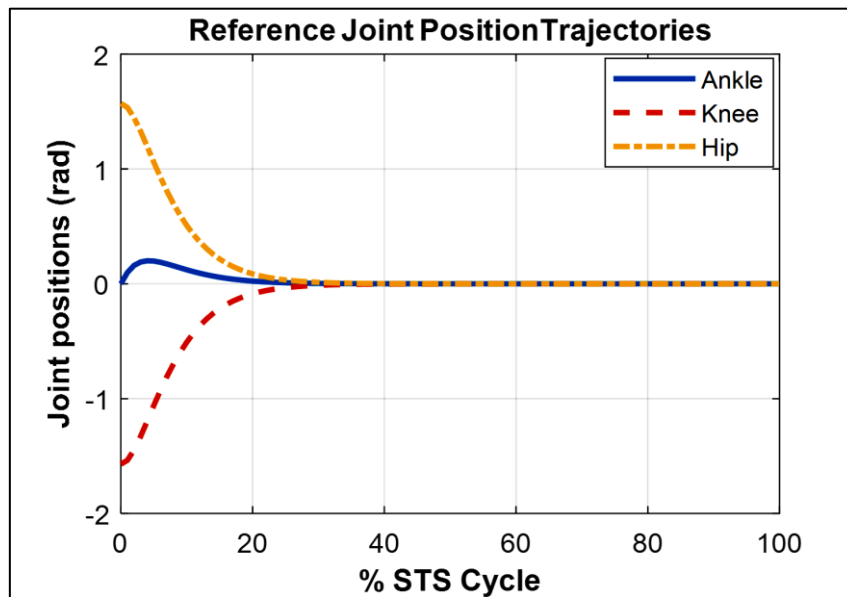


Figure 5.5. Analytically generated reference joint angle trajectories to be tracked.

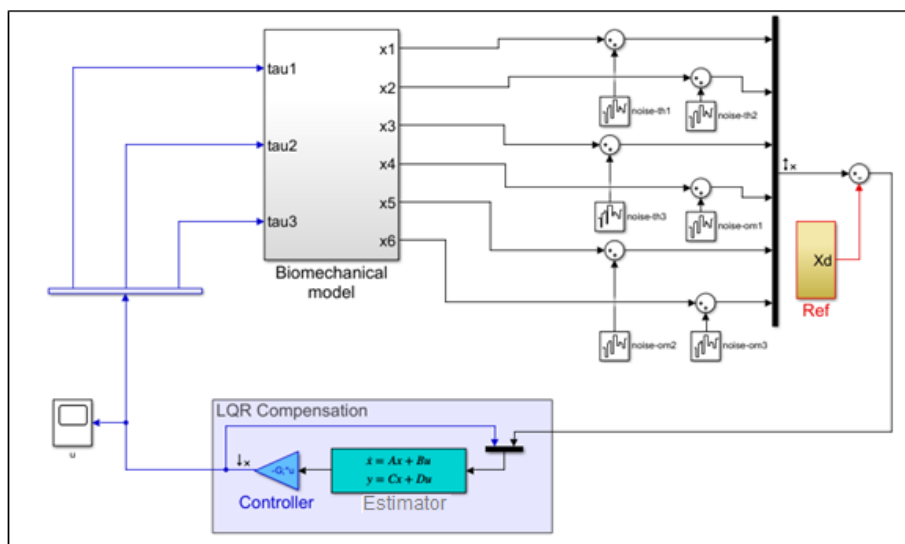


Figure 5.6. STS motion synthesis framework in SimMechanics. The CNS modeled as LQR compensator is shown in the blue rectangle

## 5.5 STS Motion Synthesis in SimMechanics

### 5.5.1 LQR scheme

The human biomechanical model shown in Figure 3.2 is used to generate physiologically relevant STS motion using the LQR control scheme as shown in Figure

5.6. LQR is implemented using the scheme shown in Figure 5.1. The ‘Ref’ or Reference block in Figure 5.6 comprises a mechanism to analytically generate joint position reference trajectories shown in Figure 5.5. Measurement noise and neuro-delays are also included in the SimMechanics modeling framework.

### 5.5.1.1 LQR scheme with noise and delay

The following are the plots of joint and torque trajectories obtained from STS motion synthesized by LQR compensation. Figure 5.7 shows joint angle estimates made by the LQE. It must be noted that since the scheme is based on full-state management, estimation is meant only for recovering noise contaminated states in pure form. The actual head positions measurements are also shown in this Figure. To depict the difference between reference and actual joint positions, the error between the two is also plotted. It can be seen that estimates of joint angles start from zero initial condition and for this reason error is large initially. But later the estimator catches up the correct value of joint angles and error is reduced.

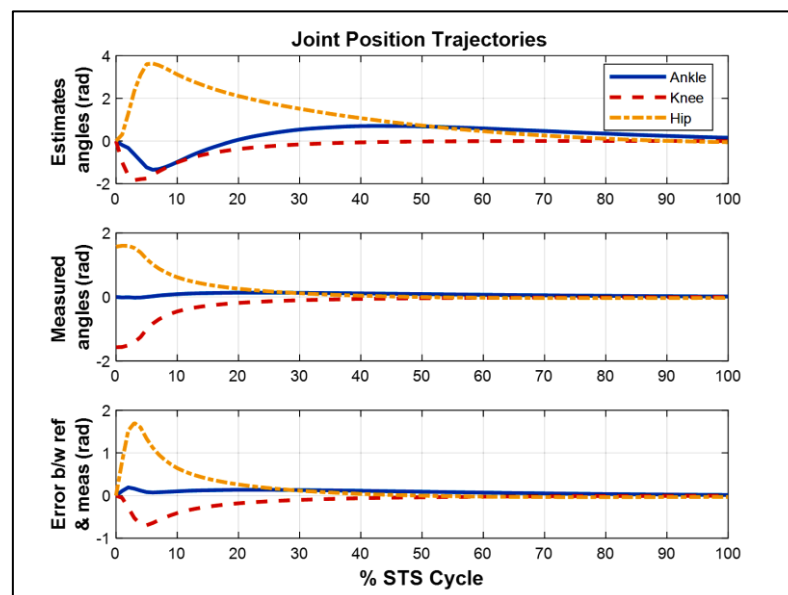


Figure 5.7. Joint angular position estimates by LQE observer (top), measured joint positions (center) and error between the reference and actual values (bottom)

Figure 5.8 shows similar plots for joint velocities. The estimates of joint velocities are very large to help reduce position error as soon as possible. Actual joint

velocities are relatively low since the error between the reference and measured joint velocities are also smaller.

Figure 5.9 shows joint torque commands generated by the LQR compensation scheme. Since large gain values are used to track the reference well, a very large knee joint torque spike can be seen. This spike, however, subsides during first 5% of STS cycle due to control action by LQR scheme. The three torque commands converge to zero showing the STS motion termination.

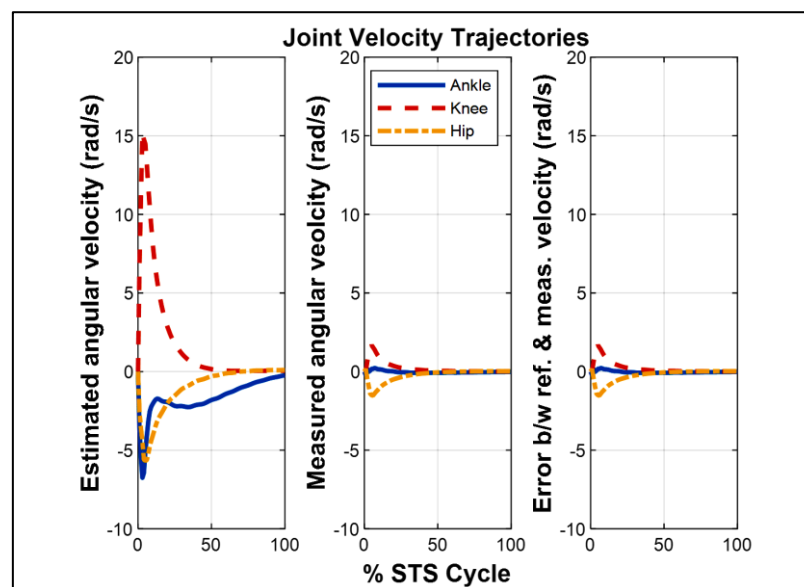


Figure 5.8. Joint angular velocity estimates by LQR observer (left), measured joint positions (center) and error between the reference and actual values (right)

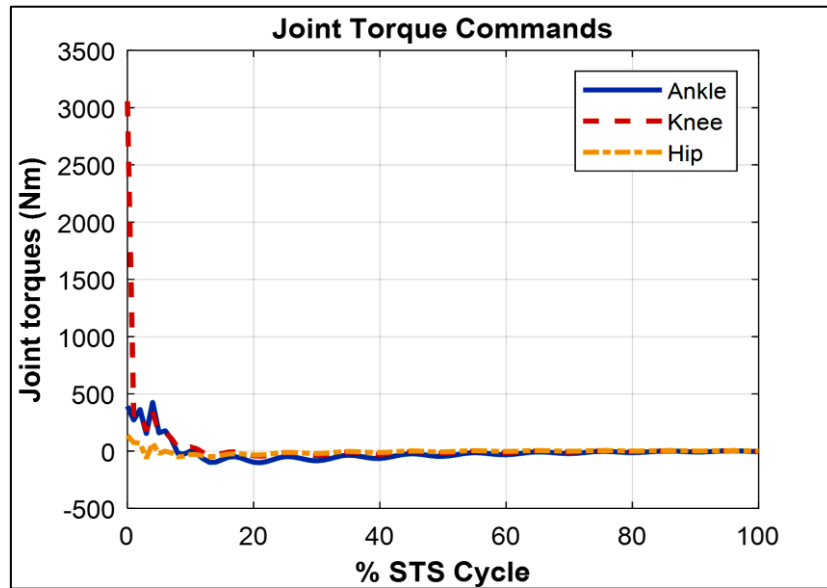


Figure 5.9. Torque inputs to joint generated by LQR controller

### 5.5.1.2 LQR scheme without noise and delay

In order to establish and quantify the robustness of LQR scheme, the same LQR compensator is used with human biomechanical model without measurement noise and neural delays. Maximum torques generated by this scheme are 2500 Nm, 611.8 Nm and 87.6 Nm for ankle, knee and hip joints respectively.

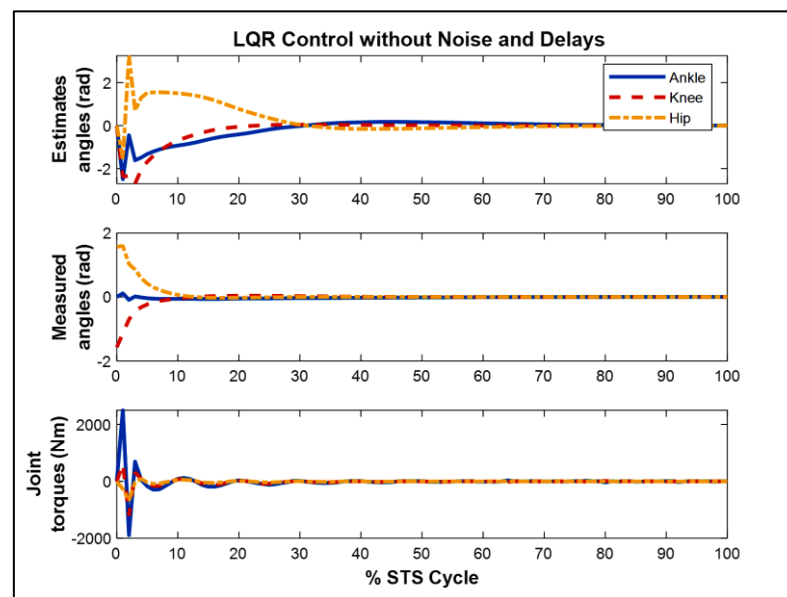


Figure 5.10. Control action of LQR without feedback delays and measurement noise

### 5.5.2 LQG scheme

Figure 5.11 shows the LQG control scheme of Figure 5.2 implemented in SimMechanics environment. Human biomechanical model is shown as ‘Biomechanical model’ block.

Figure 5.12 shows estimate of joint angles made by the LQG observer. The joint position estimates start from which is the initial condition of observer. Joint measurements show a larger angular rotation since the joint motion takes place in addition to its initial conditions. The error between the reference and measured joint positions reduces to zero showing STS motion is finally accomplished.

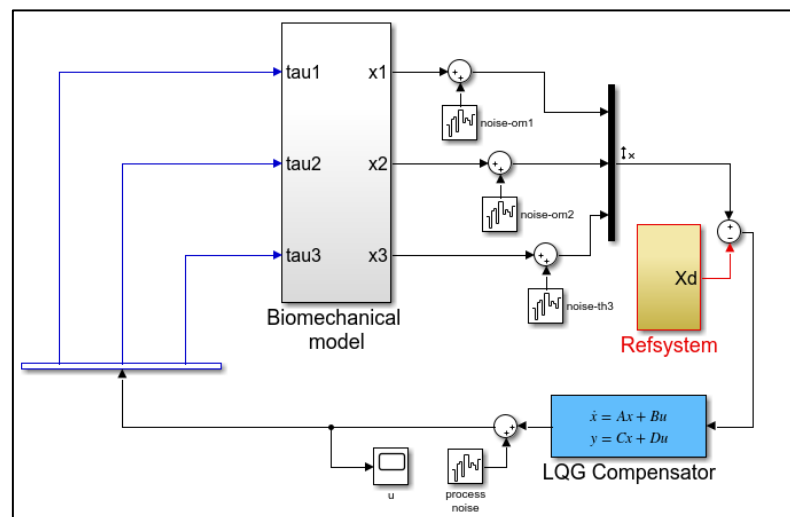


Figure 5.11. STS motion synthesis framework in SimMechanics. The CNS modeled as LQG compensator is shown in the blue rectangle

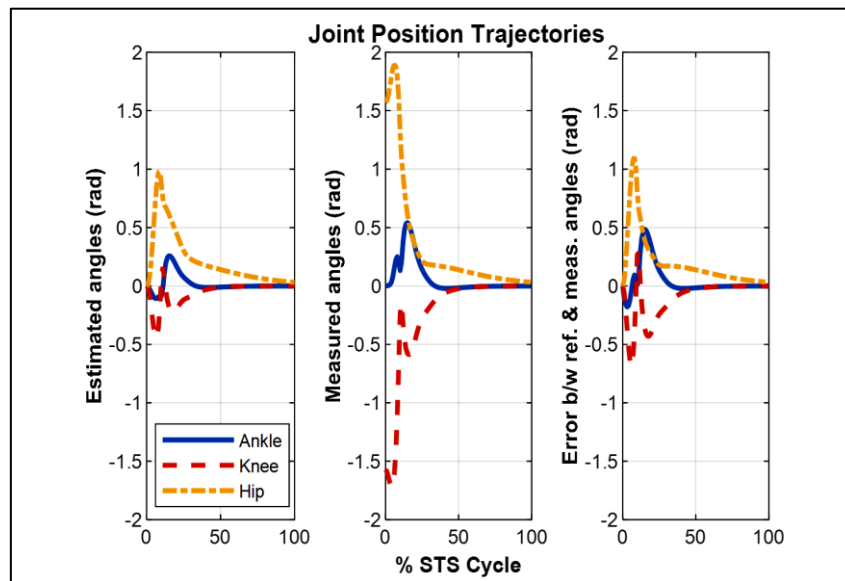


Figure 5.12. Joint angular position estimated (left), measurements (right) and error between the reference and actual values using LQG / Kalman observer scheme

Figure 5.13 shows estimate of joint velocities made by the LQG observer. It can be seen that the estimates are not smooth showing large fluctuating values. Estimates however converge to the equilibrium value of zero more quickly than done by LQR observer. It should be noted that since no velocity measurements are made in this scheme so only estimate plots are given in Figure 5.13.

Figure 5.14 shows joint torque commands generated by the LQG controller. The ankle torque is larger than knee and hip, as expected in real humans. Also, the torque values, although larger than actual joint torque values, but are much less than torques generated by the LQG scheme. Also, the torques converge smoothly and quickly as compared to LQG generated torques.

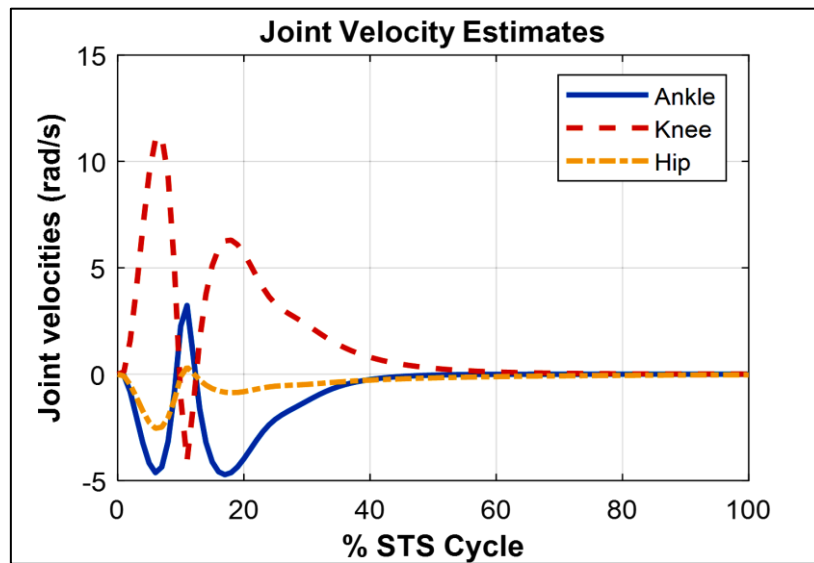


Figure 5.13. Joint velocity estimates using LQG / Kalman observer

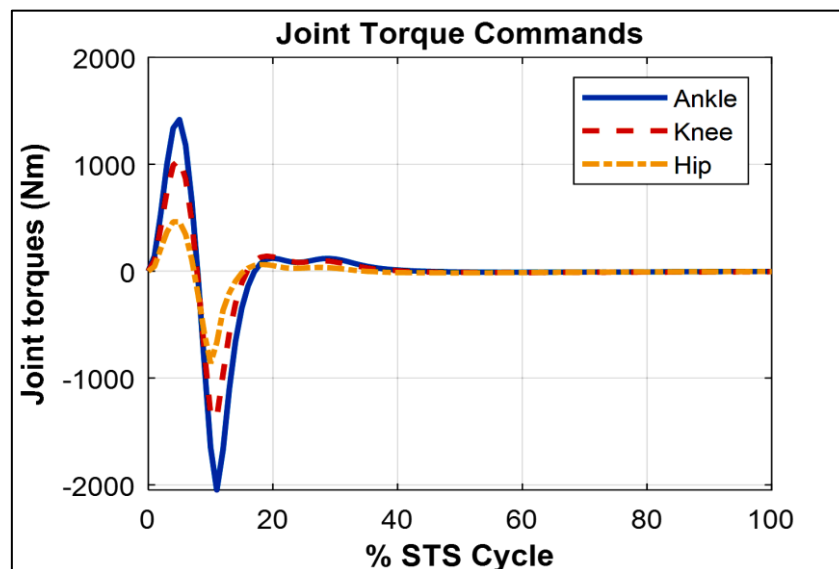


Figure 5.14. Torque inputs to joint actuators using LQG control

### 5.5.3 $\mathcal{H}_\infty$ scheme

Figure 5.15 shows the SimMechanics implementation of the control scheme shown in Figure 5.3. The measurement and process noise have also been modeled and the  $\mathcal{H}_\infty$  type compensator is used to estimate unmeasured velocities, reconstruct noise-contaminated measurements and generate joint actuation torque commands. This



system makes only joint position measurements and velocities of joints are not measured. The velocities are estimated by the  $\mathcal{H}_\infty$  observer.

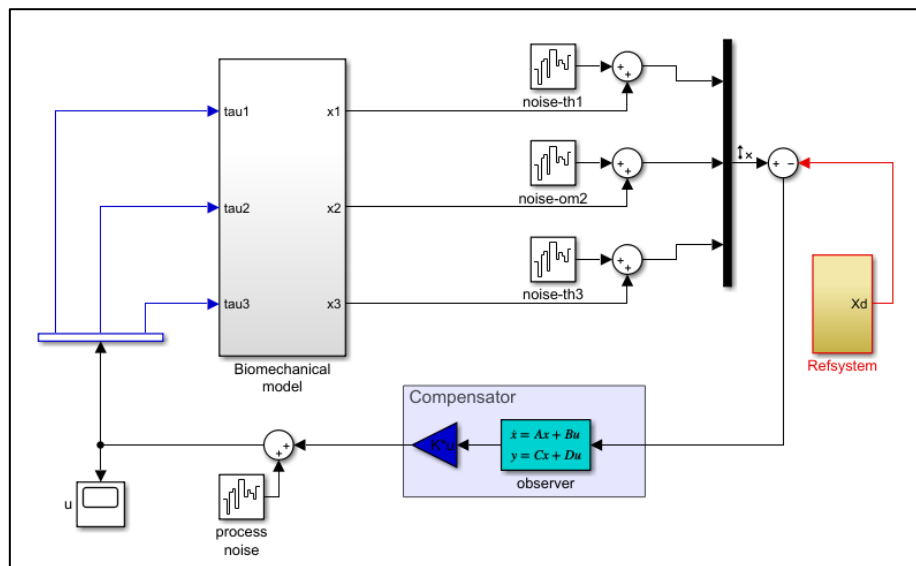


Figure 5.15. STS motion synthesis framework in SimMechanics. The CNS modeled as  $\mathcal{H}_\infty$  compensator is shown in the blue rectangle

Figure 5.16 shows joint motion measurements by  $\mathcal{H}_\infty$  compensation. The estimated joint positions start from zero initial positions, resulting in larger angular position error between the reference and measured angular trajectories. The joints however attain standing position more smoothly than attained by LQR and LQG control schemes.

Figure 5.17 shows joint velocity estimates by  $\mathcal{H}_\infty$  observer. The estimates made by this scheme are smoother than those made by the LQG observer.

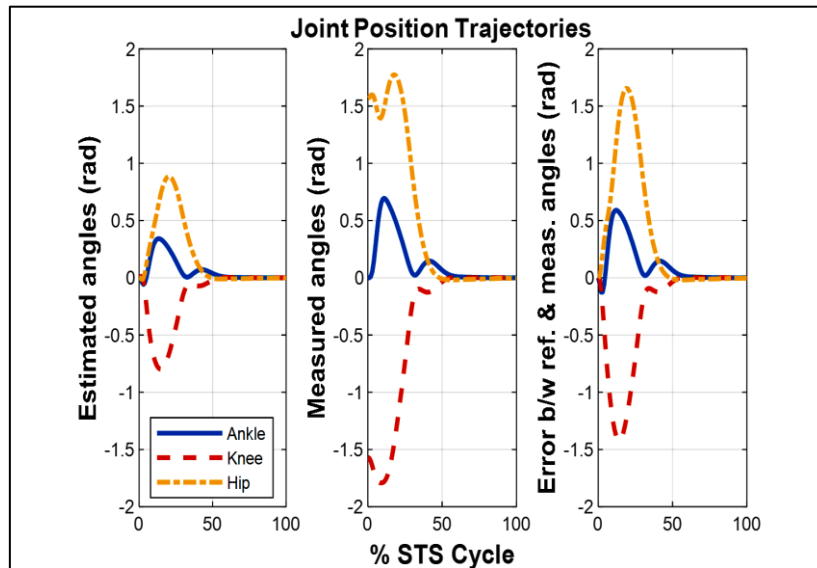


Figure 5.16. Joint angular position estimates (left), measurements (center) and error between the reference and actual values using  $\mathcal{H}_\infty$  control

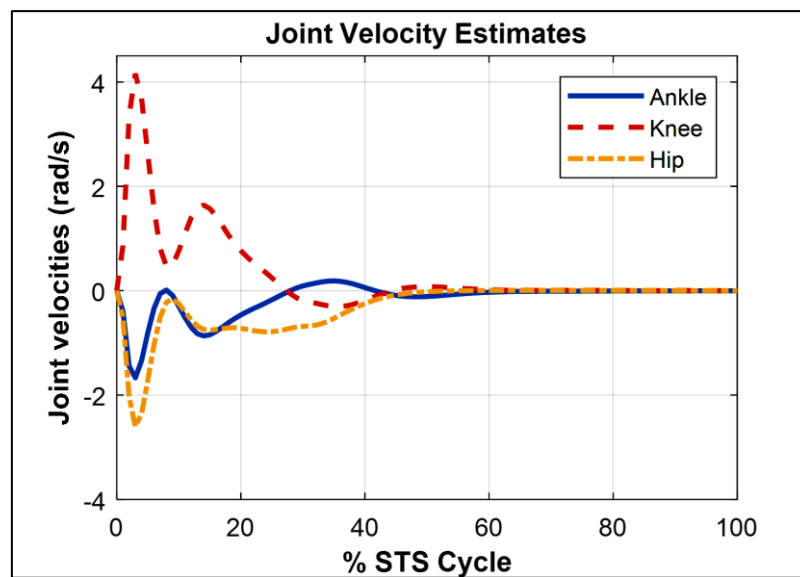


Figure 5.17. Joint velocity estimates using  $\mathcal{H}_\infty$

Figure 5.18 shows joint torque commands generated by the  $\mathcal{H}_\infty$  controller. Peak values of torques are less than those generated by LQR and LQG schemes and the trajectories are smoother as well that result in smooth and realistic STS motion.

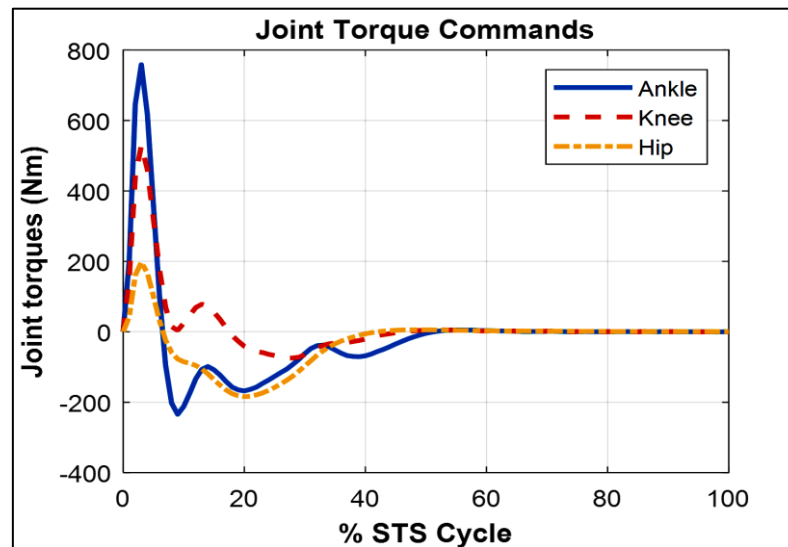


Figure 5.18. Torque inputs to joint actuators using  $\mathcal{H}_\infty$  control

## 5.6 Discussion

### 5.6.1 LQR compensation

STS motion using a 2D four-segment non-linear model developed in SimMechanics with full order observer LQR design has been synthesized as shown in Figure 5.1. All the six measurements were subject to sensor noise as well as the neuro-feedback time delay. The system tracks reference trajectories to carryout natural and physiologically relevant STS motion. Figure 5.7 (left) depicts joint position estimates by the LQR observer. The estimates are somewhat exaggerated which is the natural consequence of a large gain control strategy. The measured joint positions in Figure 5.7 (center) show that joints produce smooth STS motion and all joints settle at the standing position at around 50% of the STS cycle. A comparison of measurements with reference trajectories is depicted in Figure 5.7 (right). Initially, the error is large but very quickly the controller generates appropriate torque commands to reduce this error.

Joint velocity estimates in Figure 5.8 (left) show similar behavior; the observer estimates are again very large but as the measured velocities as shown in Figure 5.8 (center) start converging to zero value estimates too reduce to normal and error between measured and desired trajectories reduce quickly as shown in Figure 5.8 (right).

Torque commands to the three joints are shown in Figure 5.9. The sudden spike is the outcome of a simple technique for tuning the gains. The high torque values are momentary and quickly settle to the torque values of 450, 400 and 200 Nm for ankle, knee and hip joints. These values are comparable to the joint torques achieved in similar studies [40] where peak values of ankle, knee and hip joint torques were 430, 320 and 55 Nm using a hybrid LQR compensator.

The impact of joint position measurement noise and neural delays is evident from simulations shown in Figure 5.7, Figure 5.9 and Figure 5.10. It can be observed that when STS motion is synthesized in the absence of noise and delays torques generated by this scheme are lesser and smoother. This shows the lesser effort has been required by compensator to control this scheme.

### 5.6.2 LQG compensation

Our second control scheme is LQG compensation which utilizes reduced ordered measurements. Since the controller employed is again full state, we used an observer to estimate the unmeasured states. The joint positions estimate in Figure 5.12 (left) closely match the reference trajectories as shown in Figure 5.4. The measured joint positions in Figure 5.12 (center) show a large joint motion initially that quickly settles to smooth motion. Hip joint angles, however, take a longer time to converge to the equilibrium position of standing as shown in Figure 5.12 (right). Figure 5.13 shows only joint velocity estimates; since no joint velocity measurements are made. The initial conditions of zero velocity result in larger and jerky velocity estimates, but at around 50% of the STS cycle, the estimates converge to the equilibrium state of zero rad/s. The joint torques of this scheme are still high as shown in Figure 5.14. These torques are higher than the torques found in similar studies like [63], where the fuzzy-LQG controller was used and torques for ankle, knee and hip were 350, 600 and 150 Nm respectively. The torques in our scheme however show an improvement to the LQR scheme presented above, both in magnitude and smoothness. In this way, LQG provides much better and close to natural control as compared to LQR compensator, despite reduced-order measurements.

### 5.6.3 $\mathcal{H}_\infty$ compensation

The joint angular position estimates made by this scheme are shown in Figure 5.16 (left). The measurements of joint positions, shown in Figure 5.16 (center) are smooth and show a settlement to equilibrium more smoothly than LQR and LQG schemes. The error between the reference and measured values is also small as shown in Figure 5.16 (right) and is mainly attributed to the 0 value of the initial condition used for the controller. No measurements of joint velocities are made in this scheme. The missing measurements are reconstructed through estimation as shown in Figure 5.17.

Figure 5.18 shows further improvement in minimizing joint torques using. The torques generated at the joints show an improvement when compared with similar studies [63], where the fuzzy  $\mathcal{H}_\infty$  scheme resulted in joint torques as large as 100, 700 and 350 Nm compared to 750, 500 and 250 Nm for ankle, knee and hip joints respectively.

## 5.7 Summary

In this chapter, we presented a motion synthesis and control scheme that utilizes two kinematic variables i.e., joint positions and velocities as feedback elements to control STS motion. The CNS was modeled as different robust controllers. Moreover, the observer scheme is used to simulate the capability of CNS to recover and estimate noise-contaminated or missing measurements and giving a robust control against these anomalies. Next, the task level control of STS motion, using head position as the reference is presented in chapter 6.

## CHAPTER 6

### NEURO-FUZZY CONTROL OF STS MOTION USING HEAD POSITION TRACKING

Based on the clinical evidence that head position, measured by the multisensory system contributes to motion control, this study suggests a biomechanical human-CNS modeling and control framework for Sit-to-Stand (STS) motion synthesis. Motivated by the evidence for a task-oriented encoding of motion by the CNS, we propose a framework to synthesize and control STS motion using only head position trajectory in the high-level-task-control environment. Initially, the problem was posed in linear robust control setting, but we did not achieve any satisfactory results and all the controllers discussed in Chapter 5 failed to control STS motion using head position trajectory as a control variable/reference to be tracked. This chapter presents how the non-linear control scheme, based on neuro-fuzzy controller did this task very well. First, we design a generalized analytical framework comprising a human biomechanical model and an ANFIS to emulate CNS. We introduce Task-Space Training (TST) algorithm for ANFIS training. The ANFIS controller is optimized in the number of Membership Functions (MFs) and training cycles or epochs to avoid over-fitting. Next, we develop custom human-models based on anthropometric data of real subjects. Using the Weighting Coefficient method, we estimate the body segment parameter. The subject specific BSP values are used: (a) to scale human biomechanical model for real subjects, and (b) in TST to train custom ANFIS controllers. To validate our modeling and control scheme we perform extensive motion capture experiments of STS transfer by real subjects. We compare the synthesized and experimental motions using kinematic analyses. Our analytical modeling-control scheme proves to be scalable to real subjects' BSP and the TST algorithm provides a means to customize ANFIS efficiently. The customized ANFIS gives 68% to 98% improvement over general ANFIS. This study has a broader scope in the fields of rehabilitation, humanoid robotics and virtual characters' motion planning based on high-level-task-control schemes.

## 6.1 Methodology

### 6.1.1 Workflow

We formulate a motion synthesis scheme which generates joint angle positions that correspond to head position trajectory during STS transfer. The motion is controlled by a neuro-fuzzy controller, shown in Figure 6.1 as ‘ANFIS’. The reference input to the controller is head position trajectory and ANFIS infers joint angle trajectories. The inferred joint trajectories are used to actuate joints of the biomechanical model in position driven motion synthesis framework.

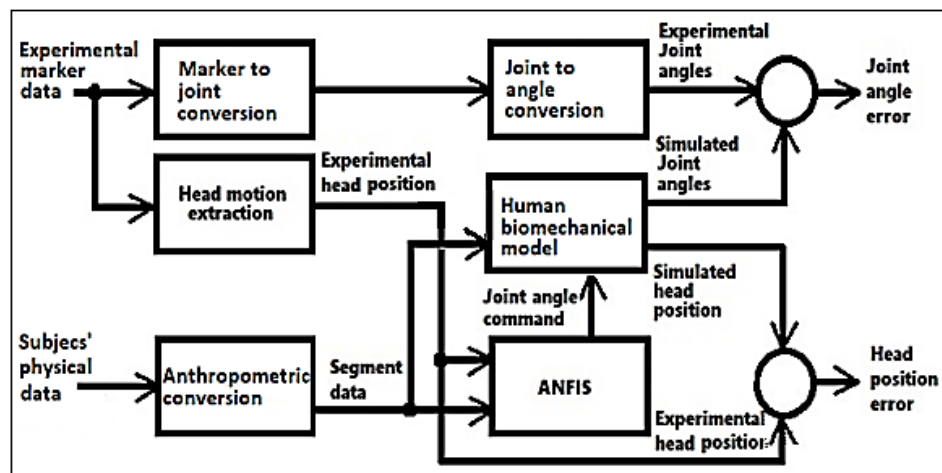


Figure 6.1. The workflow of experimental and analytical techniques

### 6.1.2 Analytical modeling

Initially, we use our general human biomechanical model based on anatomical data from [43]. Using the TST algorithm a generalized ANFIS is trained for estimation of appropriate joint angles and control of physiologically relevant STS motion. The motion control is carried out by tracking head position trajectory only, without using any other measurements.

### 6.1.3 Modeling validation on experimental data

Later we use experimental data of STS transfer from real subjects. Each subjects' physical parameter (height and mass) data are converted into the BSP values using weighting coefficient anthropometry. Segment values are then used to scale the human biomechanical model as well as for the subject-specific customization of the ANFIS controller.

STS motion of all subjects is simulated using 1) the general ANFIS controller and 2) the custom ANFIS controller. The two sets of simulations are compared with experimental results.

For a detailed description of this work refer to [15].

## 6.2 Analytical Modeling Framework

### 6.2.1 The general human biomechanical model

We define our human biomechanical model in Cartesian space and for the determination of each segments' position, we attach local reference frames with each segment. We refer shank, thigh and HAT as links  $l_1$ ,  $l_2$  and  $l_3$  respectively.  $(X, Y)$  is head position and  $(x, y)$  is the hip position in Cartesian coordinates.  $\emptyset$  is the head orientation in the World frame  $\{W\}$ . Based on forward and inverse kinematic analyses of the model, a dataset of joint angles corresponding to a range of head position trajectories are generated. Head position, in turn, is a function of segment lengths of the human biomechanical model. This dataset is used to train, validate and test the ANFIS controllers.

### 6.2.2 Forward kinematics (FK) analysis

Kinematics is the science of motion without referring to the applied force, considering only variables of displacement and its derivatives [69]. Forward kinematics



maps joint space ( $\theta_n$ ) into Cartesian space ( $x, y, \phi$ ), where  $\phi$  is the orientation of a point in the Cartesian plane with respect to the World reference  $\{W\}$ .

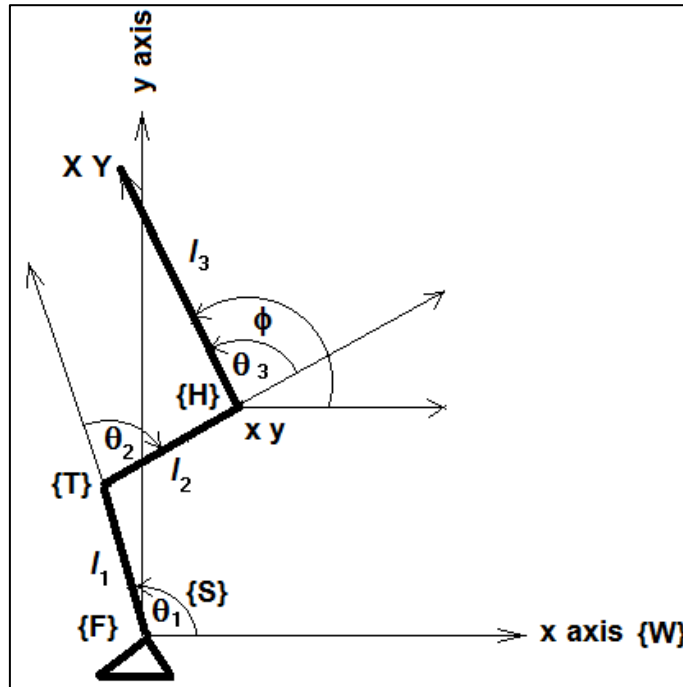


Figure 6.2. Three DoF biomechanical human biomechanical model is defined in the body frame.  $\{S\}$ ,  $\{T\}$  and  $\{H\}$  represent shank, thigh and HAT frames for segments  $l_1$ ,  $l_2$  and  $l_3$ .

To determine the head position ( $X, Y$ ), the set of kinematic equations is given as:

$$X = l_1 c_1 + l_2 c_{12} + l_3 c_{123} \quad (6.1)$$

$$Y = l_1 s_1 + l_2 s_{12} + l_3 s_{123} \quad (6.2)$$

where  $c_1$  stands for  $\cos(\theta_1)$ ,  $c_{12}$  for  $\cos(\theta_1 + \theta_2)$ ,  $s_1$  for  $\sin(\theta_1)$  and so on. Also

$$\phi = \theta_1 + \theta_2 + \theta_3 \quad (6.3)$$

where  $\phi$  is the orientation of HAT (or head) with respect to the x-axis. The generalized coordinate is a compact notation  $\vec{p} = [X, Y, \phi]$ .

### 6.2.3 Inverse kinematics (IK) analysis

To solve the IK problem, first,  $p$  is used to find a unique hip position  $(x, y)$  to reduce the problem at hand from four to three-link. To find hip position  $(x, y)$ , hip joint angle constraint, i.e.,  $0 \leq \theta_3 \leq \pi$  is imposed. The solution then simplifies:

$$x = X + l_3 c(\pi - \phi) \quad (6.4)$$

$$y = Y - l_3 s(\pi - \phi) \quad (6.5)$$

Using algebraic manipulation, the joint angles inferred from head position are:

$$\theta_2 = \text{atan2}(s_2, c_2) \quad (6.6)$$

$$\theta_1 = \text{atan2}(y, x) - \text{atan2}(l_2 s_2, (l_1 + l_2 c_2)) \quad (6.7)$$

$$\theta_1 + \theta_2 + \theta_3 = \text{atan2}(s\phi, c\phi) = \phi \quad (6.8)$$

where *atan2* is the MATLAB command for four-quadrant tan-1 with arguments representing vertical and horizontal components of position vector respectively [69].

### 6.2.4 Kinematic constraints of the human biomechanical model

To determine an accurate range of joint angle trajectories during STS is difficult owing to different experimental conditions, joint motion profiles (angle constraints) and link lengths (link-length constraints) [70]. This variety is also evident from our experimental findings in Figure 4.7, even though the number of subjects is very small. The TST algorithm works efficiently for any range of angular constraints. Segment lengths also impose a constraint on the determination of the head position subspace.

### 6.3 Determination of Head Position Subspace

Head position during STS is a subspace of head positions during all possible human body movements with stationary feet. To determine the reachable positions of the head during STS, joint and link length constraints are imposed on the human biomechanical model.

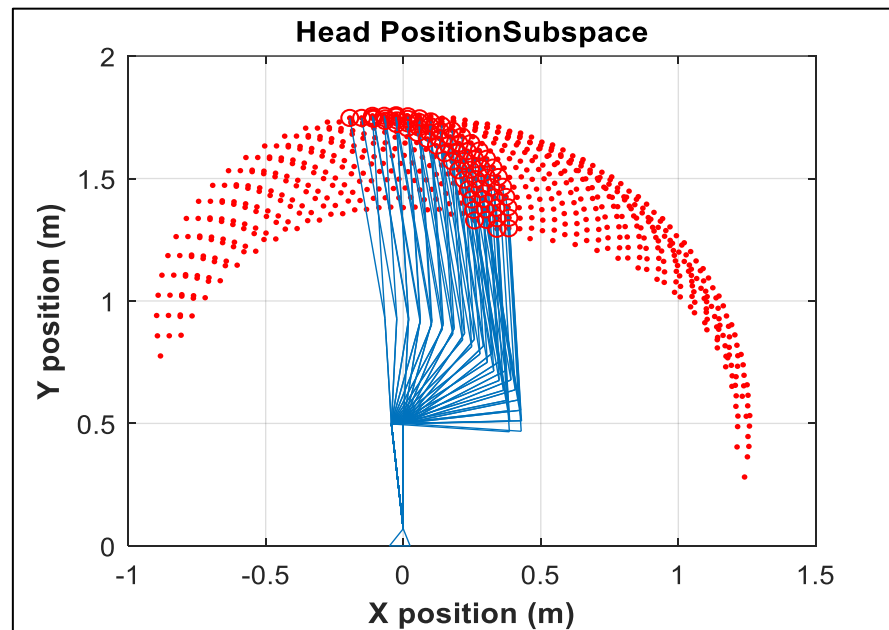


Figure 6.3. Head position subspaces with joint-angle and link-length constraints; general (dots) and during STS (circles)

Besides, we impose an additional constraint of head orientation,  $\phi$ . A dataset is generated which determines all possible head positions for all possible combinations of joint angles, head orientations and segment lengths. Figure 6.3 shows the two subspaces.

### 6.4 Joint Angle Estimation Scheme

Our scheme uses head position ( $X$ ,  $Y$ ) as a reference input to estimate joint angles ( $\theta_1$   $\theta_2$   $\theta_3$ ) using three ANFIS, which we will refer to as single ANFIS. Angle positions are commands to the human biomechanical model to rotate the three joints in the sagittal plane. The combination of three joint movements thus provides the

required position of the head in Cartesian coordinates. The complete scheme shown in Figure 6.4 gives an identity mapping.

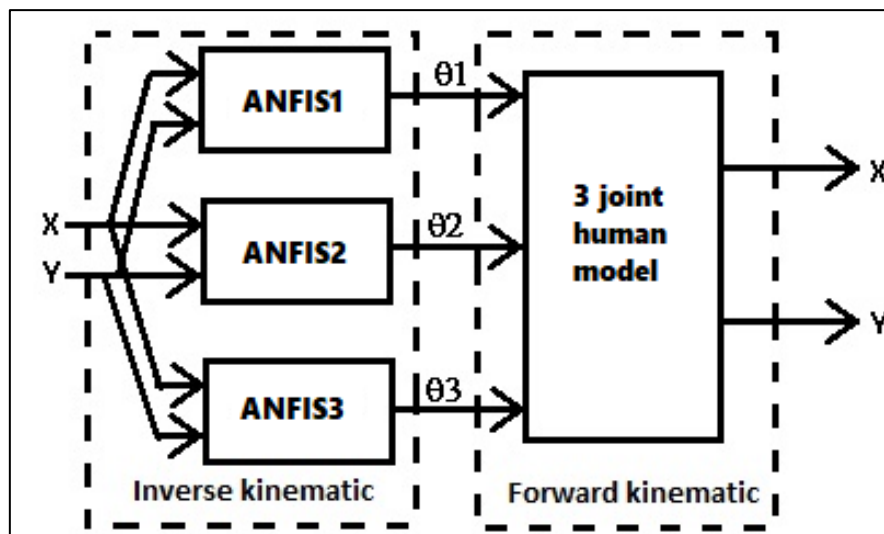


Figure 6.4. Three ANFIS controllers generate ankle, knee and hip joint angle commands

### 6.4.1 Task-space training (TST) algorithm

We propose an algorithm to generate training and validation datasets based on the task space of STS transfer:

- 1) Determine the constraints,  $l_n$ ,  $\theta_n$  and  $\phi$ , for the individual human biomechanical model,  $n=1,2,3$ .
- 2) Determine head position subspace and construct  $n$  training datasets  $[X Y \theta_n]_n$  using FK equations (6.1) to (6.3).
- 3) Determine a fictitious head subspace  $[X_f, Y_f]$  within the boundaries of the head subspace.
- 4) Using IK equations (6.4) to (6.8), predict all required joint angles;  $\theta_{np}$ . Construct test datasets  $[X_f, Y_f, \theta_{np}]_n$ .

## 6.5 Development of the ANFIS Controllers

For the  $n$  DoF system, we develop a set of  $n$  ANFIS controllers to control  $n$  joints individually. The scheme is given in Figure 6.5.

### 6.5.1 Structure of ANFIS

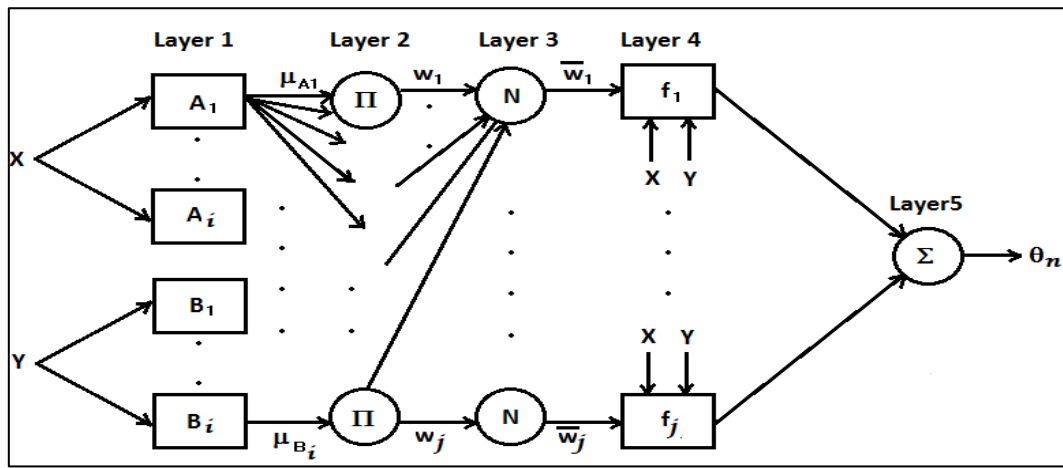


Figure 6.5. Schematic of ANFIS<sub>n</sub>: 2 inputs X, Y, 2k-input MFs, j-output MFs and one output  $\theta_n$

We apply head position X, Y data at inputs for fuzzification. Layer 1 comprises 2k membership functions; k for each inputs X and Y. Generalized bell-shape curves of MFs for input X are nonlinear functions given in (6.9).

$$\mu_{A_i}(x) = \frac{1}{1 + \left[ \left( \frac{x - c_i}{a_i} \right)^2 \right]^{b_i}}, \quad i = 1, \dots, k \quad (6.9)$$

MFs for input Y is given by

$$\mu_{B_{i-k}}(y) = \frac{1}{1 + \left[ \left( \frac{y - c_i}{a_i} \right)^2 \right]^{b_i}}, \quad i = k + 1, \dots, 2k \quad (6.10)$$

where  $\{a_i, b_i, c_i\}$  are premise parameters that define the shape of  $2k$  bell functions. Initial values of premise parameters are arbitrary such that MFs are distributed uniformly over all input space.

Specifically, for STS problem the MFs are referred to in terms of linguistic variables, i.e., SX (small X), SMX (small medium X), MX (medium X), MLX (medium large X) and LX (large X) as shown in Figure 6.6. Similarly, other set of MFs is SY (small Y), SMY (small medium Y), MY (medium Y), MLY (medium large Y) and LY (large Y).

The format of  $j$  linguistic rules is as follows:

1. If  $\{X(m) \text{ is SX}\}$  and  $\{Y(m) \text{ is SY}\}$  then  $\{\theta_n \text{ is } \theta_n \text{ mf1}(n)\}$
2. If  $\{X(m) \text{ is SX}\}$  and  $\{Y(m) \text{ is SMY}\}$  then  $\{\theta_n \text{ is } \theta_n \text{ mf2}(n)\}$
- .
- .
- j. If  $\{X(m) \text{ is LX}\}$  and  $\{Y(m) \text{ is LY}\}$  then  $\{\theta_n \text{ is } \theta_n \text{ mfj}(n)\}$

where consequent part refers to the output space governed by the rule  $j$ .

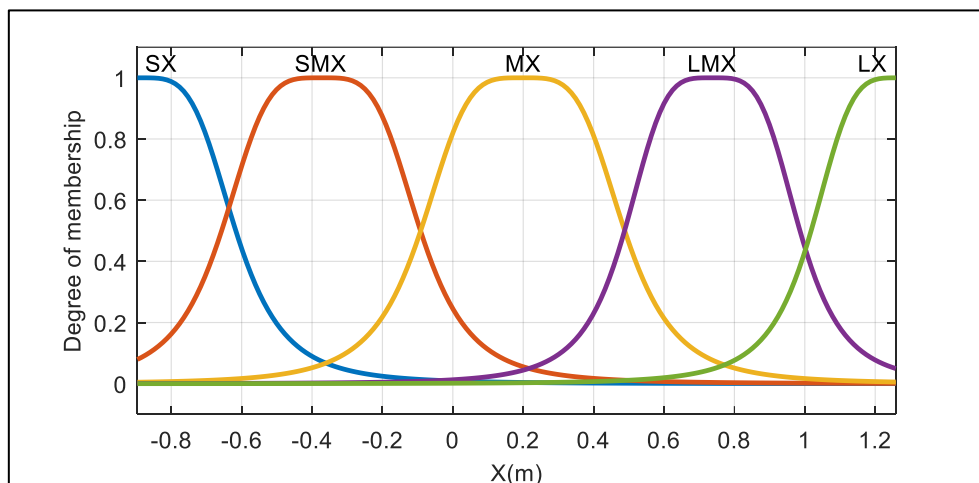


Figure 6.6. Initial MFs on X (same on Y) for ANFIS1 before training

This arrangement of MFs distributes input space into  $k^2$  uniformly distributed subspaces, each of which is governed by one fuzzy rule. Layer 2 provides the firing strength of each rule

$$w_j = \mu_{A_i}(x) \times \mu_{B_i}(y), \quad j = 1, \dots, k^2 \quad (6.11)$$

Figure 6.7 shows set of  $k^2$  rules before supervised learning starts. Note that bell shape MF curves corresponding to X and Y space are identical. Depending upon values of X and Y, one rule is selected that is used to determine corresponding joint angle.

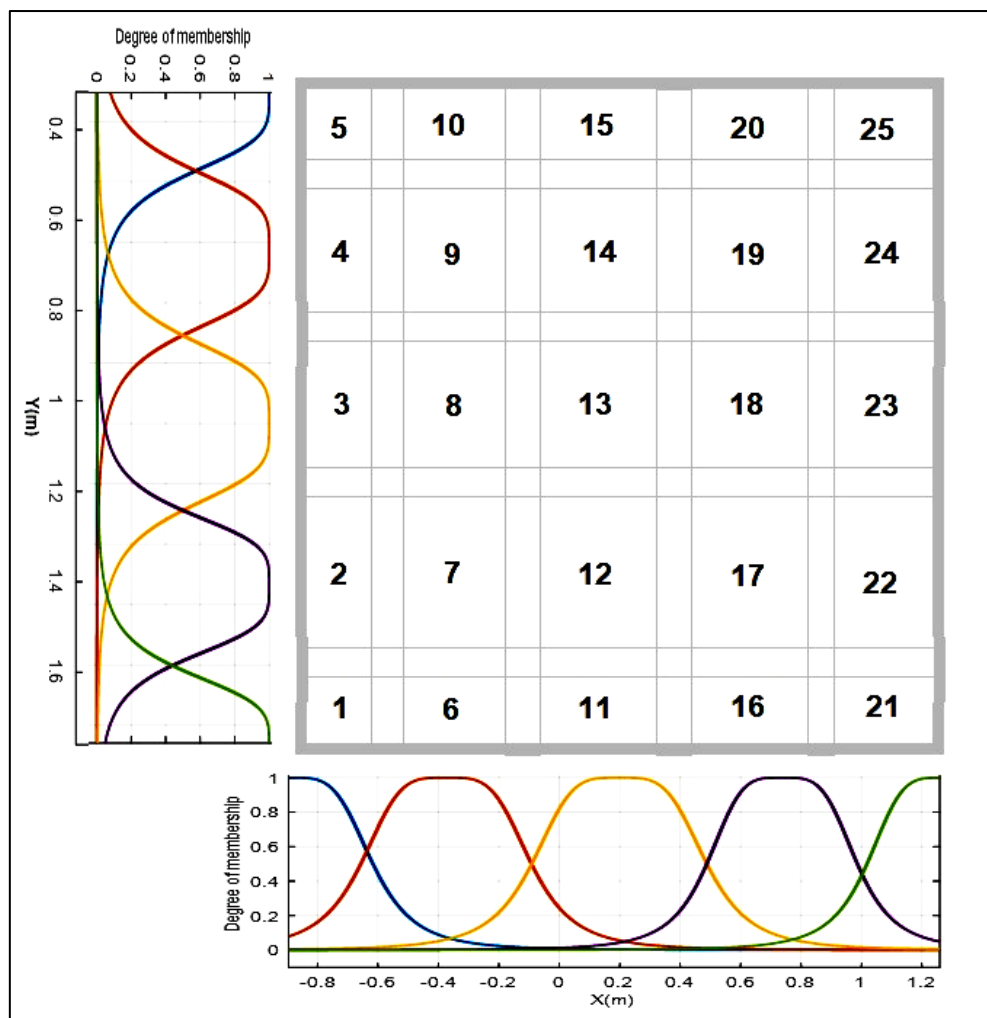


Figure 6.7. Two inputs, 10 MF ANFIS1 with 25 rules

Layer 3 provides the normalized firing strength,  $\bar{w}_j$ , given by

$$\bar{w}_j = \frac{w_j}{\sum_j w} \quad (6.12)$$

The contribution of each rule to output is given by layer 4 as

$$\bar{w}_j f_j = \bar{w}_j (p_j x + q_j y + r_j) \quad (6.13)$$

where  $f_j = \{p_j, q_j, r_j\}$  is the consequent parameter set. At the output of the last layer, all consequents are added to give the final result

$$\theta_n = \sum \bar{w}_j f_j = \sum \bar{w}_j (p_j x + q_j y + r_j) \quad (6.14)$$

where  $\theta_n$  is the ankle, knee or hip angle for  $n=1,2,3$  respectively, corresponding to X, Y head position. An ANFIS scheme utilizes Sugeno reasoning, where output is a pre-fuzzified (crisp) number, obtained from the sum of  $k^2$  linear equations and this scheme is very efficient in comparison to Mamdani reasoning for learning and generating the weights accordingly.

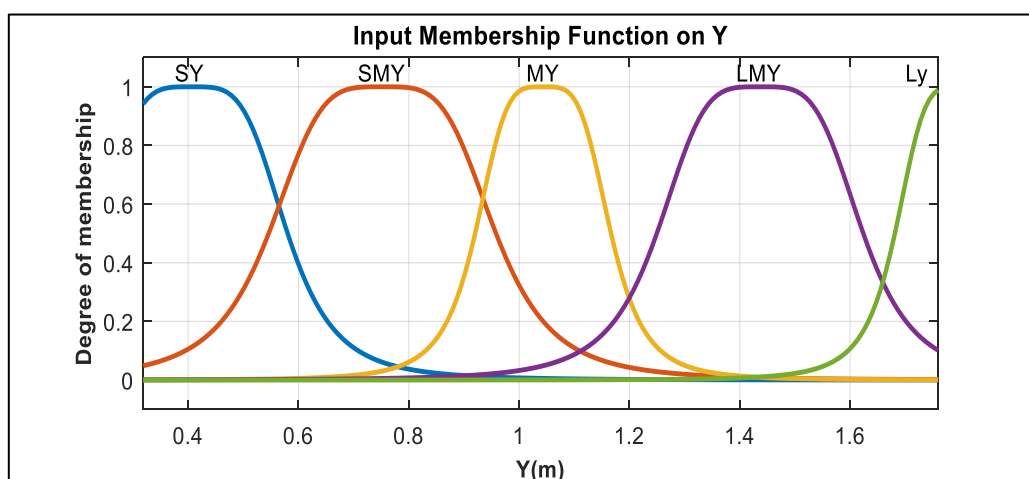


Figure 6.8. MFs on Y after training (12 epochs)



## 6.5.2 Training and optimizing ANFIS controllers

We now develop ANFIS controllers as first-order Sugeno models, using the technique described in [49]–[51]. The training algorithm uses a combination of least squares and back propagation gradient descent to minimize the error between actual and inferred values of output variables. Since  $X$ ,  $Y$  and  $\theta_n$  are used during training and  $\bar{w}_j$  are functions of premise parameters and input values, output of controller is a linear combination of consequent parameters  $\{p_j, q_j, r_j\}$ . Also, the training data points must be greater in number than consequent parameters, ANFIS obtains at least  $3k^2$  simultaneous equations in  $3k^2$  variable (unknown consequent parameters) that can be solved simultaneously. Each training cycle (epoch) is composed of two passes. In forward pass node outputs go forward until layer 4 and consequent parameters are identified (calculated) by Least Squares Estimate (LSE). In backward pass error signals propagate backward and premise parameters are updated by gradient descent. Once training is complete, a set of premise and consequent parameters is obtained. MFs change their shapes accordingly to capture local features of training data as shown in Figure 6.8. Similarly, the rules corresponding to these MFs also modify to come up with more accurate inference of joint angle.

### 6.5.2.1 Learning curves on training and validation datasets

During training (supervised learning), the Root Mean Square (RMS) error between actual joint positions and the ones inferred from ANFIS is calculated and plotted. The set of plots are called learning curves for the ANFIS. To optimize the training, different number of MFs (from 2 to 8) is used to search for the one which gives minimum error. This search is based on lowest RMS error found from learning curves on validation dataset as shown in Figure 6.9. Next, the ANFIS are trained on different number of training cycles (from 1 to 30) and the epoch corresponding to lowest RMS error is noted as shown in Figure 6.10. Training the ANFIS beyond these parameters results in over-fitting and degradation of the performance.

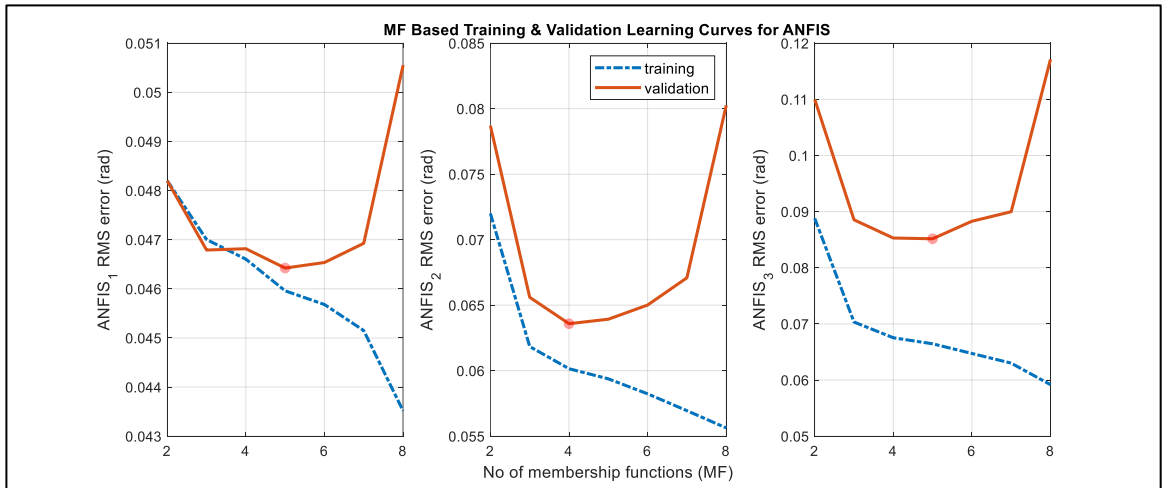


Figure 6.9. Learning curves of ANFIS on different numbers of membership function

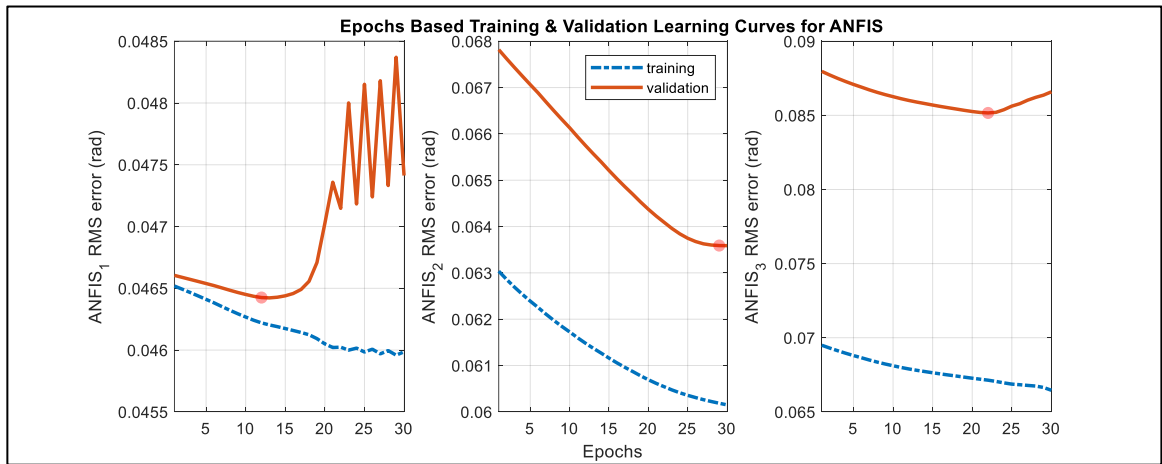


Figure 6.10. Learning curves for ANFIS controllers for training data and validation dataset.

### 6.5.3 Testing the trained ANFIS controllers

Once trained the controllers must be tested for generalization of the STS movement. Test datasets  $[X_f, Y_f, \theta_{np}]_n$  comprise 287 fictitious head positions  $(X_f, Y_f)$  and predicted joint angles  $\theta_{np}$ . These datasets are independent of training and validation datasets and hence can be relied upon to test ANFIS controllers without bias. The generated output angles  $\theta_{ng}$  are compared with predicted angles  $\theta_{np}$ . Figure 6.11 shows the error plot between the two datasets. The RMS errors for  $ANFIS_1$ ,  $ANFIS_2$  and  $ANFIS_3$  are 0.0628 rad, 0.0663 rad and 0.0299 rad respectively.

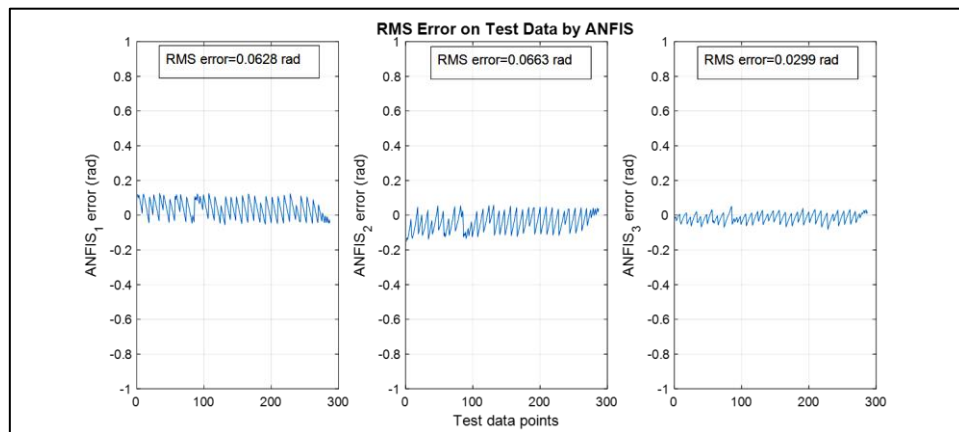


Figure 6.11. Errors of test data for ANFIS controllers

#### 6.5.4 Features of ANFIS controllers

Table 6.1 shows various features of ANFIS controllers. The three controllers operate on the same input ( $X$ ,  $Y$ ) and generate independent ankle, knee and hip joint angles. Figure 6.12 show surface plots of the three controllers for instantaneous head positions;  $X(m)$  and  $Y(m)$ .

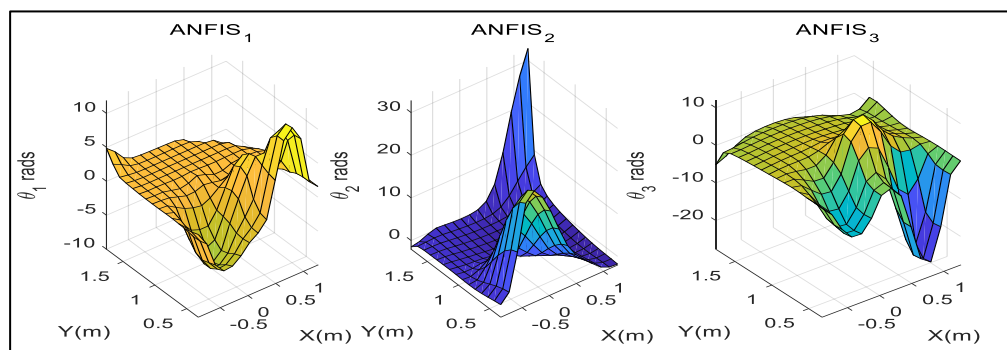


Figure 6.12. Surface plots of  $ANFIS_1$ ,  $ANFIS_2$  and  $ANFIS_3$  for three joint angles

Figure 6.12 (left) is a 3-dimensional plot showing what ankle angle will be generated by when a specific horizontal and vertical position is attained by head during STS. Figure 6.12 (center) shows knee angle range that correspond to entire head position range and Figure 6.12 (right) depicts hip angle inference based on head position.

For  $ANFIS_1$ , the number of input MF=5 each for X and Y inputs. This makes total number of input MF=10. The 3 premise parameters,  $\{a_i, b_i, c_i\}$ , for every MF make a total number of premise parameters equal to 30. Number of output MF correspond to number of rules, i.e., 25. For every output MF, there are 3 consequent parameters,  $\{p_j, q_j, r_j\}$ , which make a total of 75 parameters.  $ANFIS_1$  is trained and after 12 training cycles a minimum validation error of 0.04642 radian is obtained and  $ANFIS_1$  is finally trained. Similarly,  $ANFIS_2$  and  $ANFIS_3$  are trained.

Table 6.1. Parameters of ANFIS controllers

ANFIS serial number	1	2	3
Input parameters	30	24	30
Output parameters	75	48	75
Input membership functions	10	8	10
Output membership functions	25	16	25
Training epochs	12	29	12
Minimum validation error (RMS)	0.04642	0.06359	0.08519

For a quick overview of ANFIS implementation refer to Appendix F.

### 6.5.5 Stability of ANFIS training

Writing (6.14) in compact form

$$\theta = \vec{w}^T \vec{f} \quad (6.15)$$

where  $\vec{w}$  and  $\vec{f}$  are the functions of premise  $\{a_i, b_i, c_i\}$  and consequent parameters  $\{p_j, q_j, r_j\}$  respectively as mentioned in (6.9) and (6.10).  $\vec{w}$  represents the nonlinear mapping of head position (X,Y) into  $\theta$ . Let  $\theta_e$  be the estimation error of ANFIS during

the training.  $\vec{f}$  re-adjusts premise parameters on the basis of estimation error  $\theta_e$  using learning algorithm [48]

$$\dot{\vec{f}} = -\Gamma \vec{w} \theta_e \quad (6.16)$$

Or

$$\vec{f} = \Gamma \vec{w} \theta_e \quad (6.17)$$

where  $\tilde{f} = f_d - f$  and  $f_d$  is the desired function of consequent parameters with  $\Gamma$  learning rate given by a positive definite constant matrix. Now consider Lyapunov function

$$V = \frac{1}{2} \tilde{f}^T \Gamma^{-1} \tilde{f} \quad (6.18)$$

And

$$\theta_e = \theta_d - \theta$$

$$\theta_e = \theta_d - \vec{w}^T \vec{f}$$

$$\theta_e = \vec{w}^T \vec{f}_d - \vec{w}^T \vec{f}$$

$$\theta_e = \vec{w}^T (\vec{f}_d - \vec{f})$$

$$\theta_e = \vec{w}^T \tilde{f} \quad (6.19)$$

Differentiating V with respect to time

$$\dot{V} = \dot{\tilde{f}}^T \Gamma^{-1} \tilde{f} \quad (6.20)$$

Substituting

$$\dot{\tilde{f}} = -\Gamma \vec{w} \theta_e$$

$$\dot{V} = -\theta_e \vec{w}^T \Gamma^T \Gamma^{-1} \tilde{f}$$

$$\dot{V} = -\theta_e (\vec{w}^T \tilde{f})$$

$$\dot{V} = -\theta_e \cdot \theta_e \leq 0 \quad (6.21)$$

For any value of  $\theta_e$ ,  $\dot{V} \leq 0$ . Since  $\dot{V} = 0$  at only  $\theta_e = 0$  hence ANFIS is asymptotically stable in the sense of Lyapunov.

## 6.6 Simulation of STS Motion

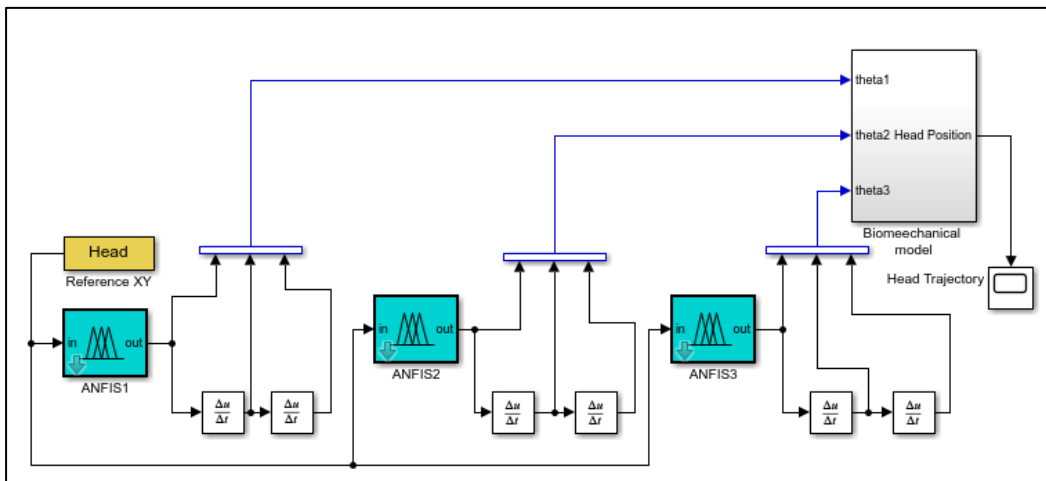


Figure 6.13. Neuro-fuzzy control-based STS motion synthesis framework in SimMechanics.

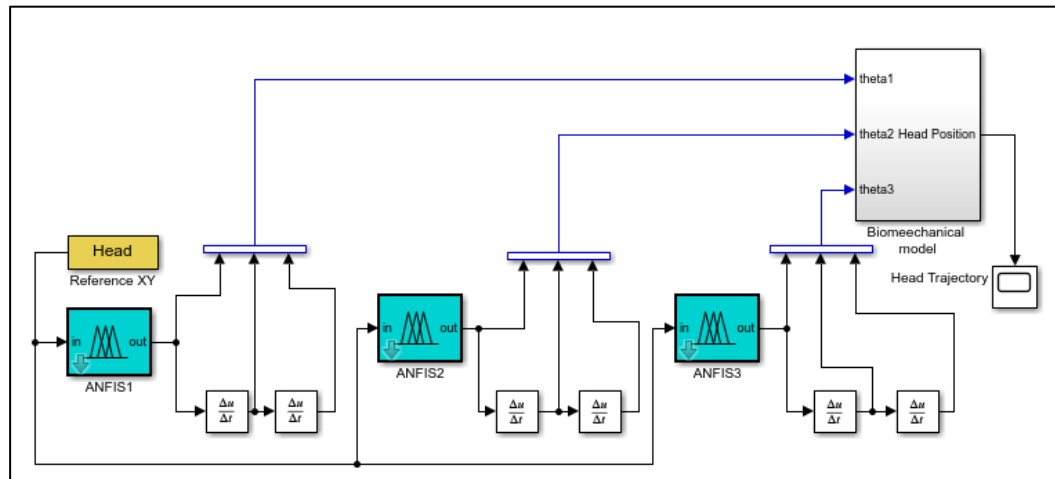


Figure 6.13 shows the modeling and motion synthesis framework of STS motion using head position trajectories in the SimMechanics simulation environment. The scheme is a variation to the model shown in Figure 4.11. In

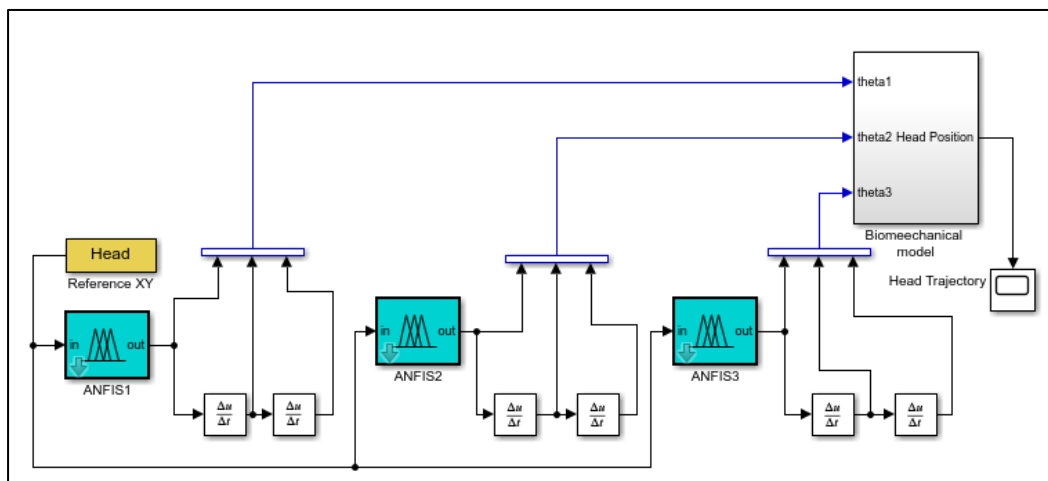


Figure 6.13 a set of three ANFIS controllers have been incorporated to actuate ankle, knee and hip joints. The system comprises a human biomechanical model of Figure 3.2 and a set of three ANFIS controllers that generate motion commands to

ankle, knee and hip joints using head position trajectories as reference input.

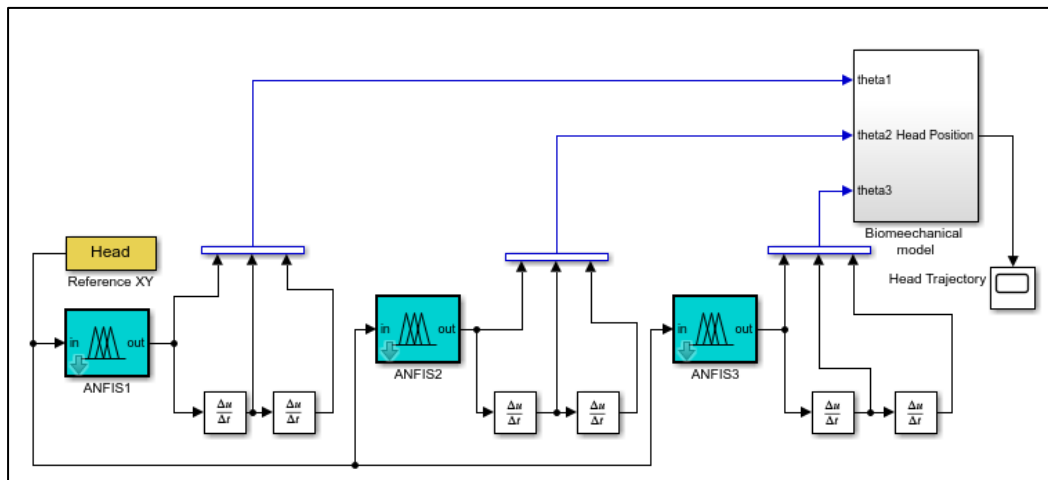


Figure 6.13 is the SimMechanics implementation of the concept presented in Figure 6.4. 'Head' block generates head position trajectories as the reference from where ANFIS infers appropriate joint angles.

### 6.6.1 Head position trajectory generation

Figure 6.14 depicts head position trajectories in Cartesian space. These trajectories are extracted from experimental motion data of marker affixed on head of a subject.

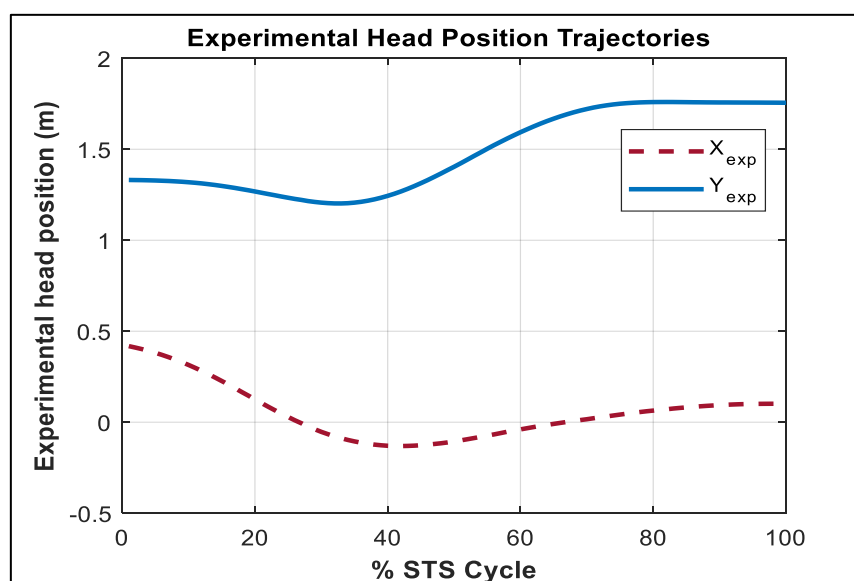


Figure 6.14. Experimentally generated head position trajectories



To simulate experimental head position trajectories as shown in Figure 6.14 generated from motion capture on the real subject, the head position reference trajectory is generated using an unforced state-space model proposed in [68] for joint angle trajectories.

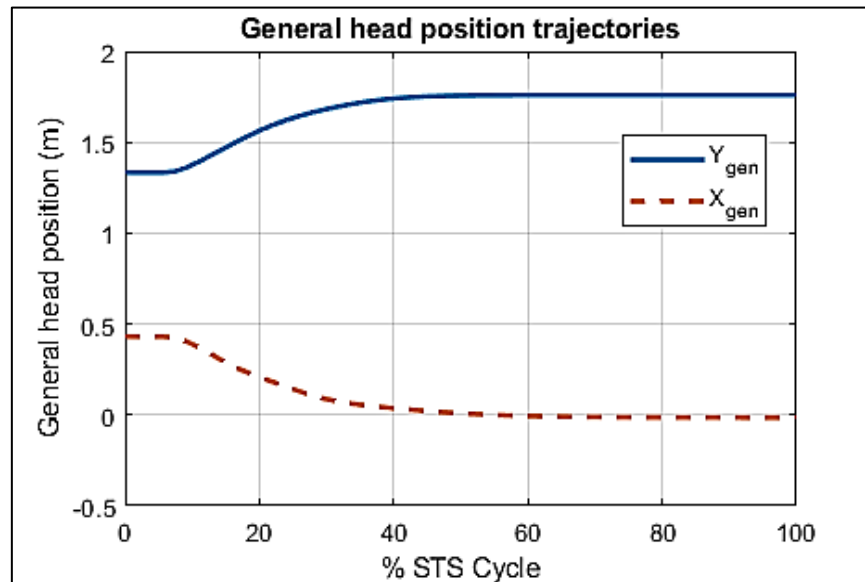


Figure 6.15. Analytically generated head position trajectories

We have modified the model for head position trajectories in Cartesian space. The analytically generated head trajectories are shown in Figure 6.15. The  $X_{gen}$  represents horizontal and  $Y_{gen}$  represents the vertical head position reference trajectory for the general human biomechanical model.

### 6.6.2 General human biomechanical model and general ANFIS control

First, the general human biomechanical model is controlled by the general ANFIS, using analytically generated head position trajectories shown in Figure 6.15. The joint angles inferred by ANFIS from reference input are plotted in Figure 6.16.

### 6.6.3 Custom human biomechanical models and general ANFIS control

BSP data of the subjects are used to customize subject-specific human biomechanical models. Subject-specific head position trajectories are used as reference input in simulations. The general ANFIS is used to simulate each subject's STS motion.

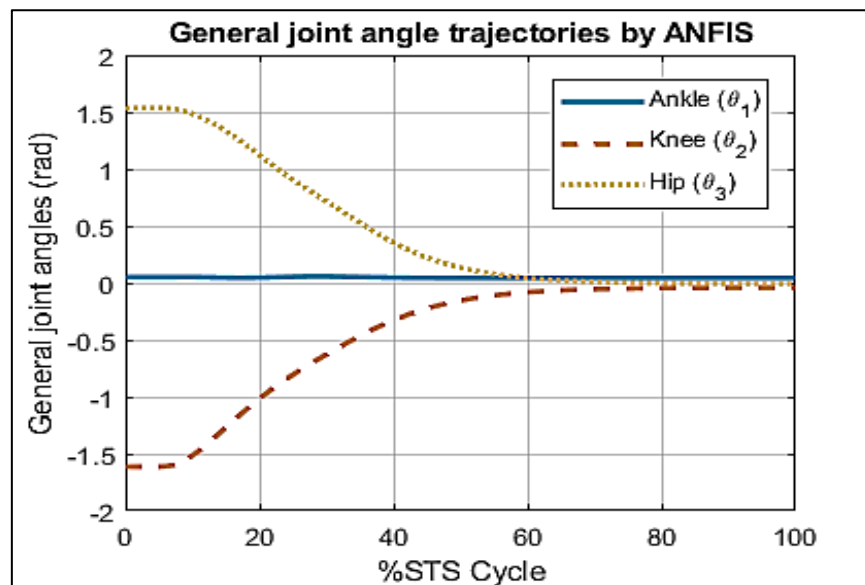


Figure 6.16. Joint angles generated by general ANFIS controller using general head trajectory

### 6.6.4 Custom human biomechanical models and custom ANFIS control

BPS data of each subject is used to generate a task-space training dataset so that custom ANFIS controllers are designed. Custom ANFIS, controls each custom human biomechanical model. The average of 6 subjects' head position measured from simulated motion, along with 1 standard deviation is plotted in Figure 6.17.

Joint angle measurements from simulated motion by custom model-controller mechanism are shown in Figure 6.18.

A comparison of motion control by general and customized ANFIS is given in Figure 6.19 in terms of error between experimental and simulated motions. The solid line curve shows the error in head position measurement in the horizontal direction between experimental and general ANFIS control-based simulation. The curve in the dashed line shows the horizontal position error between experimental and custom ANFIS control scheme. The better position control by the custom control scheme is evident from smaller errors. A similar trend can be seen in the same Figure for vertical position control error.

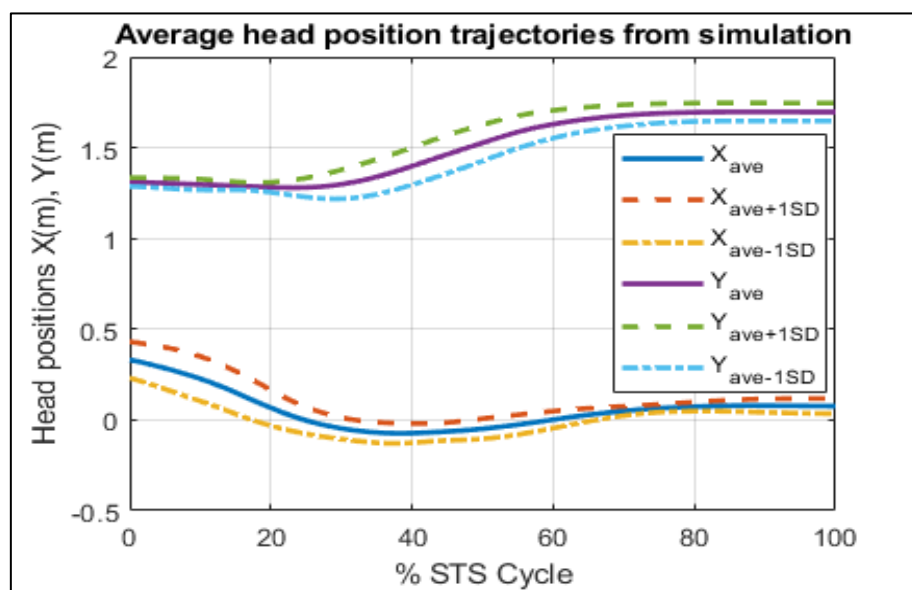


Figure 6.17. Ensemble average trajectories of head position from simulations using custom ANFIS controlled simulations. Dashed lines represent  $\pm 1SD$ , showing intra-subject variations

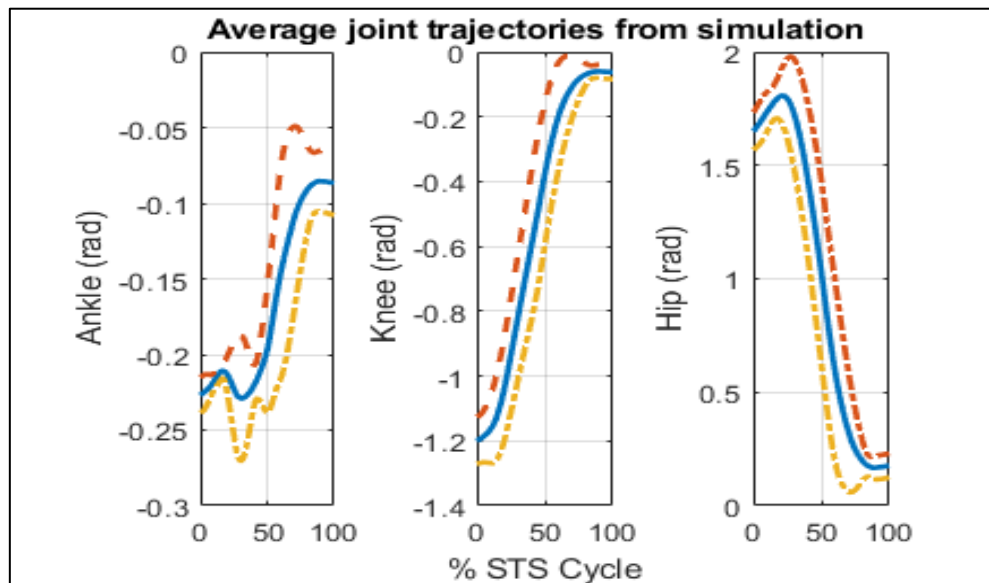


Figure 6.18. Ensemble average trajectories of joint angles using custom ANFIS controlled simulations. Dashed lines represent  $\pm 1SD$ , showing intra-subject variations

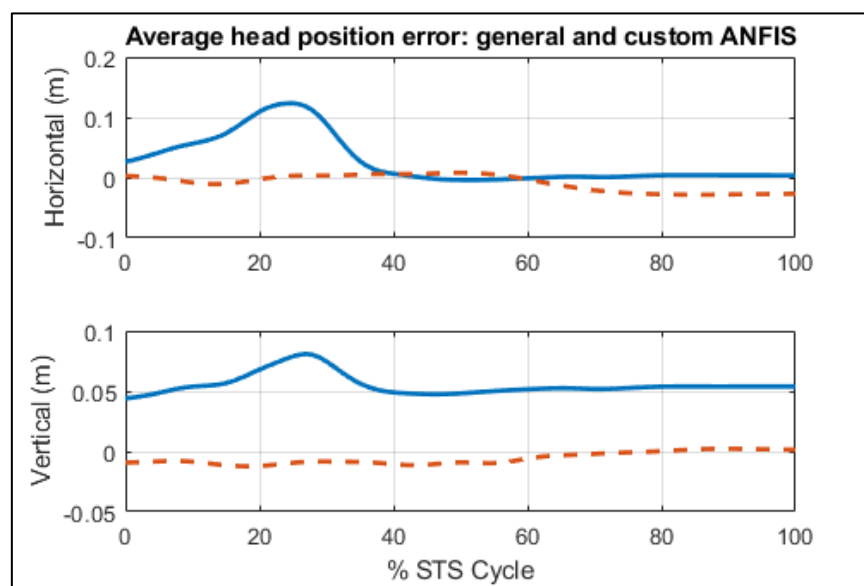


Figure 6.19. The error of head position between experimental and simulation trajectories using general (solid line) and custom (dashed line) ANFIS control

A comparison of joint angle position measurement can be seen in **Error! Reference source not found.** in terms of error between experimental and simulated motions.

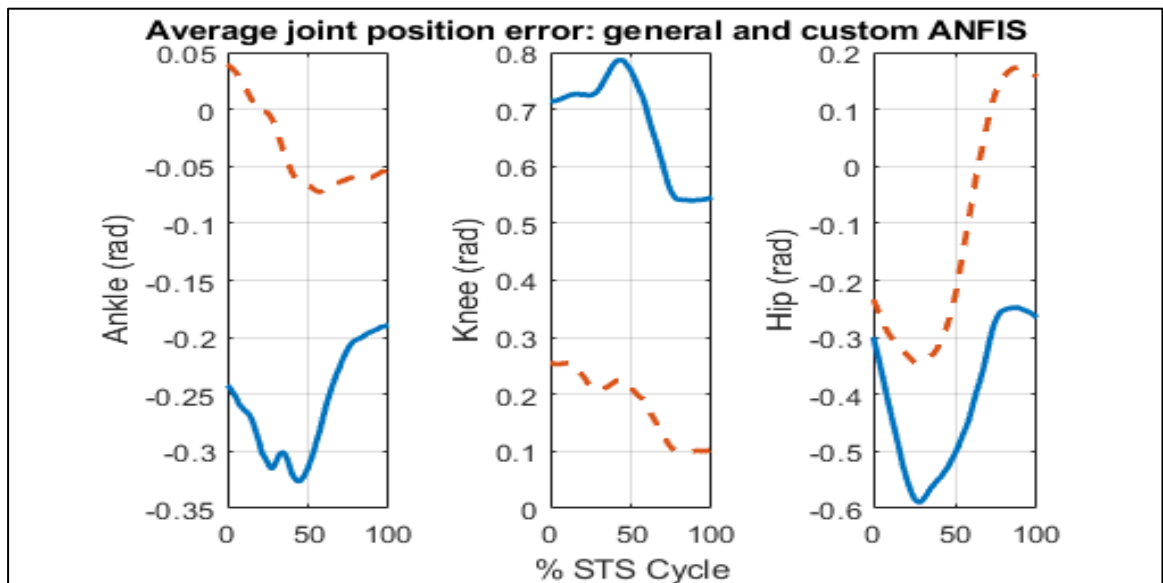


Figure 6.20. The error of joint position measurements between experimental and simulation trajectories using general (solid line) and custom (dashed line) ANFIS control

The solid line curve shows error in ankle, knee and hip position measurement between experimental and general ANFIS control-based simulation. The curve in the dashed line shows the joint position error between experimental and custom ANFIS control scheme. It can be seen that the joint position error is relatively larger in both types of control schemes. However, the custom ANFIS control scheme proves to be better here again, since the error reduces to a lower value as compared to the error in the case of the general ANFIS control scheme.

Table 6.2 gives a quantitative comparison of the two schemes: The error in head position and joint angles are quantified in terms of Root Mean Square (RMS) error. The lower error achieved by the custom ANFIS control scheme is obvious for the head position in both directions as well as in all joint angle positions. The table also shows how much % improvement is achieved by custom ANFIS as compared to the general ANFIS control scheme.

Table 6.2. A quantitative comparison of RMS errors between actual and simulated trajectories

	RMS error	
--	-----------	--

The error between experimental data and simulations	General ANFIS	Custom ANFIS	% Improvement from general to custom ANFIS
Horizontal head position (m)	0.0023	0.00025	89.13
Vertical head position (m)	0.0031	0.000057	98.16
Ankle joint position (rad)	0.0695	0.0027	96.11
Knee joint position (rad)	0.46	0.036	92.17
Hip joint position (rad)	0.18	0.057	68.33

## 6.7 Discussion

In this study, we proposed a modeling framework to evaluate the role of head position trajectory as a slow dynamic in CNS to carry out STS motion. CNS has been modeled by the ANFIS controller. We hypothesized that human CNS learns STS motion as slow dynamics; to perform STS motion the head position trajectory plays the role of a reference trajectory and CNS generates appropriate joint angles such that the head as end effector may achieve the smooth trajectory in Cartesian space while joints perform the appropriate angular motion. CNS infers the joint positions that correspond to required head positions associated with STS. Using a well-defined human biomechanical model and the simulation results from previous studies helped us design and fine-tune the ANFIS controller that could produce comparable results. As a standard procedure [10], [11], [47] we later validated our modeling and control scheme framework with laboratory data as well.

To develop general ANFIS controllers we used the TST algorithm to generate three datasets analytically. Each of these datasets  $[X, Y, \theta_n]_n$ , are bifurcated into training and validation datasets, each comprising 324 I/O data points. Initially, all three ANFIS controllers are trained for various values of MFs, starting from 3 and onwards. The number of epochs was varied between 10 and 50. Figure 6.9 shows a comparison between training and validation error plots of ANFIS controllers for difference number of MFs. Although training error curves show better convergence, validation error plots

are considered a true measure of model performance [49]. ANFIS controllers are then trained on the optimal number of MFs and for different number of epochs using both training and validating data set as shown in Figure 6.10. Error-values obtained through test data are very low, as shown in Figure 6.11, showing good learning of controllers. Surface plots in Figure 6.12 relate to the head position subspace in Figure 6.3. ANFIS controllers are capable of providing suitable angle commands to a much wider range of angles for which they were trained. This makes the controllers flexible and robust for various STS patterns.

ANFIS controller is then customized for each subject using BSP data and the TST algorithm. Using the same subject's head position trajectory constructed from experimental data, subject-specific STS motion is controlled. Figure 6.19 and **Error! Reference source not found.** give a comparison of errors between experimental trajectories and simulated ones; by the general ANFIS and custom ANFIS. Plots show that subject-specific tuning improves ANFIS control of the STS motion as compared to the general ANFIS scheme and matches more closely to experimental results. An overall comparison of performance by two control schemes is given in Table 6.2. RMS error due to general  $ANFIS_3$  was already very small for hip joint, hence there was little room for improvement by customized  $ANFIS_3$ . Performance of ANFIS can be further improved in two stages: first, the simulation can be run with subject-specific joint initial conditions and second, for each subject the ANFIS controller may be optimized for the number of membership functions and training cycle epochs and tested for minimum error. For now, we have used a scheme, which is less time-consuming due to its non-iterative nature and even then, shows good results.

## 6.8 Summary

This chapter has outlined the development of a technique that easily maps motion capture data into a simulation environment by customizing both the human biomechanical model as well as the ANFIS controller to a real human being performing STS motion. ANFIS controller is presented as an inference mechanism to model human CNS that estimates and controls appropriate joint angles needed to perform STS motion

using a pre-learned head position trajectory as a reference to be tracked. Next, task-level control of STS motion in close loop is presented. Chapter 7 gives details of STS motion synthesis using Cartesian control.



## CHAPTER 7

# CARTESIAN CONTROL OF SIT-TO-STAND MOTION USING HEAD POSITION FEEDBACK

In this chapter, we evaluate the clinical hypothesis that besides numerous other factors, the CNS controls STS motion by tracking a pre-learned head position trajectory. Motivated by the evidence for a task-oriented encoding of motion by the CNS, we adopt a robotic approach for the synthesis of STS motion and propose this scheme as a formulation of this hypothesis in simulation framework as an analysis tool. We propose an analytical biomechanical human-CNS modeling framework where the head position trajectory defines the high-level task control variable. The motion control is divided into low-level task generation and motor execution phases. We model CNS as STS Controller and its Estimator subsystem plans joint trajectories to perform the low-level task. The motor execution is done through the Cartesian Controller subsystem that generates torque commands to the joints. We performed motion and force capture experiments on human subjects to validate our analytical modeling scheme. We first scale our biomechanical model to match the anthropometry of the subjects. We do dynamic motion reconstruction through the control of simulated custom human-CNS models to follow the captured head position trajectories in real-time. We perform kinematic, kinetic analyses and comparison of experimental and simulated motions. For head position trajectories RMS errors are 0.0118m in horizontal and 0.0315m in vertical directions. Errors in angle estimates are 0.55 rad, 0.93 rad, 0.59 rad and 0.0442 rad for ankle, knee, hip and head orientation respectively. RMS error of Ground Reaction Force (GRF) is 50.26N, and the correlation between ground reaction torque and the support moment is 0.72. Low errors in our results validate technique for customization of human biomechanical models and the high-level task control framework and human-CNS modeling as a solution to the hypothesis.

## 7.1 Methodology

### 7.1.1 Workflow

We design a biomechanical human-CNS model to synthesize and control STS motion by tracking only head trajectory  $\mathcal{X}_d$  as a reference and head position  $\mathcal{X}$  as the only measurement. Force measurement does not play a role in motion synthesis or control, it is meant only for modeling scheme validation.

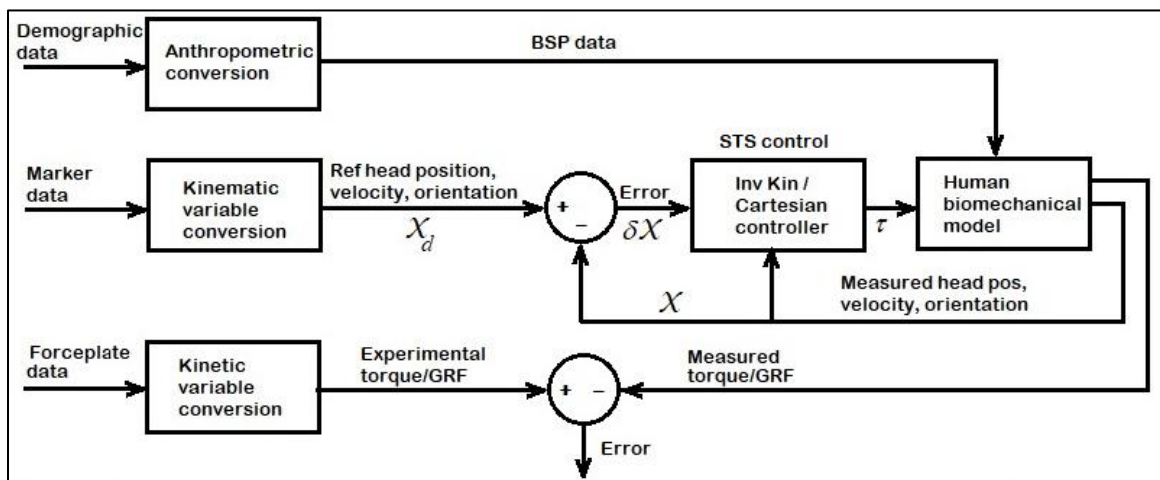


Figure 7.1. The workflow of the STS motion control scheme

### 7.1.2 Analytical modeling

We develop an analytical human-CNS modeling framework to generate STS motion. Our modeling scheme comprises the following steps:

- 1) A general four-segment human biomechanical model in the sagittal plane based on BSP from the literature [12], [37], [40], [41], [53], [62] is realized in SimMechanics.
- 2) We analytically generate head trajectory [68] to be used as the reference.
- 3) We design the STS Controller to emulate human CNS, capable to:

a) Estimate joint angles using inverse kinematics, based on head position measurements.

b) Generate joint actuation torque commands  $\vec{\tau}$  by Cartesian control based on head position error  $\overline{\delta\mathcal{X}}$ .

### **7.1.3 Modeling validation on experimental data**

1) The physical parameter data collected from 7 subjects are converted into BSP using the Weighing Coefficient method of anthropometry. BSP values are used to realize custom/subject-specific human biomechanical models.

2) We capture motion and force data of STS maneuver from subjects using multiple infra-red cameras and passive reflective markers. We extract custom head trajectories from motion data and torques and GRFs from force data.

3) STS motion is reconstructed for each custom human-CNS model. Custom head trajectories are used as the reference for respective models. Simulated motions are analyzed and compared with experimental motion.

## **7.2 Analytical Modeling Framework**

### **7.2.1 CNS modeling: STS controller design**

The CNS is modeled as an STS controller comprising two subsystems: an Estimator and a Cartesian controller:

### 7.2.1.1 Estimator

The estimation of joint angles is based on the inverse kinematics of the human biomechanical model as explained in Chapter 6.

### 7.2.1.2 Cartesian control

Cartesian control refers to the position control of the head, following a required trajectory in Cartesian space.

#### 1) Equation of motion

The dynamic equation of motion of the n DoF human biomechanical model in joint space is given by

$$\vec{\tau} = \mathbf{D}(\theta)\ddot{\theta} + \mathbf{H}(\theta, \dot{\theta})\dot{\theta} + \vec{G}(\theta) \quad (7.1)$$

where  $\ddot{\theta}$ ,  $\dot{\theta}$  and  $\theta$  are  $n \times 1$  joint angular acceleration, velocity and position vectors respectively.  $\mathbf{D}(\theta)$  is the  $n \times n$  inertia matrix of the model,  $\mathbf{H}(\theta, \dot{\theta})$  is  $n \times n$  matrix of centrifugal and Coriolis terms,  $\vec{G}(\theta)$  is the  $n \times 1$  vector of gravity terms and  $\vec{\tau}$  is the  $n \times 1$  torque vector.

Modifying dynamic equation from joint space to Cartesian space [69],

$$\vec{\mathcal{F}} = \mathbf{D}_x(\mathbf{x})\ddot{\mathcal{X}} + \mathbf{H}_x(\dot{\mathbf{x}}, \mathbf{x})\dot{\mathcal{X}} + \vec{G}_x(\mathbf{x}) \quad (7.2)$$

where  $\vec{\mathcal{F}}$  is the appropriate force-torque vector and  $\vec{\mathcal{X}}$  is the position and orientation of the head in Cartesian space.  $\mathbf{D}_x(\mathbf{x})$  is the mass-inertia matrix in Cartesian space and so on.

A trajectory conversion process thus required is:

$$\vec{\theta}_d = \text{inv kin}(\vec{\mathcal{X}}) \quad (7.3)$$

where  $\vec{\mathcal{X}}$  is the measured head position trajectory in Cartesian space and  $\vec{\theta}_d$  is the vector of corresponding joint angles and the *inv kin* operator refers to the inverse kinematic procedure used for the inference of joint angles from the position of the end effector.

## 2) Transpose Jacobian control

In this scheme measured position  $\vec{\mathcal{X}}$  is compared to desired position  $\vec{\mathcal{X}}_d$  to form an error  $\delta\vec{\mathcal{X}}$  in Cartesian space. The error vector is then applied to control law to compute the Cartesian force vector,  $\vec{\mathcal{F}}$ , which is that fictitious force if applied at the head, will tend to reduce Cartesian error. The Cartesian force vector is then mapped into joint torque vector  $\vec{\tau}$  using transpose Jacobian conversion.

## 3) The velocity of the head

Description of angular velocity  $\vec{\omega}$  of link i+1 with respect to respective frame is given by

$${}^{i+1}\vec{\omega}_{i+1} = {}^{i+1}\mathbf{R} \ {}^i\vec{\omega}_i + \dot{\theta}_{i+1} \ {}^{i+1}\mathbf{Z}_{i+1} \quad (7.4)$$

where i=0,1,2 refer to link number,  $\mathbf{R}$  is a rotation matrix and  $\mathbf{Z}$  is the axis of joint rotation. The linear velocity  $\vec{v}$  is given by

$${}^{i+1}\vec{v}_{i+1} = {}^{i+1}\mathbf{R} \left( {}^i\vec{v}_i + {}^i\vec{\omega}_i \times {}^i\vec{p}_{i+1} \right) \quad (7.5)$$

where  $\vec{p}$  is the head position vector. For the model shown in Figure 6.2, the angular and linear velocity components of the head in three axes are given respectively:

$${}^3\vec{\omega}_3 = {}^2\vec{\omega}_2 = \begin{bmatrix} 0 \\ 0 \\ \dot{\theta}_1 + \dot{\theta}_2 \end{bmatrix} \quad (7.6)$$

$${}^3\vec{v}_3 = \begin{bmatrix} l_1 s_2 \dot{\theta}_1 \\ l_1 c_2 \dot{\theta}_1 + l_2 (\dot{\theta}_1 + \dot{\theta}_2) \\ 0 \end{bmatrix} \quad (7.7)$$

To find these velocities with respect to fixed foot-shank frame {F}, we use the rotation matrix

$${}^0\mathbf{R}_3 = {}^0\mathbf{R}_1 {}^1\mathbf{R}_2 {}^2\mathbf{R}_3 = \begin{bmatrix} c_{12} & -s_{12} & 0 \\ s_{12} & c_{12} & 0 \\ 0 & 0 & 1 \end{bmatrix} \quad (7.8)$$

$${}^0\vec{v}_3 = {}^0\mathbf{R}_3 {}^3\vec{v}_3 = \begin{bmatrix} -l_1 s_1 \dot{\theta}_1 - l_2 s_{12} (\dot{\theta}_1 + \dot{\theta}_2) \\ l_1 c_1 \dot{\theta}_1 + l_2 c_{12} (\dot{\theta}_1 + \dot{\theta}_2) \\ 0 \end{bmatrix} \quad (7.9)$$

#### 4) The Jacobian

Jacobian is a nonlinear time-varying matrix that relates joint angular velocities to linear head velocity:

$${}^0\vec{v} = {}^0\mathbf{J}(\theta) \vec{\dot{\theta}}$$

$${}^0\vec{v} = \begin{bmatrix} -l_1 s_1 - l_2 s_{12} - l_3 s_{123} & -l_2 s_{12} - l_3 s_{123} & -l_3 s_{123} \\ l_1 c_1 + l_2 c_{12} + l_3 c_{123} & l_2 c_{12} + l_3 c_{123} & l_3 c_{123} \\ 1 & 1 & 1 \end{bmatrix} \begin{bmatrix} \dot{\theta}_1 \\ \dot{\theta}_2 \\ \dot{\theta}_3 \end{bmatrix} \quad (7.10)$$

### 5) Static forces in the human biomechanical model

Forces and moments propagate from segment to segment. Torques on joints must be applied to keep the system in static equilibrium. Jacobian (  $J$  ) in force domain maps force on the head into torques on joints:

$$\vec{\tau} = J^T \vec{F}, \quad (7.11)$$

where  $\vec{F}$  is the Cartesian force required to act on the head.

### 7.2.2 Cartesian controller for STS

The control scheme is based upon the hypothesis that the feedback of head position  $\vec{X}$  to CNS, i.e., the STS controller, plays a role in carrying out STS motion. As shown in Figure 7.2, using the measured position of head  $\vec{X}$  and comparing with desired/reference head trajectories  $\vec{X}_d$ , the CNS generates error signal  $\delta\vec{X}$ . From head position measurements, the Estimator part of CNS infers joint positions ( $\vec{\theta}_d$ ), required to reduce the error  $\delta\vec{X}$ . Similarly, the head position errors fed back to CNS generate torque command to the joints using Cartesian control law. Since Cartesian control is usually implemented in force domain, the controller generates a force command  $\vec{F}$ . Then the transpose Jacobean converts force command  $\vec{F}$  into torque command  $\vec{\tau}$ , for joint actuation.

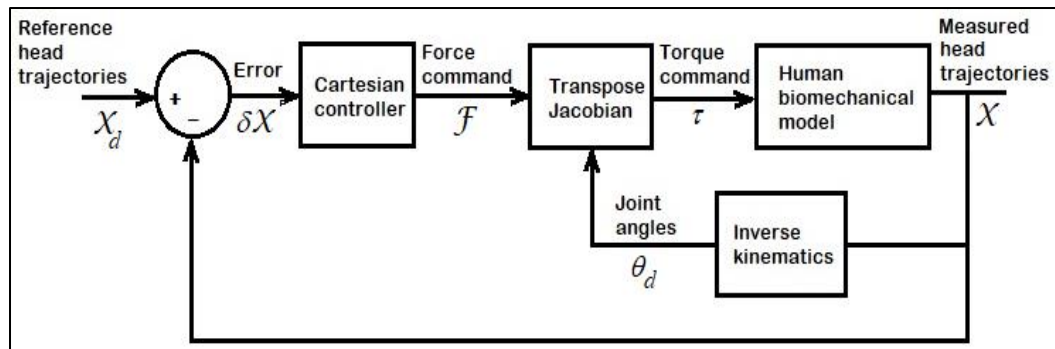


Figure 7.2. STS control scheme to emulate CNS

### 7.2.3 Stability of the Cartesian control

The overall control scheme in joint space using transpose Jacobian is given by

$$\mathbf{D}(\boldsymbol{\theta})\ddot{\boldsymbol{\theta}} + \mathbf{H}(\boldsymbol{\theta}, \dot{\boldsymbol{\theta}})\dot{\boldsymbol{\theta}} + \vec{G}(\boldsymbol{\theta}) = \mathbf{J}^T \vec{F} \quad (7.12)$$

The scheme can be represented in Cartesian space

$$\mathbf{D}_x(x)\ddot{\mathcal{X}} + \mathbf{H}_x(\dot{x}, x)\dot{\mathcal{X}} + \vec{G}_x(x) = \vec{\tau}_x \quad (7.13)$$

Using the control law [71] with  $\mathbf{k}_p$  and  $\mathbf{k}_d$  the diagonal positive definite matrices

$$\vec{\tau}_x = \mathbf{k}_p \delta \mathcal{X} - \mathbf{k}_d \dot{\mathcal{X}} + \vec{G}(\vec{x}) \quad (7.14)$$

Equating (7.13) and (7.14)

$$\mathbf{D}_x(x)\ddot{\mathcal{X}} + \mathbf{H}_x(\dot{x}, x)\dot{\mathcal{X}} = \mathbf{k}_p \delta \vec{\mathcal{X}} - \mathbf{k}_d \dot{\mathcal{X}}$$

Left multiplying with  $\dot{\mathcal{X}}^T$

$$\dot{\mathcal{X}}^T \mathbf{D}_x(x)\ddot{\mathcal{X}} + \dot{\mathcal{X}}^T \mathbf{H}_x(\dot{x}, x)\dot{\mathcal{X}} = \dot{\mathcal{X}}^T \mathbf{k}_p \delta \vec{\mathcal{X}} - \dot{\mathcal{X}}^T \mathbf{k}_d \dot{\mathcal{X}}$$

$$\dot{\mathcal{X}}^T \mathbf{D}_x(x)\ddot{\mathcal{X}} - \dot{\mathcal{X}}^T \mathbf{k}_p \delta \vec{\mathcal{X}} = -\dot{\mathcal{X}}^T \mathbf{H}_x(\dot{x}, x)\dot{\mathcal{X}} - \dot{\mathcal{X}}^T \mathbf{k}_d \dot{\mathcal{X}} \quad (7.15)$$

Defining

$$u(\mathbf{k}_p, \delta \mathcal{X}) = \frac{\delta \mathcal{X}^T \mathbf{k}_p \delta \mathcal{X}}{2}$$

Using Lyapunov candidate function



$$V(\dot{\mathcal{X}}, \delta \vec{\mathcal{X}}) = \frac{\dot{\mathcal{X}}^T \mathbf{D} \dot{\mathcal{X}}}{2} + u(\mathbf{k}_p, \delta \vec{\mathcal{X}}) \quad (7.16)$$

Differentiating the Lyapunov function

$$\dot{V}(\dot{\mathcal{X}}, \delta \mathcal{X}) = \frac{\dot{\mathcal{X}}^T \dot{\mathbf{D}} \dot{\mathcal{X}}}{2} + \dot{\mathcal{X}}^T \mathbf{D} \dot{\mathcal{X}} - \dot{\mathcal{X}}^T \mathbf{k}_p \delta \mathcal{X} \quad (7.17)$$

From ((7.15))

$$\dot{V}(\dot{\mathcal{X}}, \delta \mathcal{X}) = \frac{\dot{\mathcal{X}}^T \dot{\mathbf{D}} \dot{\mathcal{X}}}{2} - \dot{\mathcal{X}}^T \mathbf{H}_x(\dot{x}, x) \dot{\mathcal{X}} - \dot{\mathcal{X}}^T \mathbf{k}_d \dot{\mathcal{X}}$$

Also,

$$\frac{\dot{\mathcal{X}}^T \dot{\mathbf{D}} \dot{\mathcal{X}}}{2} = \dot{\mathcal{X}}^T \mathbf{H}_x(\dot{x}, x) \dot{\mathcal{X}}$$

$$\dot{V}(\dot{\mathcal{X}}, \delta \mathcal{X}) = -\dot{\mathcal{X}}^T \mathbf{k}_d \dot{\mathcal{X}}$$

Also, the  $\mathbf{k}_d$  is positive definite it fulfills the condition

$$\dot{V}(\dot{\mathcal{X}}, \delta \mathcal{X}) \leq 0 \quad (7.18)$$

And verifies asymptotic stability with LaSalle theorem

$$\dot{V}(\dot{\mathcal{X}}, \delta \mathcal{X}) < 0 \quad (7.19)$$

And hence close-loop system is locally stable and positioning aim is achieved as:

$$\lim_{t \rightarrow \infty} \vec{x}(t) = \mathcal{X}_d \quad \text{and} \quad \lim_{t \rightarrow \infty} \dot{\vec{x}}(t) = 0$$

## 7.3 Simulation of STS Motion

Figure 7.3 is the SimMechanics implementation of scheme given in Figure 7.2. The 'Head' represents head position trajectory  $\vec{\mathcal{X}}_d$  generator that provides reference head position and orientation trajectories. The human biomechanical model is represented by the 'Biomechanical model' block. The Cartesian controller generates force command  $\vec{\mathcal{F}}$  which is converted into required torque  $\vec{\tau}$ , for the actuation of ankle, knee and hip joints. Head position  $\vec{\mathcal{X}}$  is measured and is used to infer joint angles by 'Estimator' block.

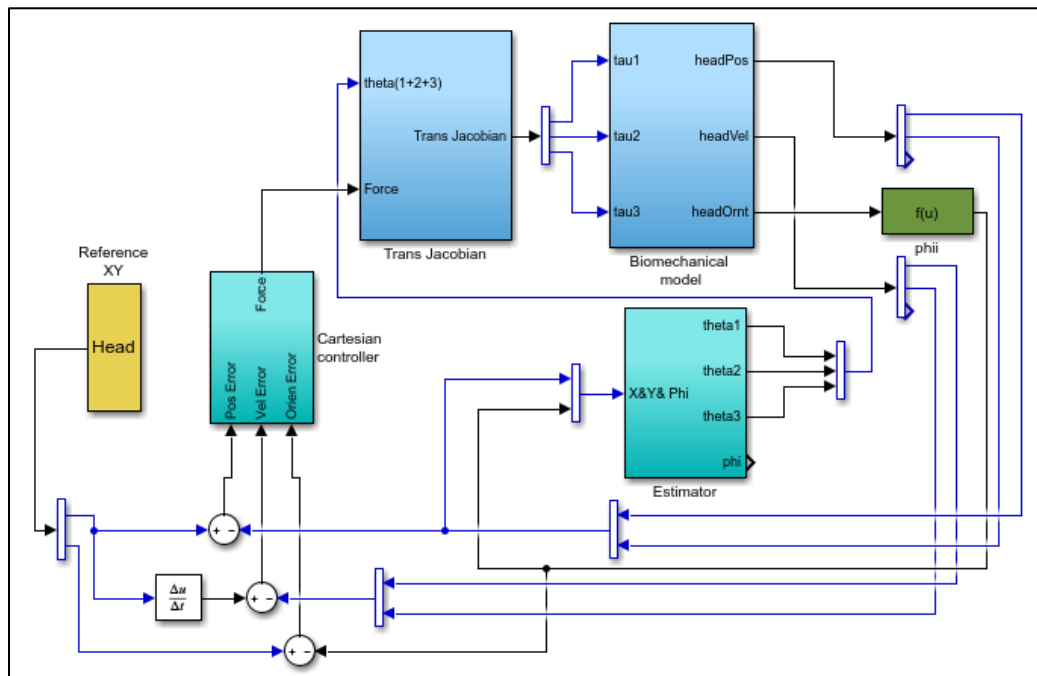


Figure 7.3. STS control scheme implemented in SimMechanics

### 7.3.1 Simulation using the analytical scheme

The SimMechanics model is first used for the analytical human biomechanical model discussed in Chapter 3. Refer to Table 3.1 and Figure 3.2 for more details of the model. The analytical model tracks analytically generated reference trajectory using an unforced system discussed in section 6.7. Figure 7.4 shows reference head position

trajectories as  $X_d$  and  $Y_d$ , generated analytically. The measured head position trajectories  $X_m$  and  $Y_m$  are also shown. The tracking by the controller is good and the human biomechanical model tracks the reference well.

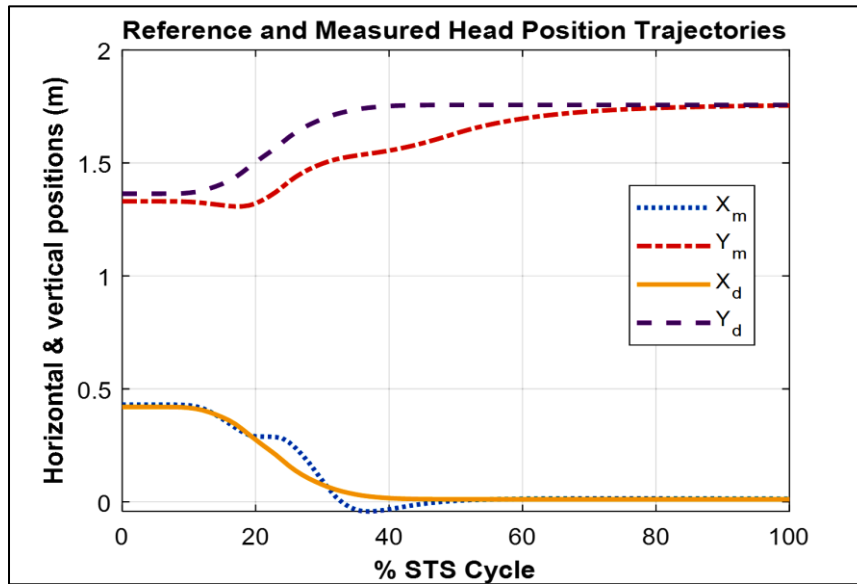


Figure 7.4. Comparison of reference and measured head position trajectories

Figure 7.5 shows measurements of joint angles during STS motion. For the sake of comparison Figure 5.4 is redrawn as Figure 7.6, which shows actual joint angles by real humans. The biomechanical model generates the joint angles that are to some extent resemble the angles in Figure 7.5. Ankle follows a larger flexing angle as compared to the real ankle motion pattern. Also, knee motion is a bit jerky in Figure 7.4 and the knee does not unfold completely to zero radians by the end of the STS cycle.

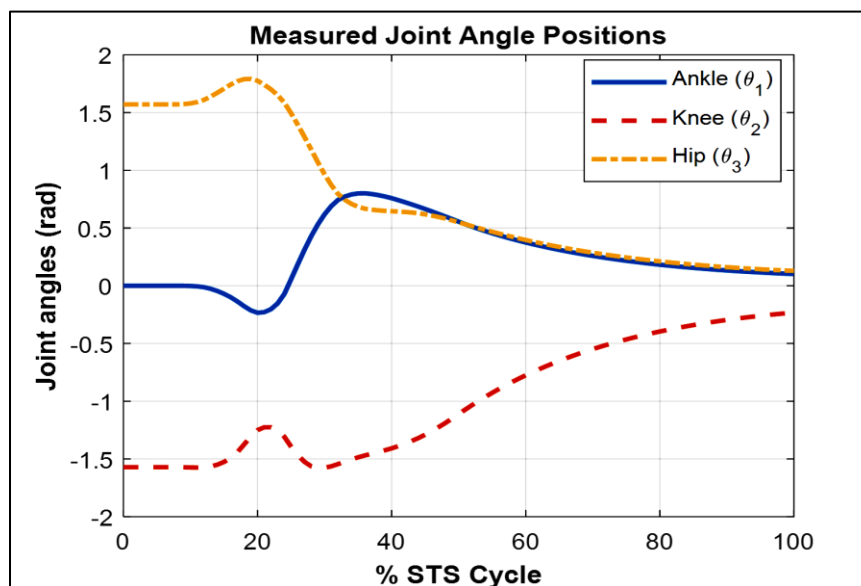


Figure 7.5. Ankle, knee and hip joint angle trajectories measured during STS

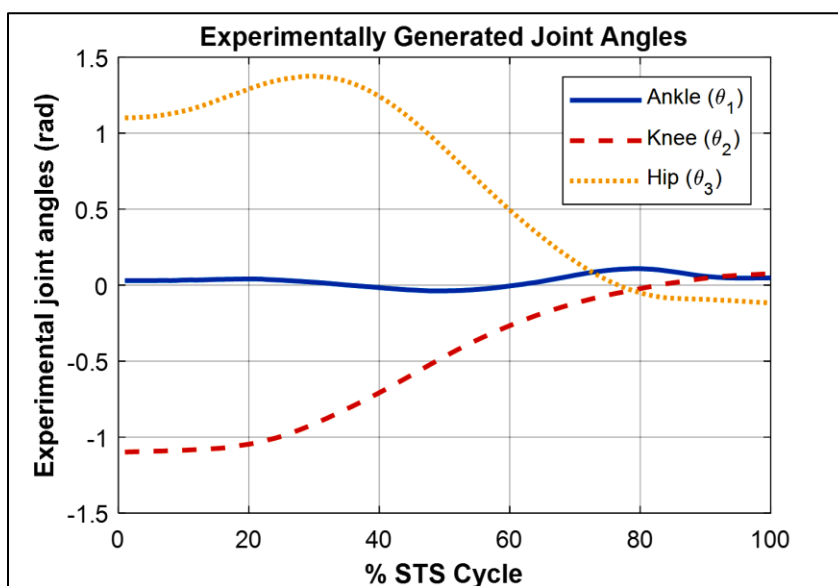


Figure 7.6. The actual joint positions measured from STS motion by actual humans

Since the human biomechanical model is redundant by nature, it can follow the head position trajectory using multiple combinations of joint angles. To restrict the joint angular motion such that a human-like STS transfer may result, the head orientation reference provides the required motion constraint. The reference head orientation trajectory

as shown in Figure 7.7 is generated analytically. The measured head orientation curve shows a peak deviation of less than 0.1 radians from reference.

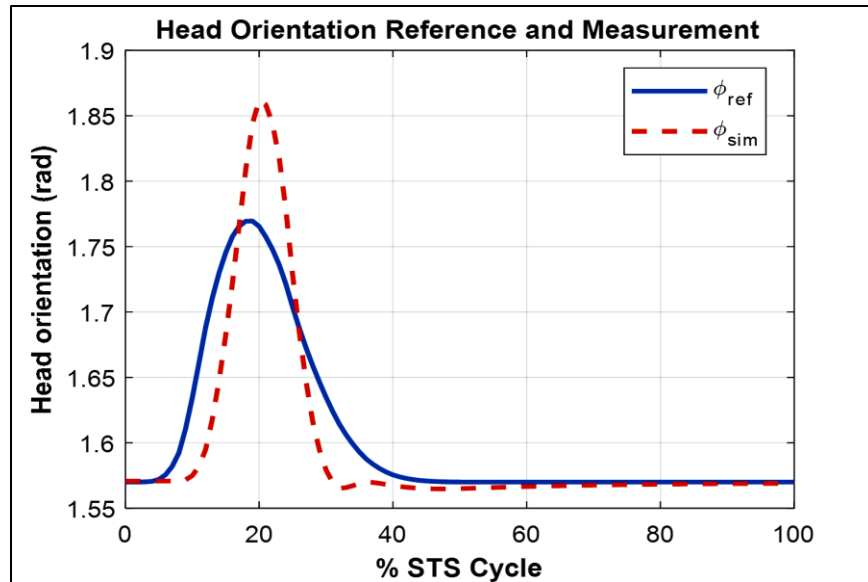


Figure 7.7. Head orientation reference generated analytically and measured from simulation

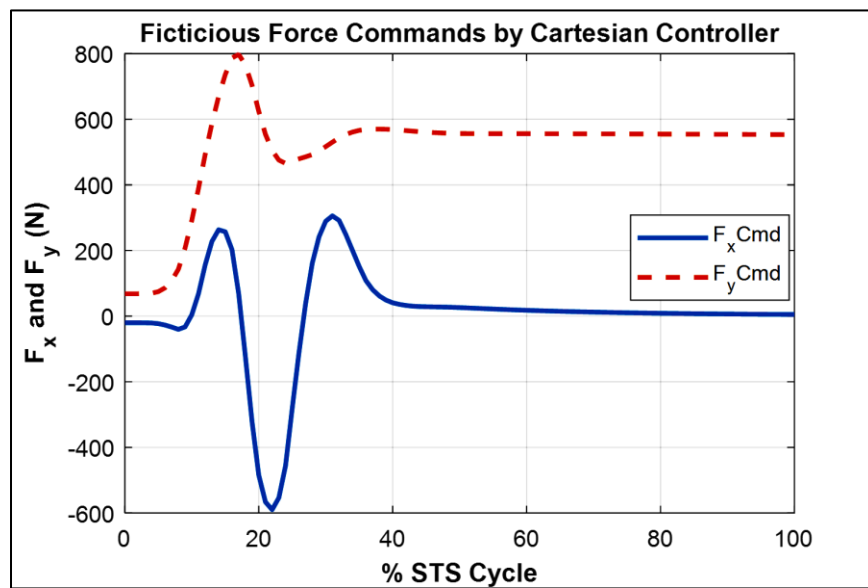


Figure 7.8. Force command generated by Cartesian control law

The Cartesian controller generates motion command in the force domain. Figure 7.8 shows the force command components  $F_xCmd$  and  $F_yCmd$  that refer to the force vector needed to be applied on end effector i.e., head to move the model from sitting to standing. It can be noted from the Figure that the horizontal component of force starts and finishes with a value of 0 N that corresponds to the horizontal motion of the head at the start and the end of STS. The vertical force component  $F_yCmd$  takes a large spike initially that corresponds to the initial upward thrust of the body. The vertical force component settles at approximately 600 N, showing the force needed to hold the body upward against gravitational pull equal to body weight.

Since the application of force on the head is only a conceptual way to estimate the force needed to do STS, the actual method is to apply torques of ankle, knee and hip joints. The transpose Jacobean transforms force from Cartesian space to torque in the joint space. Joint commands finally generated are shown in Figure 7.9. The curves show somehow jerky movement that eventually settles to values close to 0 Nm showing termination of STS motion.

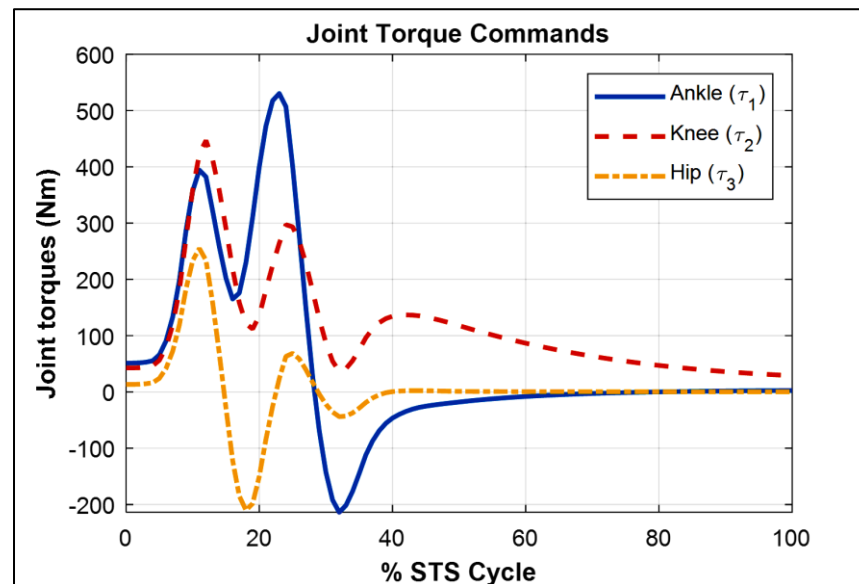


Figure 7.9. Torque commands generated by the controller for ankle, knee and hip joints

Figure 7.10 shows the measurement of force variation underneath the feet of the human biomechanical model during STS. It is interesting to observe the similarity between the curves shown here with those shown in Figure 7.8.

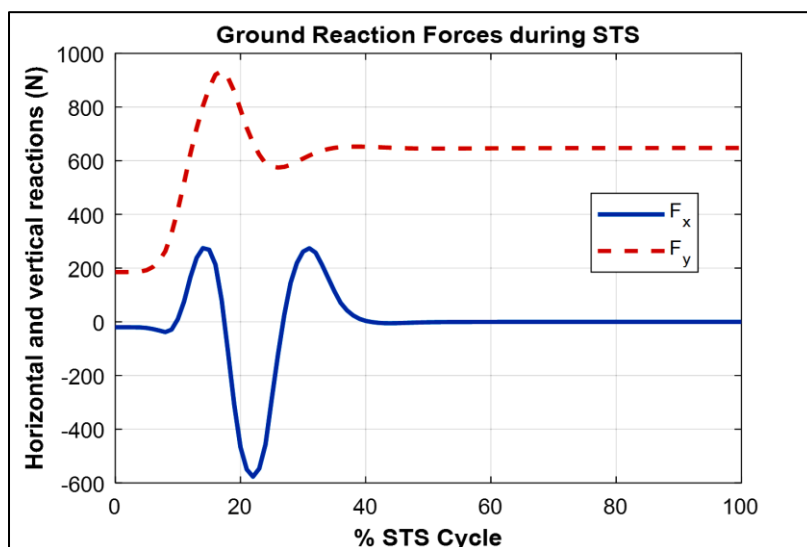


Figure 7.10. Ground reaction forces under the feet of the analytical human biomechanical model

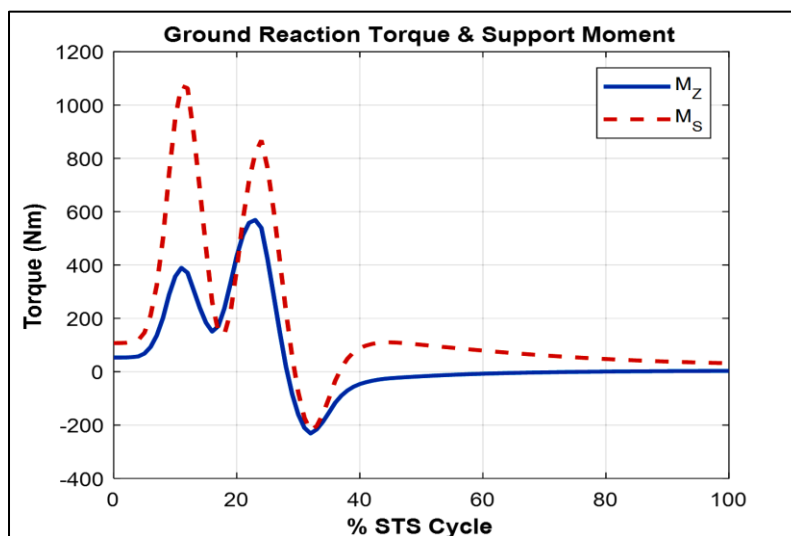


Figure 7.11. Kinetic analysis of STS simulation; ground reaction torque and the sum of joint torques

Ground reaction torque is measured using a torque sensor under the feet of the model as shown in Figure 7.11. Joint torques are measured during simulation using joint sensors. The similarity between the ground reaction torque curve plotted as  $M_z$  and the sum of joint torques  $M_s$ , also called support moment, is frequently discussed in the literature. Refer to section 4.3 and Figure 4.14 for details on the relation between these two variables.

### 7.3.2 Simulation using the custom biomechanical model

The human-CNS modeling scheme to synthesize STS motion was designed in a purely analytical framework. To validate our modeling framework and the hypothesis that CNS control of STS motion has a dependence on head position trajectory feedback, we must check the model for its ability to replicate experimental STS motion using custom/subject-specific models. A comparison of simulations and experimental findings will be the basis of the validity of our control framework. The second phase of our study starts from scaling our analytical human-model to custom models: We reconstruct STS motion using the SimMechanics model of Figure 7.3 with a custom human biomechanical model and an analytical STS controller framework. Subject-specific head position trajectories extracted from motion capture data are used as the reference.

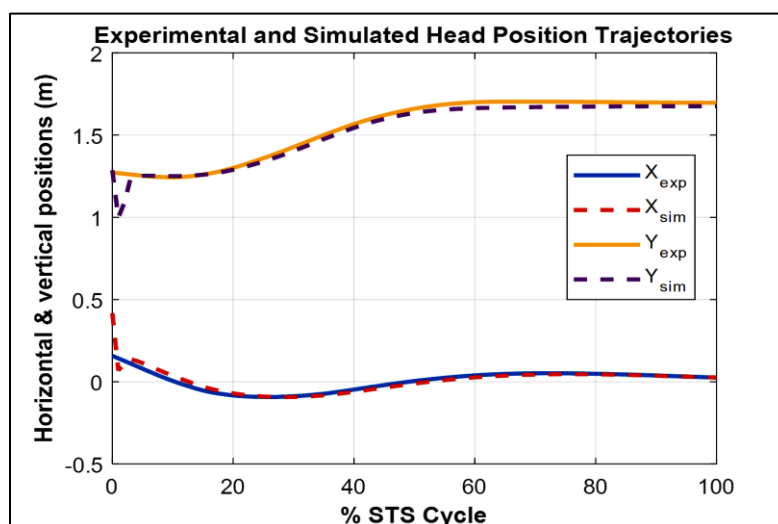


Figure 7.12. Average reference and measured head position trajectories from simulations



The ensemble averages of all motion and force data obtained from the experiment and simulations are calculated and compared. Figure 7.12 shows the experimentally generated head position trajectories in bold line curves that act as references to be tracked. The reference trajectory is the ensemble average of experimentally generated head positions using the head marker of the subjects. The measured output of the same variable, head position, is also plotted in the same Figure in broken line curves. The output is the average head position measured from the simulations where subject-specific / custom human biomechanical models were operated using the STS controller. It can be seen from Figure 7.12 that trajectory tracking is not smooth for a small duration initially. Very quickly excellent head position tracking can be seen that shows good tracking of reference input.

The tracking of head position trajectory can also be measured in terms of error between the reference input and the measured output as shown in Figure 7.13. RMS error for horizontal position  $X=0.0118\text{m}$  and for  $Y=0.0315\text{m}$ .

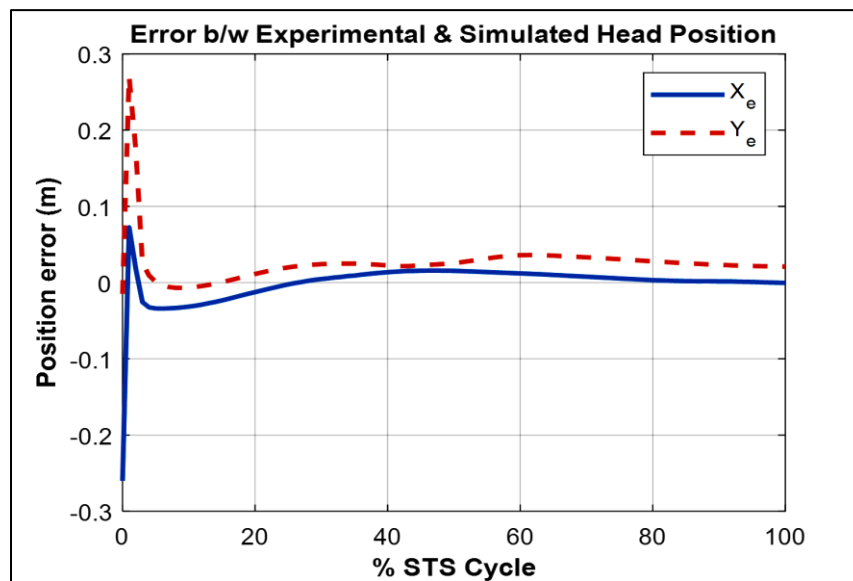


Figure 7.13. Comparison of ensemble average head position trajectories from motion capture experiments and simulations.

Figure 7.14 gives a detailed analysis of tracking performance in terms of joint angles. Joint angle measurements are only made for analysis and this measurement is not used as a feedback element for controller operation. Using head position measurement the

Inverse Kinematics part of the scheme shown in Figure 7.2 and **InvKin** block in Figure 7.3, the control scheme utilizes an inference mechanism for joint positions estimation. Figure 7.14 shows three types of joint angles: Bold line curves represent experimentally obtained joint angle positions. The dashed-dotted line curves depict the inference of joint positions made from head position measurement by the Inverse Kinematic mechanism. It can be seen that the difference between experimental and estimated values of joint angles is large. The RMS error between experimental and estimated ankle joint trajectory is 0.55 rad, for knee it is 0.93 rad and for hip 0.59 rad. The joint angles measured from the simulation are shown in dashed line curves. It can be seen that measurements almost exactly coincide with the estimated joint angles. But the error between experimental and measured joint angles is large again; 0.54 rad, 0.93 rad and 0.59 rad for ankle, knee and hip joints respectively.

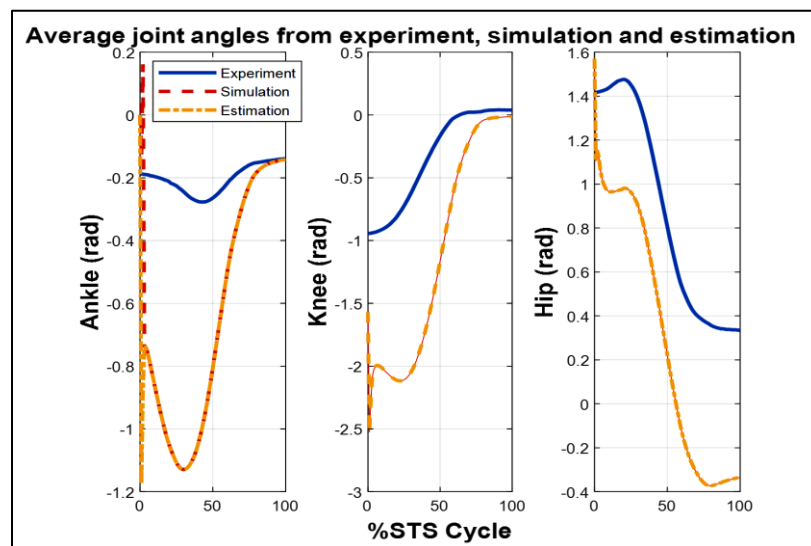


Figure 7.14. Comparison of average experimental joint trajectories with estimated and simulated trajectories.

Figure 7.15 shows how head orientation is followed by this scheme. Experimentally measured head orientation is shown in a bold line curve and the one measured from the simulation is drawn in broken line. Despite the large and very brief initial spike, the tracking is satisfactory and an RMS error of 0.0442 rad is found between the two curves.

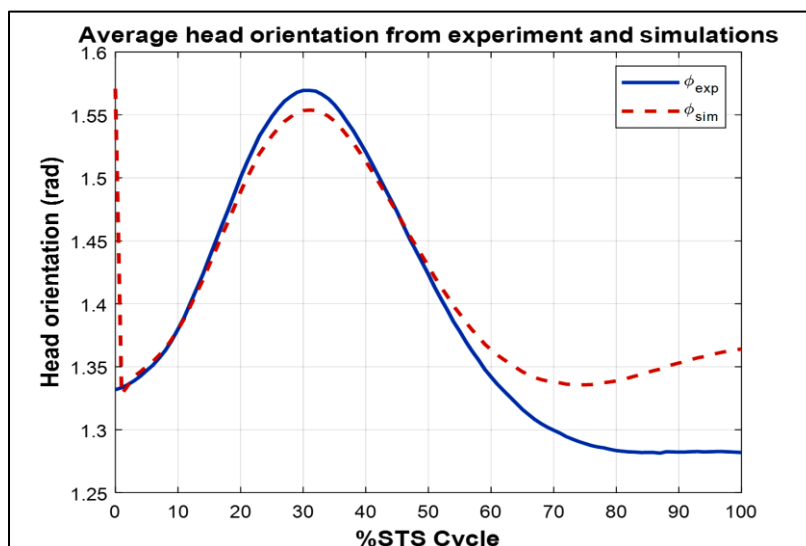


Figure 7.15. Reference head orientation trajectory obtained from the average of experimental and head orientation measurements from simulations

The plots of kinetic variables are presented below. GRF is experimentally measured from subjects using a force platform.

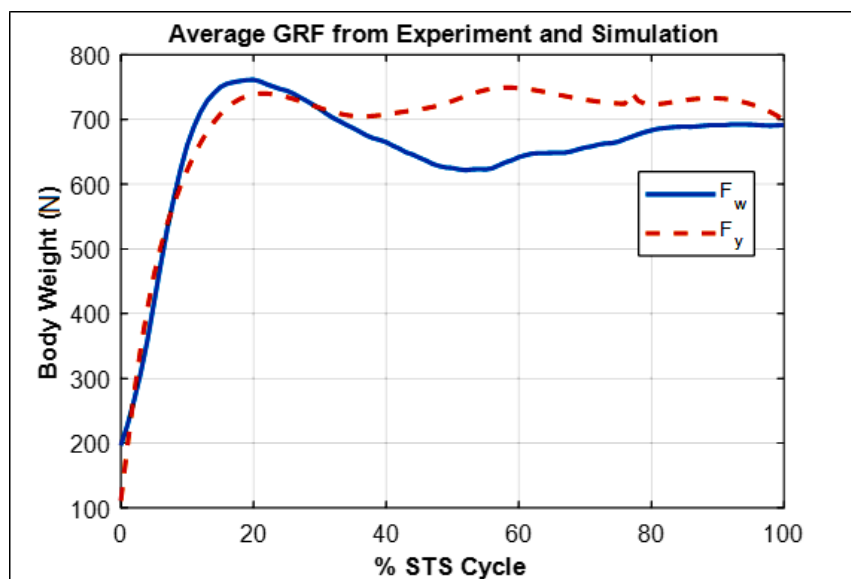


Figure 7.16. Average ground reaction force curve  $F_w$ , measured by the force platform, showing the trajectory of body weight variation during STS by the subjects.  $F_y$  shows the same variable measured during subject-specific simulations.

Figure 7.16 shows the vertical component of force  $F_W$  to depict variation in body weight during the STS movement. The broken line curve represents the measurement of the same variable from simulations. It can be seen that the two trajectories adopt the same trend, showing that simulated motion is close to real motion. The RMS error between the two curves = 50.26 N.

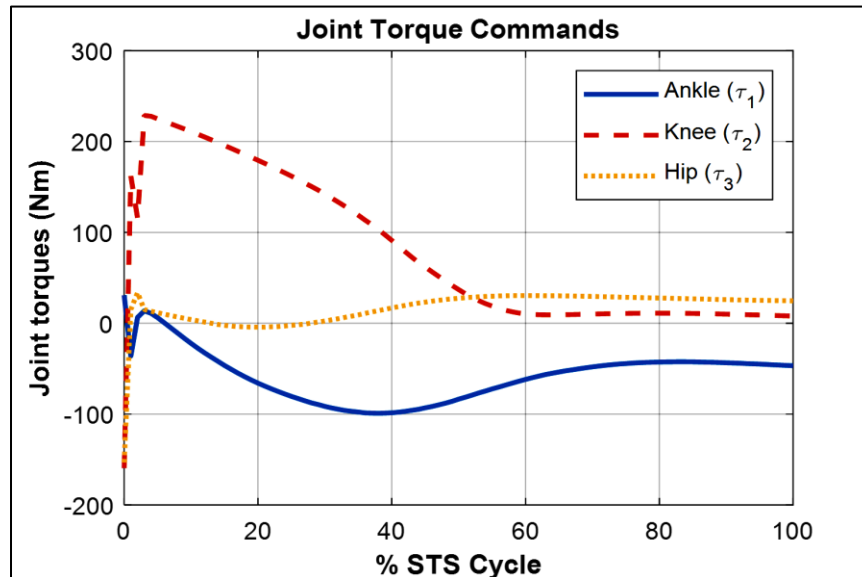


Figure 7.17. Joint torque command by motion controller for ankle, knee and hip

Figure 7.17 shows torque commands generated by the controller. The torque vector comprises motion commands for ankle, knee and hip joints. A deviation from actual trends of torques can be observed here; the largest torque is generated at the ankle joint, whereas in this diagram knee is having the largest torque. The peak values of torques are -100 Nm, 228Nm and 33Nm for ankle, knee and hip joints respectively. Moreover, knee torque is subject to large spikes that result in non-smooth motion at the start of STS motion simulation.

Figure 7.18 shows the ground reaction torque  $M_z$  and sum of joint torques, also called support moment  $M_s$ , both measured from simulations. It can be seen that the two curves appear similar to each other and the correlation between the two curves is considerably high, *i.e.*,  $R=0.72$ . The correlation between these variables is used as a tool to

measure physiologically relevant motion, especially in a simulated environment, hence, to validate a modeling and control scheme.

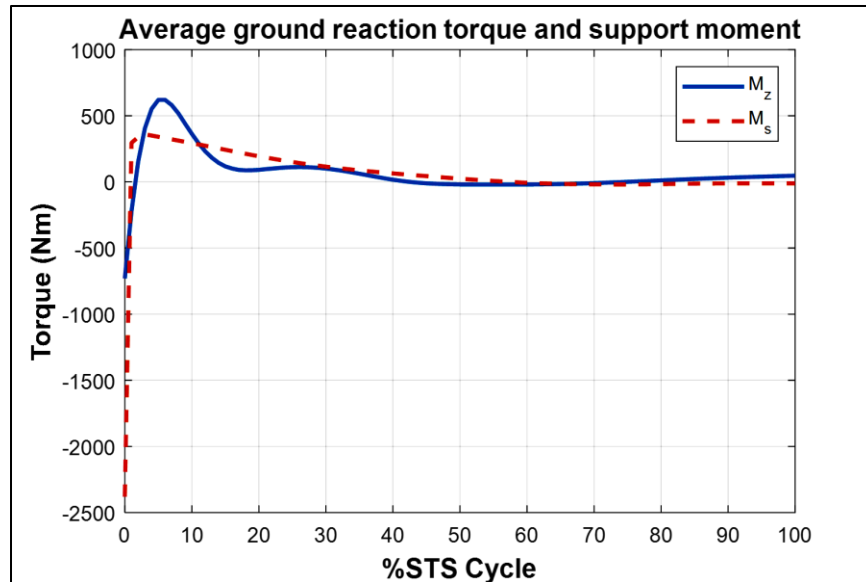


Figure 7.18. Average ground reaction torque  $M_z$  and support moment  $M_s$  (sum of joint torques)

## 7.4 Discussion

We propose a modeling and motion control solution to evaluate the clinical hypothesis that besides numerous other factors, CNS controls the STS motion by tracking a pre-learned head position trajectory. CNS compares this anticipated head motion pattern with actual head position measured by vestibular, proprioception and vision senses. Based on the head position error, CNS generates torque commands for joints actuation so that a smooth STS motion may result.

First, we realized our generalized analytical human biomechanical model based on anatomical proportions [43] in the sagittal plane. We modeled the CNS as an STS Controller having two subsystems; an Estimator to automatically plan a lower level of motion by joints and the Cartesian controller to generate appropriate joint torque commands to reduce head position error. We used this scheme to tune the controller to

come up with satisfactory results. Figure 7.3 through Figure 7.10 depict results obtained from this scheme.

In the next phase, we validated our modeling scheme by extending its application to simulate real human beings' STS motion. We customized the human biomechanical model to simulate real subjects' STS motion. We used the same STS controller to replicate STS motion of all customized human biomechanical models. Since the human biomechanical model was customized for each subject but the controller was used without retuning for a specific model, the achieved STS motions, in general, were somehow jerky and at times did not terminate in straight standing postures. Very often the final standing postures were a bit crouching.

Figure 7.11 gives a comparison of experimental and simulated head position trajectories in horizontal (X) and vertical (Y) directions. The Cartesian control part of the STS controller provides appropriate joint torques to minimize head position error  $\delta\mathcal{X}$ . The RMS error for X= 0.0118m and for Y=0.0315m. This shows very good tracking of reference input  $\mathcal{X}_d$  by the STS Controller. Experimental, estimated and simulated joint angles are plotted in Figure 7.14. Estimates and simulated joint angles are compared with experimental joint angles. RMS error for ankle=0.55 rad (estimation), 0.54 rad (simulation), for knee=0.93 rad (both) and for hip=0.59 rad (both). The joint angle errors are relatively high and attribute to the use of the same controller for a variety of custom human biomechanical models and head position trajectories that exhibit relatively large intra-subject variations. The joint angle error can be reduced significantly if 1) the controller is tuned for each custom model 2) simulation is run with subject-specific initial conditions. Figure 7.14 plots head orientation curves  $\emptyset$ , measured from experiments and simulations. A small RMS error of 0.0442 rad for head orientation shows good estimation and tracking of the head trajectory by the controller. Kinetic variables are plotted and analyzed next. Figure 7.14 shows how the force  $F_w$  exerted by the bodyweight during STS changes. At the start of the STS cycle, the initial force of 200N shows the average weight of the two feet, shanks and partially of thighs, while seated. With the seat off, the weight on the force plate increases and so does the vertical component of the ground reaction force.

The GRF measured from simulations is plotted as  $F_y$ . The two forces match closely (RMS error 50.26N only) and settle to the final value of the subjects' average weight. Support moment  $M_s$  is the sum of ankle, knee and hip joint torques. Ground reaction torque is a function of ankle joint torque [36]. We have found that a relatively high correlation (0.72) exists between ground reaction moment  $M_z$  and the support moment  $M_s$  as can be seen in Figure 7.18. The low RMS errors between experimental and simulated measurements validate our modeling framework.

## 7.5 Summary

This chapter presents an STS motion synthesis and control scheme using robotic control to position the end effector following the desired path. In the STS perspective, we have considered human biomechanical as a multi-segment robotic manipulator and the head as the end effector. The trajectory to be followed is the head position trajectory extracted from real human subjects' STS motion capture. We have modeled human CNS as a controller that comprises two parts: one is responsible to infer joint angles to achieve the head position in a human-like joint position combination. The second part generates appropriate joint torques using the Cartesian control scheme using head position measurement as a feedback element.

## CHAPTER 8

### CONCLUSIONS & FUTURE DIRECTIONS

This study was aimed at establishing the role of various kinematic variables in accomplishing physiologically relevant STS motion control using a biomechanical modeling and simulation platform. We studied the role of joint angular positions and head position trajectories fed back to CNS as variables of interest in STS motion control. The framework of the study was based on a general human biomechanical model comprising four rigid segments, *i.e.*, foot, shank, thigh and HAT. The model has three joints *i.e.*, ankle, knee and hip. This model is extensively studied in the literature for the synthesis and control of STS motion.

#### 8.1 Biomechanical Model Validation

Since the reliability of any motion synthesis scheme is primarily linked with good modeling technique, we first validated the general human biomechanical model using motion and force capture of STS transfer on real subjects. We used the weighting coefficient method for human anthropometry to infer body segment parameters to scale the general human model into subject-specific models. Our study suggests a set of protocols specifically for 2D motion capture. We used motion capture data to reconstruct experimental kinematic variables like joint angles and head position trajectories. The force data were used to obtain ground reaction forces. The scaled human biomechanical model was then used for the synthesis and control of STS motion using various controllers to model CNS and using different kinematic variables as reference trajectories to be tracked by this human-CNS modeling framework. To validate the modeling scheme the kinematic and kinetic analyses then followed. The similarity of experimental and simulated results



was measured in terms of head position trajectories, joint angles, ground reaction forces and ground reaction torques.

## **8.2 Joint Position and Velocity Feedback**

Initially, the study worked out the role of joint position feedback to CNS to Figure out this variable as a contributor to motion control. We used a full state control scheme, *i.e.*, all joint positions and velocity measurements and an LQR compensator to estimate noise-contaminated measurements. The resulting motion proved to be very realistic and physiologically relevant. The joint torques resulted were however larger than real owing to the cheap control optimization technique used in robust control design.

## **8.3 Joint Position Feedback**

The scheme was later extended for reduced ordered measurements, using only joint position measurements and velocities were estimated using LQG and  $\mathcal{H}_\infty$  observers. The robust control mechanism worked well in realizing human-like motion and achieving joint torques close to the values observed in real human-beings. This scheme resulted in joint torques closer to the values observed in real humans. This framework helped us establish the role of joint position feedback to CNS in carrying out STS motion. Moreover, the role of CNS as an estimator of missing data from the sensory organ is also presented in a biomechanical setting.

## **8.4 Head Position Feedback**

Finally, we worked out the role of head position trajectory as a single variable of interest, used as a feedback element, in synthesis and control of STS motion. Head position trajectory as a reference input to be tracked by the human biomechanical model is included

to model slow dynamics in CNS regarding the STS motion control strategy. We hypothesized that CNS has as an inference mechanism to generate appropriate joint angles that correspond to the required head position. We proposed a system that synthesizes human motion using a high-level task control framework, for which low-level motion control is automatically generated.

#### **8.4.1 Neuro-fuzzy inference and control**

We proposed a modeling framework to emulate the role of head position trajectory in physiologically relevant STS motion control by the CNS modeled as ANFIS controller. The neuro-fuzzy inference mechanism is based on humans like decision making and hence is frequently chosen to model the human biomechanical system's motion control mechanism. The slow dynamics in CNS regarding the STS motion control strategy is hypothesized as an inference mechanism to generate appropriate joint angles that correspond to the required head position. Hence, we synthesize human motion using a high-level task control framework, for which low-level motion control is automatically generated. We propose the TST algorithm to create a task-space for ANFIS training. The analytically trained ANFIS is robust enough to simulate real subjects' STS motion. Our scheme provides a further improvement in motion control by subject-specific tuning of biomechanical models and ANFIS controllers. Although a high-level task framework results in redundant solutions. We have resolved the problem by implementing kinematic model constraints through ANFIS training. ANFIS inference ensures physiologically relevant STS motions and also avoids joints from hitting their limits. Low errors between experimental and simulated motions prove the validity of the modeling framework. Our scheme provides a further improvement in motion control by subject-specific tuning of biomechanical models and ANFIS controllers. The modeling scheme is validated using kinematic analyses of simulated and motion capture data of real subjects.

### **8.4.2 Robotic control**

Lastly, the STS motion synthesis was done using a robotic approach employing a task-level control approach. The CNS is modeled as the STS controller. The subsystems of this control scheme comprise 1) an inverse dynamic based Estimator to infer joint angle based on measured head position and 2) a Cartesian controller to generate appropriate joint torques based on the error in head position. We did the analytical design in the first phase to relate and compare our current study with the previous work. Using a well-defined human model and simulation results from previous studies helped us design and fine-tune the STS Controller that could produce comparable results. As a standard procedure, we validated our modeling and control scheme framework with laboratory data as well. The analytically designed STS Controller proved to be robust enough to simulate real subjects' STS motion. Low errors between experimental and simulated motion measurements not only prove the validity of the modeling framework but support the clinical hypothesis that there exists a role of head position measurement feedback to CNS in controlling a smooth STS motion.

## **8.5 Assumptions and Limitations**

The subjects' physical parameters were converted into a complete set of BSP using the Weighting Coefficient method, which is a mathematical method of anthropometry. Despite the risk of high error in estimation [46], this method is widely accepted in the research community due to its convenience as compared to other methods that need special equipment for body segment measurements. The estimation error, however, leads to modeling error that becomes a source of mismatch in experimental and simulation results. Moreover, there is a lack of protocols for motion capture in 2D. We devised a set of protocols for this experiment which we kept modifying until a satisfactory level of reliable results was achieved. There was some limitation associated with experimental equipment as well: 1) We did not have specialized skin-tight garments for subjects. Since markers pose problems in the segment and joint position assessment due to skin or loose garment

artifacts, a set of markers on each segment were applied using rigid rulers. 2) The motion capture equipment and force plate were not synchronized electronically; the two variables were visually analyzed from captured data for time synchronization. Another assumption was made by using the same motion controller for all subject-specific human biomechanical models. Further improvement in work could be made if the controller were tuned separately for each scaled model. For this study our modeling scheme was based on rigid body segments; such assumption leads to modeling errors of the systems like the human body that are not exactly rigid.

## **8.6 Future Outlook**

Our scheme may find its application in the diagnosis and rehabilitation of patients with physical impairments, training of athletes and design of machines for physical therapy and sports training. In case of rehabilitation, a force augmentation or therapy mechanism would benefit a patient to infer and actuate joint level motions for any required motion tasked at a higher level. In computer graphics, this scheme can be extended to autonomously generating realistic motion for virtual characters. Instead of providing joint trajectories for detailed motion, only head position trajectories can be assigned to make the virtual characters follow a required path. The relation between head position trajectory and an EMG signal generated by CNS needs to be analyzed. Moreover, how this EMG signal differs in elderly and pathological individuals when compared with normal ones can be very beneficial in clinical applications. Moreover, how this signal is correlated with kinematics and kinetics of STS motion needs to be analyzed.

Our hypothesis and findings can be further generalized to all kinds of human motion syntheses like walking and stair climbing etc.

## References

- [1] M. A. Schenkman Richard Berger Patrick, R. W. Robert Mann ---M Schenkman, R. Berger, and P. Riley, "Whole-Body Movements During Rising to Standing kom Sitting."
- [2] R. Chiba, K. Takakusaki, J. Ota, A. Yozu, and N. Haga, "Human upright posture control models based on multisensory inputs; in fast and slow dynamics," *Neuroscience Research*, vol. 104. Elsevier Ireland Ltd, pp. 96–104, Mar. 01, 2016. doi: 10.1016/j.neures.2015.12.002.
- [3] T. W. Lu and C. F. Chang, "Biomechanics of human movement and its clinical applications," *Kaohsiung Journal of Medical Sciences*, vol. 28, no. 2 SUPPL. Feb. 2012. doi: 10.1016/j.kjms.2011.08.004.
- [4] T. Xiao and Y. F. Fu, "Biomechanical Modeling of Human Body Movement," *Journal of Biometrics & Biostatistics*, vol. 7, no. 3, pp. 5–8, 2016, doi: 10.4172/2155-6180.1000309.
- [5] F. C. T. van der Kooij, Herman and Koopman, Bart and van der Helm, "Human Motion Control," *Reader for Delft*, no. January, 2008.
- [6] V. De and R. Che, "A Task-Level Biomechanical Framework for Motion Analysis and Control Synthesis," *Human Musculoskeletal Biomechanics*, 2012, doi: 10.5772/22417.
- [7] J. A. Reinbolt, A. Seth, and S. L. Delp, "Simulation of human movement: Applications using OpenSim," *Procedia IUTAM*, vol. 2, pp. 186–198, 2011, doi: 10.1016/j.piutam.2011.04.019.

- [8] J. F. Nunes, L. P. Reis, R. J. F. Rossetti, P. M. Moreira, and J. M. R. S. Tavares, “Dynamic simulation of human motion,” *Modelling and Simulation 2014 - European Simulation and Modelling Conference, ESM 2014*, pp. 395–397, 2014.
- [9] J. F. Nunes, P. M. Moreira, and J. M. R. S. Tavares, “Human Motion Analysis and Simulation Tools,” in *Handbook of Research on Computational Simulation and Modeling in Engineering*, no. September, 2016, pp. 359–388. doi: 10.4018/978-1-4666-8823-0.ch012.
- [10] M. K. Cullen, “Muscle-Driven Simulations of Sit to Stand Transfer in Persons with Severe Osteoarthritis,” 2015.
- [11] E. J. Caruthers *et al.*, “Muscle forces and their contributions to vertical and horizontal acceleration of the Center of mass during sit-to-stand transfer in young, healthy adults,” *Journal of Applied Biomechanics*, vol. 32, no. 5, pp. 487–503, 2016, doi: 10.1123/jab.2015-0291.
- [12] S. Rafique *et al.*, “Position driven sit-to-stand simulation using human body motion and force capture,” *Proceedings - 22nd International Multitopic Conference, INMIC 2019*, 2019, doi: 10.1109/INMIC48123.2019.9022738.
- [13] A. M. Mughal and K. Iqbal, “Experimental Analysis of Kinetic Variables for Biomechanical Sts Movement.,” *Conference Proceedings of the Annual Meeting of the American Society of Biomechanics*, pp. 821–822, 2010.
- [14] S. Rafique, M. Najam-Ul-Islam, M. Shafique, and A. Mahmood, “Cartesian Control of Sit-to-Stand Motion Using Head Position Feedback,” *Applied Bionics and Biomechanics*, vol. 2020, 2020, doi: 10.1155/2020/1979342.
- [15] S. Rafique, M. Najam-ul-Islam, M. Shafique, and A. Mahmood, “Neuro-fuzzy control of sit-to-stand motion using head position tracking,” *Measurement and Control (United Kingdom)*, vol. 53, no. 7–8, pp. 1342–1353, 2020, doi: 10.1177/0020294020938079.

- [16] K. Knudson, *The Fundamentals of Biomechanics*. Springer Science & Business Media, 2018. doi: 10.1007/978-1-4757-5298-4.
- [17] A. Veeraraghavan, A. R. Chowdhury, and R. Chellappa, "Role of shape and kinematics in human movement analysis," *Proceedings of the IEEE Computer Society Conference on Computer Vision and Pattern Recognition*, vol. 1, 2004, doi: 10.1109/cvpr.2004.1315104.
- [18] A. M. Mughal and K. Iqbal, "Bipedal modeling and decoupled optimal control design of biomechanical sit-to-stand transfer," *ROSE 2008 - IEEE International Workshop on Robotic and Sensors Environments Proceedings*, no. October, pp. 46–51, 2008, doi: 10.1109/ROSE.2008.4669179.
- [19] A. M. Mughal and K. Iqbal, "H $\infty$  controller synthesis for a physiological motor control system modeled with bond graphs," *Proceedings of the IEEE International Conference on Control Applications*, pp. 947–952, 2006, doi: 10.1109/CACSD-CCA-ISIC.2006.4776772.
- [20] F. Iida, Y. Minekawa, J. Rummel, and A. Seyfarth, "Toward a human-like biped robot with compliant legs," *Robotics and Autonomous Systems*, vol. 57, no. 2, pp. 139–144, 2009, doi: 10.1016/j.robot.2007.12.001.
- [21] F. Iida, "Cheap design approach to adaptive behavior: Walking and sensing through body dynamics," *International symposium on adaptive motion of animals and machines*, 2005.
- [22] M. Schenkman, R. A. Berger, P. O. Riley, R. W. Mann, and W. A. Hodge, "Whole-body movements during rising to standing from sitting," *Physical Therapy*, vol. 70, no. 10, pp. 638–651, 1990, doi: 10.1093/ptj/70.10.638.
- [23] A. Kerr, A. H. Deakin, J. V. Clarke, J. M. Dillon, P. Rowe, and F. Picard, "Biomechanical Analysis Of The Sit-To-Stand Movement Following Knee

Replacement: A Cross-Sectional Observational Study,” *Congress of International Society of Biomechanics*, 2013.

- [24] C. Cachia, “A Biomechanical Analysis of the Sit-to-Stand transfer in Parkinson’s disease By Carl Cachia,” pp. 25–70, 2008.
- [25] J. Kang, B. Badi, Y. Zhao, and D. K. Wright, “Human motion modeling and simulation by anatomical approach,” *WSEAS Transactions on Computers*, vol. 5, no. 6, pp. 1325–1332, 2006.
- [26] R. C. van Lummel, “Assessing Sit-to-Stand for Clinical Use,” *Department of Human Movement Sciences*, vol. Ph.D, pp. 10–25, 2017.
- [27] M. Kok, J. D. Hol, and T. B. Schön, “An optimization-based approach to human body motion capture using inertial sensors,” *IFAC Proceedings Volumes (IFAC-PapersOnline)*, vol. 19, pp. 79–85, 2014, doi: 10.3182/20140824-6-za-1003.02252.
- [28] E. van der Kruk and M. M. Reijne, “Accuracy of human motion capture systems for sport applications; state-of-the-art review,” *European Journal of Sport Science*, vol. 18, no. 6, pp. 806–819, 2018, doi: 10.1080/17461391.2018.1463397.
- [29] A. Bilesan *et al.*, “Marker-based motion tracking using Microsoft Kinect,” *IFAC-PapersOnLine*, vol. 51, no. 22, pp. 399–404, 2018, doi: 10.1016/j.ifacol.2018.11.575.
- [30] G. Liu and L. McMillan, “Estimation of missing markers in human motion capture,” *Visual Computer*, vol. 22, no. 9–11, pp. 721–728, 2006, doi: 10.1007/s00371-006-0080-9.
- [31] M. Loper, N. Mahmood, and M. J. Black, “MoSh,” *ACM Transactions on Graphics*, vol. 33, no. 6, pp. 1–13, 2014, doi: 10.1145/2661229.2661273.



- [32] W. G. Janssen, H. B. Bussmann, and H. J. Stam, “Determinants of the Sit-to-Stand Movement : A Review,” *Physical Therapy*, vol. 82, no. 9, pp. 866–879, 2002, doi: <https://doi.org/10.1093/ptj/82.9.866>.
- [33] R. Chiba, K. Takakusaki, J. Ota, A. Yozu, and N. Haga, “Human upright posture control models based on multisensory inputs; in fast and slow dynamics,” *Neuroscience Research*, vol. 104, pp. 96–104, 2016, doi: [10.1016/j.neures.2015.12.002](https://doi.org/10.1016/j.neures.2015.12.002).
- [34] J. P. Scholz, D. Reisman, and G. Schöner, “Effects of varying task constraints on solutions to joint coordination in a sit-to-stand task,” *Experimental Brain Research*, vol. 141, no. 4, pp. 485–500, 2001, doi: [10.1007/s002210100878](https://doi.org/10.1007/s002210100878).
- [35] A. Czaplicki, M. Silva, and J. Ambrosio, “Biomechanical modelling for whole body motion using natural coordinates,” *Journal of Theoretical and Applied Mechanics (Warsaw)*, vol. 42, no. 4, pp. 927–944, 2004.
- [36] J. S. Matthis and B. R. Fajen, “Humans exploit the biomechanics of bipedal gait during visually guided walking over complex terrain,” *Proceedings of the Royal Society B: Biological Sciences*, vol. 280, no. 1762, 2013, doi: [10.1098/rspb.2013.0700](https://doi.org/10.1098/rspb.2013.0700).
- [37] A. M. Mughal and K. Iqbal, “Optimization of biomechanical sts movement with linear matrix inequalities,” *Mechatronic Systems and Control*, vol. 47, no. 1, pp. 1–11, 2019, doi: [10.2316/J.2019.201-2753](https://doi.org/10.2316/J.2019.201-2753).
- [38] A. Siriphorn, D. Chamonchant, and S. Boonyong, “The effects of vision on sit-to-stand movement,” *Journal of Physical Therapy Science*, vol. 27, no. 1, pp. 83–86, 2015, doi: [10.1589/jpts.27.83](https://doi.org/10.1589/jpts.27.83).
- [39] P. A. Forbes, G. P. Siegmund, A. C. Schouten, and J. S. Blouin, “Task, muscle and frequency dependent vestibular control of posture,” *Frontiers in Integrative Neuroscience*, vol. 8, no. JAN, pp. 1–12, 2015, doi: [10.3389/fnint.2014.00094](https://doi.org/10.3389/fnint.2014.00094).

- [40] A. M. Mughal and K. Iqbal, "Physiological LQR Design for Postural Control Coordination of Sit-to-Stand Movement," *Cognitive Computation*, vol. 4, no. 4, pp. 549–562, 2012, doi: 10.1007/s12559-012-9160-5.
- [41] S. Rafique, Najam-ul-Islam, and A. M. Mahmood, "Sit-to-stand motion control using head position feedback to CNS," *Basic & Clinical Pharmacology & Toxicology*, vol. 124, no. S3, pp. 3–379, Apr. 2019, doi: 10.1111/bcpt.13217.
- [42] M. Geravand, P. Z. Korondi, C. Werner, K. Hauer, and A. Peer, "Human sit-to-stand transfer modeling towards intuitive and biologically-inspired robot assistance," *Autonomous Robots*, vol. 41, no. 3, pp. 575–592, 2017, doi: 10.1007/s10514-016-9553-5.
- [43] K. Iqbal and Y.-C. Pai, "Predicted region of stability for balance recovery:," *Journal of Biomechanics*, vol. 33, no. 12, pp. 1619–1627, Dec. 2000, doi: 10.1016/S0021-9290(00)00129-9.
- [44] M. Raison, M. Laitenberger, A. Sarcher, C. Detrembleur, J.-C. Samin, and P. Fisette, "Methodology for the Assessment of Joint Efforts During Sit to Stand Movement," *Injury and Skeletal Biomechanics*, 2012, doi: 10.5772/49996.
- [45] K. Iqbal and A. M. Mughal, "Fuzzy Modeling and Optimal Control of Biomechanical Sit-to-Stand Movement."
- [46] R. Riemer and E. T. Hsiao-Wecksler, "Improving net joint torque calculations through a two-step optimization method for estimating body segment parameters," *Journal of Biomechanical Engineering*, vol. 131, no. 1, 2009, doi: 10.1115/1.3005155.
- [47] O. Khatib, E. Demircan, V. De Sapió, L. Sentis, T. Besier, and S. Delp, "Robotics-based synthesis of human motion," *Journal of Physiology Paris*, vol. 103, no. 3–5, pp. 211–219, 2009, doi: 10.1016/j.jphysparis.2009.08.004.

- [48] L. Peng and P. Y. Woo, "Neural-Fuzzy Control System for Robotic Manipulators," *IEEE Control Systems*, vol. 22, no. 1, pp. 53–63, 2002, doi: 10.1109/37.980247.
- [49] J. Jang, "Fuzzy Modeling Using Generalized Neural Networks and Kalman Filter Algorithm.," *Proceedings of the 9th National Conference on Artificial Intelligence*, vol. 91, pp. 762–767, 1991.
- [50] J.-S. R. Jang, "ANFIS: adaptive-network-based fuzzy inference system," *IEEE Transactions on Systems, Man, and Cybernetics*, vol. 23, no. 3, pp. 665–685, 1993, doi: 10.1109/21.256541.
- [51] J. S. R. Jang, "Input selection for ANFIS learning," *IEEE International Conference on Fuzzy Systems*, vol. 2, pp. 1493–1499, 1996, doi: 10.1109/fuzzy.1996.552396.
- [52] A. M. Mughal, S. Perviaz, and K. Iqbal, "LMI based physiological cost optimization for biomechanical STS transfer," *Conference Proceedings - IEEE International Conference on Systems, Man and Cybernetics*, pp. 1508–1513, 2011, doi: 10.1109/ICSMC.2011.6083885.
- [53] S. Rafique, A. Mahmood, and M. Najam-ul-Islam, "Robust control of physiologically relevant sit-to-stand motion using reduced order measurements," *Advances in Intelligent Systems and Computing*, vol. 881, no. November, pp. 783–796, 2019, doi: 10.1007/978-3-030-02683-7\_56.
- [54] Y. C. Pai, J. D. Wening, E. F. Runtz, K. Iqbal, and M. J. Pavol, "Role of movement stability in reducing slip-related balance loss and falls among older adults," *International IEEE/EMBS Conference on Neural Engineering, NER*, vol. 2003-Janua, pp. 253–256, 2003, doi: 10.1109/CNE.2003.1196806.
- [55] W. Li and E. Todorov, "ITERATIVE LINEAR QUADRATIC REGULATOR DESIGN FOR NONLINEAR BIOLOGICAL MOVEMENT SYSTEMS," in *Proceedings of the First International Conference on Informatics in Control*,

- Automation and Robotics*, 2004, no. January 2004, pp. 222–229. doi: 10.5220/0001143902220229.
- [56] D. A. Winter, *Biomechanics and Motor Control of Human Movement*. Hoboken, NJ, USA: John Wiley & Sons, Inc., 2009. doi: 10.1002/9780470549148.
- [57] I. Y. Campos Padilla, “Biomechanical Analysis of the Sit-to-Stand Transition,” [Thesis]. Manchester, UK: The University of Manchester; 2016., 2016.
- [58] G. Hettich, L. Fennell, and T. Mergner, “Double Inverted Pendulum Model of Reactive Human Stance Control,” *Multibody Dynamics 2011*, no. July, pp. 4–7, 2011.
- [59] S. Sasagawa, M. Shinya, and K. Nakazawa, “Interjoint dynamic interaction during constrained human quiet standing examined by induced acceleration analysis,” *Journal of Neurophysiology*, vol. 111, no. 2, pp. 313–322, 2014, doi: 10.1152/jn.01082.2012.
- [60] A. M. Mughal and K. Iqbal, “Fuzzy optimal control of sit-to-stand movement in a biomechanical model,” *Journal of Intelligent and Fuzzy Systems*, vol. 25, no. 1, pp. 247–258, 2013, doi: 10.3233/IFS-2012-0632.
- [61] S. Rafique, M. Najam-I-Islam, and A. Mahmood, “Synthesis of Sit-to-Stand Movement Using SimMechanics,” in *Smart Innovation, Systems and Technologies*, vol. 150, 2019, pp. 386–392. doi: 10.1007/978-3-030-22964-1\_43.
- [62] A. M. Mughal and K. Iqbal, “A FUZZY BIOMECHANICAL MODEL FOR  $H_\infty$  SUBOPTIMAL CONTROL OF SIT-TO-STAND MOVEMENT,” 2005.
- [63] A. M. Mughal and K. Iqbal, “A fuzzy biomechanical model with  $H_2$  control system for sit-to-stand movement,” *Proceedings of the American Control Conference*, vol. 2006, pp. 3427–3432, 2006, doi: 10.1109/acc.2006.1657248.

- [64] G. Model, H. P. Dynamics, and S. Plane, “Biological Cybernetics 9,” vol. 50, pp. 37–50, 1989.
- [65] B. Burger and P. Toiviainen, “Mocap Toolbox – a Matlab Toolbox for Computational Analysis of Movement Data,” *In R. Bresin (Ed.), Proceedings of the Sound and Music Computing Conference 2013, SMC 2013, Logos Verlag Berlin, Stockholm, Sweden*, pp. 172–178, 2013.
- [66] B. Friedland, *CONTROL SYSTEM DESIGN An Introduction to State-Space Methods*. Mineola, New: Dover Publications, Inc., 2012.
- [67] D. Xue, Y. Chen, and D. P. Atherton, *Linear Feedback Control*. Society for Industrial and Applied Mathematics, 2007. doi: 10.1137/1.9780898718621.
- [68] A. M. Mughal and K. Iqbal, “Synthesis of angular profiles for bipedal sit-to-stand movement,” *Proceedings of the Annual Southeastern Symposium on System Theory*, pp. 293–297, 2008, doi: 10.1109/SSST.2008.4480240.
- [69] J. Craig, John, *Introduction to Robotics: Mechanics and Control*, 3rd ed. Pearson Prentice Hall, 2005.
- [70] S. P. Balasubramaniam, “Influence of joint kinematics and joint moment on the design of an active exoskeleton to assist elderly with sit-to-stand movement,” University of Cincinnati, 2016.
- [71] P. Sánchez-sánchez and F. Reyes-cortés, “Cartesian Control for Robot Manipulators,” no. March, 2010, doi: 10.5772/9186.
- [72] “US Army exoskeletons: which companies are designing military suits?” <https://www.army-technology.com/features/us-army-exoskeletons/> (accessed Feb. 12, 2021).
- [73] M. Sone, H. Wagatsuma, K. Tachibana, and K. Sakamoto, “Robotic rehabilitation tool supporting up and down motions in the bathroom – analyses of the catapult-

assisted taking-off mechanism,” *Proc. 9th Intl Conf. on Disability, Virtual Reality and Assoc. Technologies*, pp. 10–12, 2012.


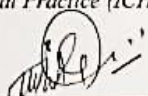
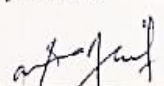

- [74] D. G. de Sousa *et al.*, “Two weeks of intensive sit-to-stand training in addition to usual care improves sit-to-stand ability in people who are unable to stand up independently after stroke: a randomised trial,” *Journal of Physiotherapy*, vol. 65, no. 3, pp. 152–158, 2019, doi: 10.1016/j.jphys.2019.05.007.

## **PART III**

### **Appendices**

Appendices B to H give a brief overview of methodologies/tools used for data acquisition, data processing, simulations and analyses. Only some of those aspects are quickly touched upon which have been utilized in this research. Readers can use this material as a startup or tutorial.

## APPENDIX A. Ethics Committee Certificate

 <p><b>RESEARCH ETHICS COMMITTEE</b>  <b>FACULTY OF ENGINEERING AND APPLIED SCIENCES</b>  <b>RIPHAH INTERNATIONAL UNIVERSITY</b>          ADDRESS : SECTOR I-14 ISLAMABAD          TELEPHONE : 0092-51-8446000</p>	<p><b>RIPHAH/MERC/BME-19-03</b>          Date: June 06, 2019</p>
	<p><b>TITLE OF RESEARCH:</b> Physiologically relevant sit to stand movement with output feedback tracking</p>
<p><b>PRINCIPAL INVESTIGATOR:</b> Samina Rafique</p>	
<p><b>PROTOCOL.NO</b> (if applicable):</p>	
<p>The Research Ethics Committee (FEAS) has reviewed and discussed the above-mentioned research. We approve the research to be conducted in the presented form.</p>	
<p>The following item [<input checked="" type="checkbox"/>] have been received and reviewed in connection with the above study to conducted by the above investigator.</p>	
<p><input checked="" type="checkbox"/> Application to Conduct Research Project(form)</p>	
<p><input checked="" type="checkbox"/> Study Protocol</p>	
<p><input checked="" type="checkbox"/> Research Proposal</p>	
<p><input checked="" type="checkbox"/> Participant information sheet</p>	
<p><input checked="" type="checkbox"/> Investigator's CV</p>	
<p>and the decision is [<input checked="" type="checkbox"/>]</p>	
<p><input checked="" type="checkbox"/> Approved</p>	
<p><input type="checkbox"/> Rejected (reasons specified below or in accompanying letter)</p>	
<p>Comments:</p> <p>-</p>	
<p><i>Investigator are required to:</i></p>	
<p>1) follow instructions, guidelines and requirements of the Research Ethics Committee.</p>	
<p>2) report any protocol deviations/violations to Research Ethics Committee.</p>	
<p>3) comply with International Conference on Harmonization – Guidelines for Good Clinical Practice (ICH-GCP) and Declaration of Helsinki.</p>	
<p>          _____  <b>Dr. Haris Shehzad</b>          Member, Research Ethics Committee</p>	<p>          _____  <b>Dr. Sana Arif</b>          Member, Research Ethics Committee</p>
<p>          _____  <b>Dr. Muhammad Shauqat</b>          Convener, Research Ethics Committee</p>	



## **APPENDIX B. Human Anthropometry**

### **B.1 Weighing Coefficient Method [56]**

Anthropometry is an important branch of anthropology, i.e., the study of humans' biological and physiological characteristics. To be specific anthropometry deals with the physical measurements of the human body that help determine and distinguish an individual from others. To accomplish a set of characteristics with sufficient parameters required to describe and differentiate the characteristics of race, sex, age, and body type a large number of measurements of body parts are required which is costly, time-consuming, dangerous, erroneous or even impossible at some time. Specifically, the human movement analysis requires kinetic measurements also which include masses, moments of inertia, and their locations on or inside the body or body part. The weighing coefficient method is used in this research to infer Body Segment Parameters from body mass and length/height.

### **B.2 Segment dimensions ( $l$ )**

The segment dimension is defined as the length between two joints. Since joint must be defined at the center of rotation, this definition also poses some difficulties in the accurate measurement of segment length. Also, typical values of a particular segment vary with body build, sex, and racial origin.

### **B.3 Segment mass ( $m$ ) and CoM ( $k$ )**

Segment mass is a function of individual masses of bones, muscles, fat, and other tissues. The density of each mass type within a given segment is also not uniform. Generally speaking, the density of distal segments is greater than that of proximal segments because of the higher proportion of bone.

The terms center of mass and center of gravity are often considered as the same parameters. The center of mass is defined by the geometrical center of the body on which force of gravity is being applied. Since the total body mass is a function of individual masses of body segments, it is possible to express the mass of each segment as a percentage of the total body mass. This assumption is the basis of the Weighing Coefficient method used in this study.

#### B.4 Mass moment of Inertia ( $I$ )

The human body as a whole and its segments and joints generate translational as well as rotational motion. To study the human translational motion center of mass location of each segment is needed. Similarly in rotational movement, as in the case of joints, mass moment of inertia or inertia tensor, denoted by  $I$ , should be known. Inertia Tensor is the constant of proportionality that measures the ability of the segment to resist changes in angular velocity. The value of  $I$  depends on the point about which rotation is taking place and is a minimum when the rotation takes place about its center of mass. The Weighing Coefficient method uses a proportionality relation between total body length and mass with individual segments' lengths and masses. To conduct this study we measured heights (total body lengths) and weights (total body masses) of 7 subjects using head marker position and force platform respectively. Using formulas listed in Table B. 1 the lengths, masses, the center of masses and inertia tensor of individual segments i.e., foot, shank, thigh and HAT are determined. Using the coefficient for conversion depicted in Table B. 1, the subjects' data in Table 4.1 is converted into BSP. See Table B. 2.

Table B. 1. Anthropometric conversion table based on subject's height and mass

Total Body		HAT	Thigh	Shank	Foot
Lengths (m)	L	$l_3=0.47L$	$l_2=0.245L$	$l_1=0.246L$	$l_f=0.039L$
Mass (kg)	M	$m_3=0.678M$	$m_2=2x0.1M$	$m_1=2x0.0465M$	$m_f=2x.0145M$
CoG (m)		$k_3=0.374 l_3$	$k_2=0.567 l_2$	$k_1=0.567 l_1$	
Inertia tensor (kg-Nm)		$I_3=m_3x(l_3x0.496)^2$	$I_2=m_2x(l_2x0.323)^2$	$I_1=m_1x(l_1x0.302)^2$	

Table B. 2. Subjects' physical parameter data

Subjects' ID		1	2	3	4	5	6	7	Gen1[41]
Ages		21	22	21	22	22	23	23	NA
Height	Verbal2	5'4"	5'8"	5'5"	163cm	5'7"		5'8"	1.76m
	Verbal(m)	1.6	1.7	1.625	1.63	1.675		1.7	
	Head Marker(m)	1.705	1.703	1.702	1.619	1.675	1.724	1.78	
Weight	Verbal(kg)	76.2	75	54		80		78	66kg
	FP3(N)	751	783	491	653	833	697	776	
	FP(kg)	76.555	79.817	50.051	66.565	84.913	71.050	79.103	
Segment Lengths (m)	Foot lf	0.0665	0.0664	0.0664	0.0631	0.0653	0.0672	0.0694	0.07
	Shank l1	0.4194	0.4189	0.4187	0.3983	0.4121	0.4241	0.4379	0.43
	Thigh l2	0.4177	0.4172	0.4170	0.3967	0.4104	0.4224	0.4361	0.43
	HAT l3	0.8014	0.8004	0.7999	0.7609	0.7873	0.8103	0.8366	0.83
CoG(m)	Shank k1	0.2378	0.2375	0.2374	0.2258	0.2336	0.2405	0.2483	0.25
	Thigh k2	0.2369	0.2366	0.2364	0.2249	0.2327	0.2395	0.2473	0.25
	HAT k3	0.2997	0.2994	0.2992	0.2846	0.2944	0.3030	0.3129	0.31
Segment Mass(kg)	Foot mf	2.2201	2.3147	1.4515	1.9304	2.4625	2.0604	2.2940	1.91
	Shank m1	7.1196	7.4229	4.6547	6.1905	7.8969	6.6076	7.3566	6.14
	Thigh m2	15.3109	15.9633	10.0102	13.3129	16.9827	14.2100	15.8206	13.2
	HAT m3	51.9040	54.1156	33.9346	45.1309	57.5713	48.1719	53.6318	44.75
Segment Moment of Inertia (kg-m <sup>2</sup> )	Shank I1	0.1142	0.1188	0.0744	0.0896	0.1223	0.1084	0.1286	0.11
	Thigh I2	0.2787	0.2899	0.1816	0.2185	0.2984	0.2645	0.3139	0.26
	HAT I3	8.1999	8.5292	5.3422	6.4288	8.7780	7.7809	9.2347	7.53

<sup>1</sup> Parameters of the general human biomechanical model from [43]

<sup>2</sup> The height as told by the subjects.

<sup>3</sup> Weight of subjects measured by the force plate

## APPENDIX C. Motion & Force Capture Operation

### C.1 Experiment Apparatus

The motion capture system used in this study comprised:

- 1) 04 infra-red Optitrack model Flex 3 cameras,
- 2) Data acquisition software Motive version 2.0.1
- 3) Passive, spherical reflecting markers
- 4) Calibration wand: Internally calibrated for distances of attached markers.
- 5) Calibration square: Internally calibrated for X and Z axes and origin due to 3 markers attached to it at 900. It is for Reference frame/ground setting.

### C.2 Procedure

For 2D STS motion all cameras are placed in a line facing the area of motion capture.



Figure C. 1. Four Flex 3 cameras set up to capture STS motion

The calibration wand is rotated slowly in all motion capture area. A ground calibration tool is placed on the ground to establish a world reference frame.

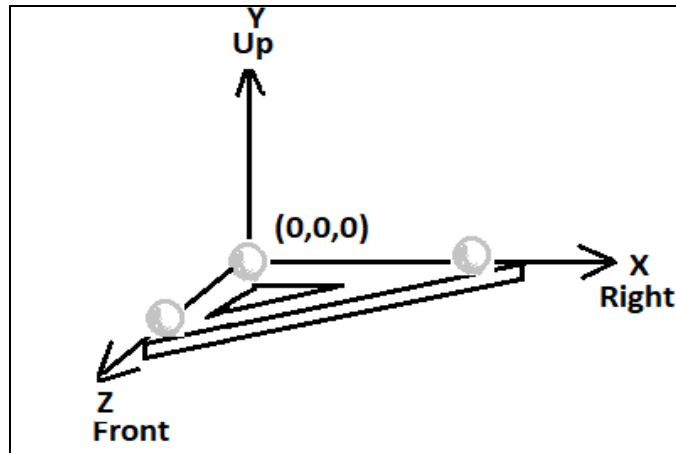


Figure C. 2. Calibration square is used to establish a reference frame



Figure C. 3. A calibration wand is used to tune camera measurements

Markers are attached to the subject and the subject sits on a chair with his sagittal side facing the cameras. The force platform is placed under the subject's feet at the origin

of the motion capture area. Force data is captured using CapStone software. The sampling frequency of both motion and force data acquisition systems is 100Hz.

Force plate data are checked in the CapStone screen for zero error before each STS trial. Data are recorded on the same computer running two programs simultaneously for force and motion capture. Since the two instruments are not synchronized, a verbal 'stand' command is given to the subject and after 5 seconds another command 'sit' is given.

### C.3 Data Acquisition & Motive Screen

In LIVE mode, on the upper part of the screen 3D motion of marker is shown and cameras are also shown on their respective positions. In the lower part, separate 2D images (marker movements) from individual cameras can be seen. Movement is recorded and video is played back to check if all markers were visible throughout the clip. In EDIT mode, each marker is assigned a number and a group of markers is labeled as segments; foot, shank, thigh and HAT. The data file is exported in CSV and C3D formats to be analyzed in the MoCap environment.

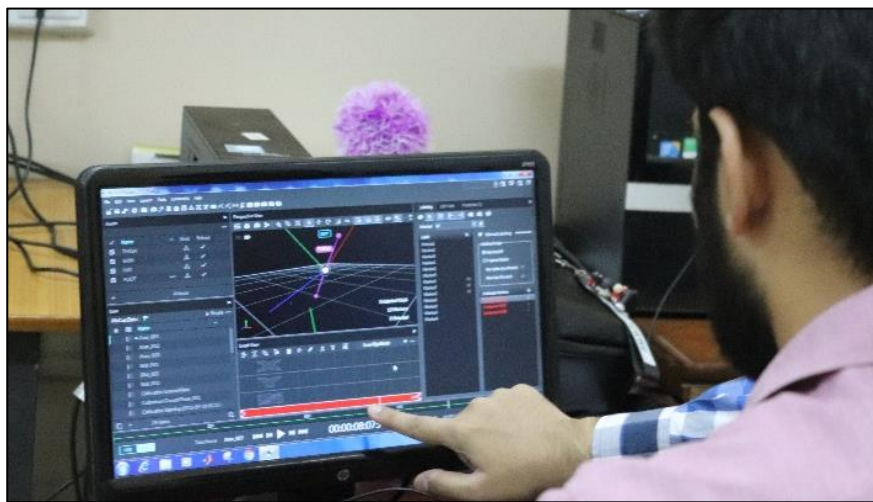


Figure C. 4. Motive environment showing markers movement

## APPENDIX D. Introduction to MoCap Toolbox

The MoCap Toolbox is a freely available MATLAB® toolbox that contains functions for the analysis and visualization of motion capture data. It supports the generic *.c3d* file format, in which our motion data was captured. Before using it, the toolbox has to be added to the MATLAB path variable.

### D.1 Reading & Plotting the MoCap Data

Given that the motion capture data is available in the file, for example, '*sub1.c3d*', The following m file will generate animation. The initial part of the code plots marker as white dots on a black background:

```
A=mcread('sub1.c3d');      %Creates data structure variable A

B=mcinitanimpar           %Initiates animation in marker space

mcplotframe(A,100) %Plots 100th frame
```

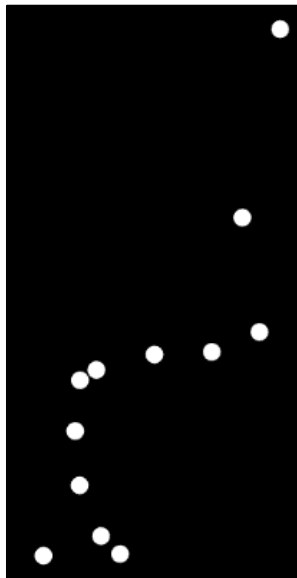


Figure D. 1. Marker positions while the subject is sitting

To change marker size and color of marker and background:

```

B.colors='wkkkk';           %Set marker color black on white

B.msize=5;                 %Set marker size

B.conn=[1 2;2 3;3 1;6 5;5 4;9 8;8 7;12 11;11 10]; %Join markers

mcplotframe(A,100,B)      %Plot 100th frame with markers connected

```

## D.2 Defining the Segments

The markers are joined to define segments

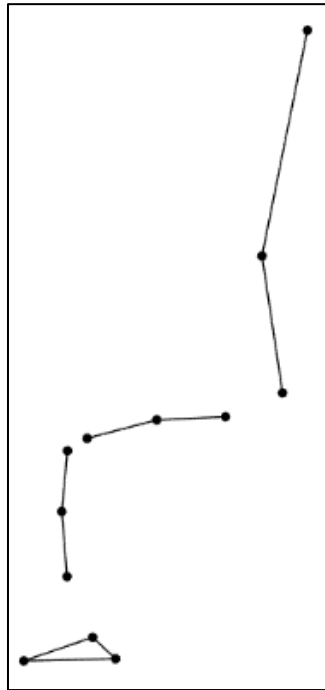


Figure D. 2. Marker connected as segments

```

B.fps=15;                  %Set frame/sec rate

B.conn=[1 2;2 3;3 1;1 9;9 12;12 10]; %Connect end markers only

```



### D.3 Animation in Joint Space

The marker data is used to define joints and joints are used to define segment terminals

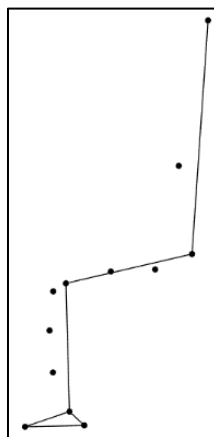


Figure D. 3. Markers at terminals of each segment

It must be noted that segment determination using markers does not give accurate results; actually, the first joints between the segments must be determined. For now, this crude solution is used as an introductory method to obtain animation.

`stsMot=mcanimate(A,B)`

`% Animate the motion`

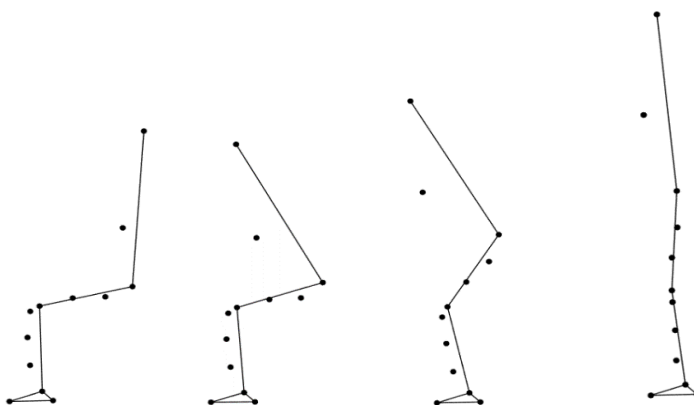


Figure D. 4. Animation of STS motion. Note middle marker on HAT is dis aligned due to garment artifact

## APPENDIX E. Introduction to SimMechanics/Simscape

Simscape Multibody software models, simulates, and visualizes mechanical systems, together with Simulink® and MATLAB®. The greatest advantage of this simulation environment is that the model is implemented using components of the physical system without considering underlying modeling equations. Simscape Multibody software is a set of block libraries and mechanical modeling and simulation tools for use with Simulink. You connect Simscape Multibody blocks to normal Simulink blocks through Sensor and Actuator blocks.

### E.1 Modeling Biomechanical Systems: Lower leg model

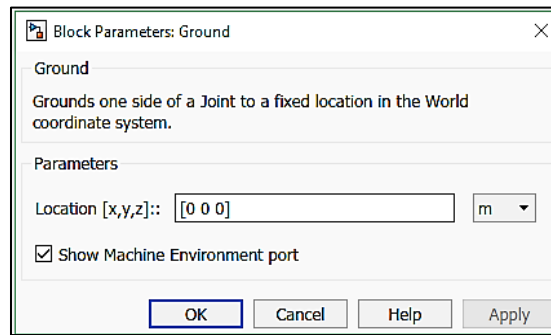
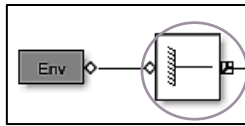
Biomechanical systems are modeled as machines in SimMechanics. Following is a brief tutorial for implementing a simple biomechanical model:

Here a simple model of the lower leg is implemented which comprises two segments: shank and foot. The two segments are connected through the ankle joint. Shank is stationary and foot moves due to revolute ankle joint

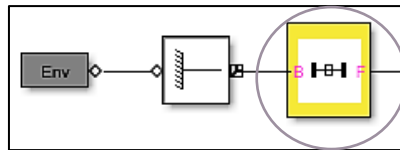
The model is implemented in the machine environment, hence *Machine Env* is the first block to be included in the model.



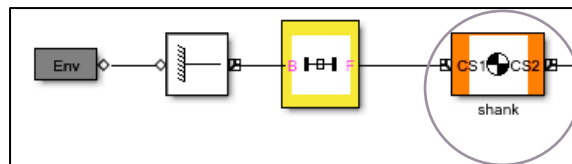
The motion of the system must be measured with a reference represented by a *Ground* block. There should be at least one Ground block in any model. The location of the Ground block is entered in a menu which appears when double-clicked on the block.

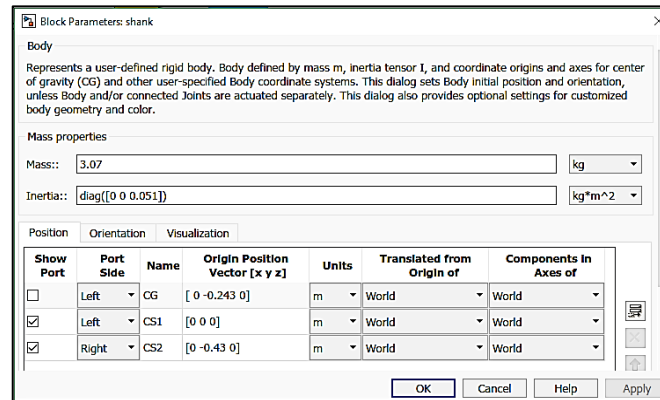


Any segment must be connected to the ground through a joint. Since the shank segment is not mobile in this model, a Weld joint may be used.

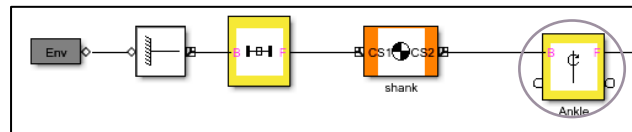


The shank is modeled as a Body block. Physical parameters of the shank i.e., mass, inertia tensor, position and orientation are entered in the menu of the Body block.

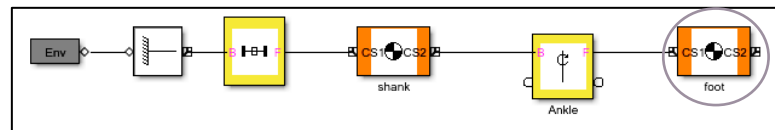




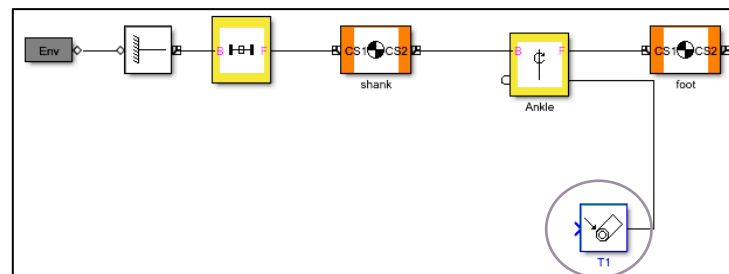
The ankle joint is modeled by Revolute block



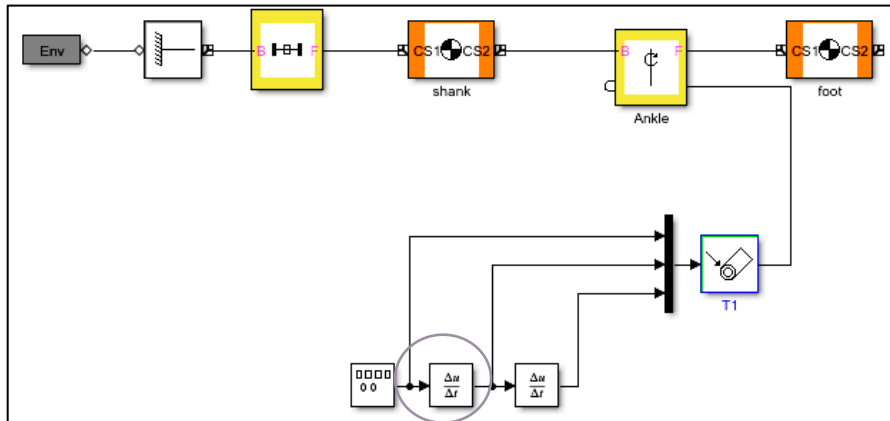
The foot is implemented by another Body block.



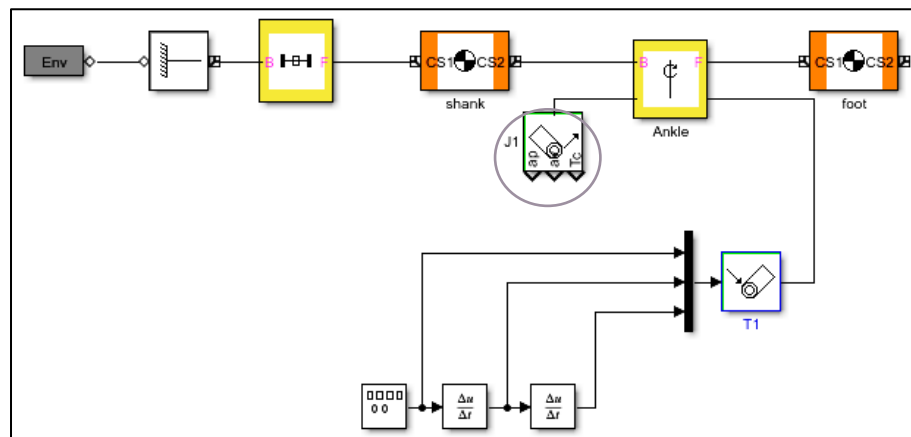
A Joint Actuator block is needed to rotate the foot about the ankle joint.



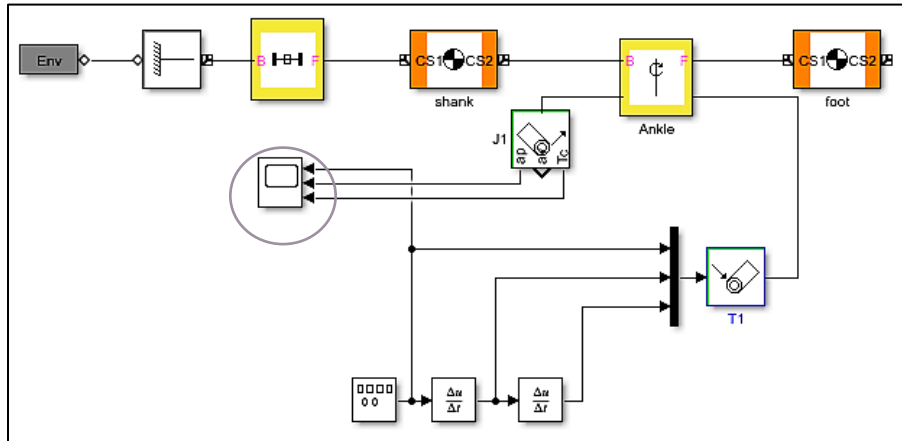
The actuation signal is provided by a Signal Generator block that generates a sinusoidal signal to produce simple harmonic motion in the ankle joint. The actuation mode of the Joint Actuator is the position, so velocity and acceleration of actuation signals are also needed, for this Derivative block are used.



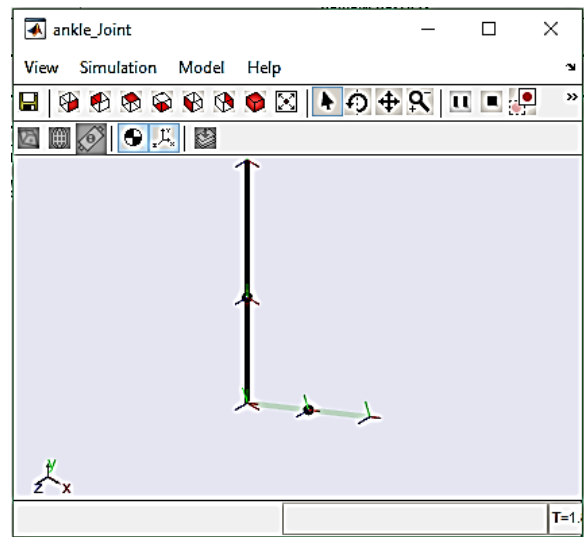
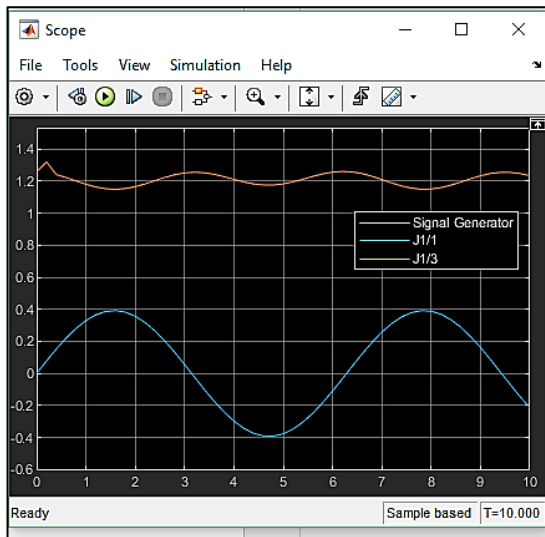
To measure position and acceleration Joint Sensor block is used.



The measured position and acceleration can be seen on the Scope block



## E.2 Animation visualization



SimMechanics provides the user with the visualization of the model and its motion as well. The signals can be visualized on the scope as well as motion animation is also visible.

## **APPENDIX F. Introduction to ANFIS**

ANFIS is an adaptive inference system that is built upon the concept of inference mechanism using fuzzy logic. The general concept is called FIS.

### **F.1 Fuzzy Inference System (FIS)**

Fuzzy inference systems are built upon fuzzy logic. These systems work well where significance should be preferred over precision. Fuzzy logic is a convenient way to map an input space to an output space. It is one of many black-box-like solutions that include linear systems, differential equations or lookup tables. Fuzzy logic is however more simple, flexible and can be used to model and control nonlinear systems. Input and output data is mapped through a set of curves called membership functions (MF). Typically, MFs are constructed in the form of triangles, bells or trapezium etc. For a set of  $n$  input variables,  $n$  sets of such MFs are used to map whole input space(s) to output space.

### **F.2 Adaptive Neuro-Fuzzy Inference System (ANFIS)**

Adaptive Neuro-fuzzy Inference Mechanism is an estimation algorithm that is based on fuzzy logic. The basic principle of fuzzy logic is based on flexible rules that are inspired by phenomena in nature, especially estimation and decision making just like humans do. An ANFIS is, therefore, capable to perform control operations. This type of controller is developed through a learning mechanism: first, a training data which comprises a set of inputs and the required output is collected and ANFIS learns the rules to generate required outputs for given inputs. Following is a simple example to implement an ANFIS based biomechanical control mechanism.

#### **F.2.1 Example: Ankle Motion Control**

Figure F. 1 depicts the SimMechanics model of a stationary foot connected with a shank through the ankle joint. The model needs to produce a motion in shank about the ankle. The required motion XY1 is in the Cartesian coordinate system and the actuator at

the ankle receives angular position command from ANFIS (Fuzzy Logic Controller). In this way, the ANFIS gives a mapping from Cartesian space to Joint space. The foot-ankle-shank model is a slight modification to the model shown in Appendix E.

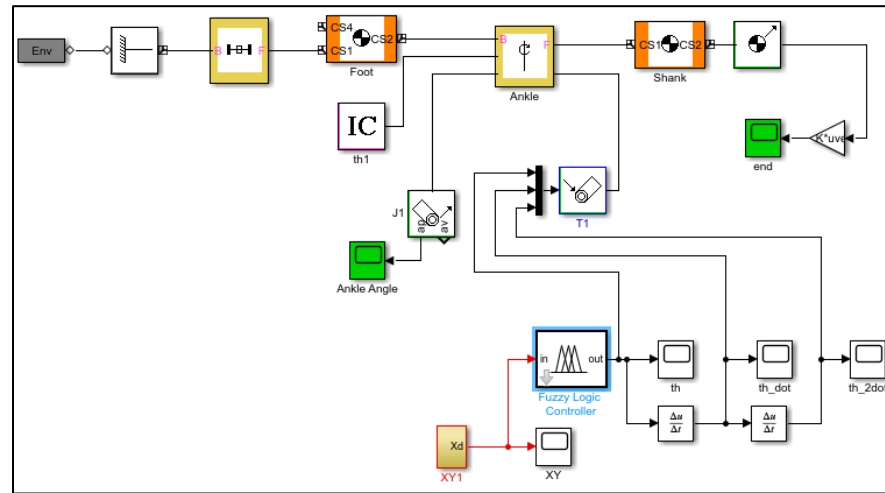


Figure F. 1. SimMechanics model of shank-ankle-foot with ANFIS controller

### F.3 Training and Test Data for ANFIS

The inverse dynamic equation governing the system is used to generate a master dataset that comprises  $X$ ,  $Y$  position as inputs and joint angle  $\theta$  as output. This dataset is bifurcated into two sets; first, the training dataset `trnData1` and the second one `chkData1` are test datasets that comprise on  $X$  and  $Y$  position data points. MATLAB command 'anfis' is used for training the ANFIS controller `anfis_shank`

```
anfis_shank=anfis(trnData1,4,20,[0,0,0,0]);
```

The ANFIS controller is then evaluated on test data `chkData1`, which comprises only inputs  $X$  and  $Y$  and the angles corresponding to each set of  $X$  and  $Y$  data points:

```
u1=evalfis(chkData1,anfis_shank);
```

The obtained outputs in the process of evaluation are compared with training data outputs and the error plot gives a measure of ANFIS estimation level. This process is



iterative and is tried for various values of epochs and membership functions until a minimum level of error is achieved.

The ANFIS can be saved as a variable called `anfis_shank.fis`

Various features of the ANFIS can be viewed using command line instructions:

```
>>A=readfis('anfis_shank.fis');
```

```
>>fuzzy(A)
```

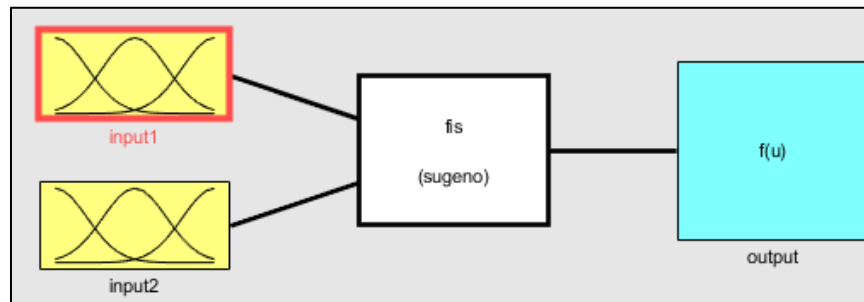


Figure F. 2. Two input and one output representation of Sugeno type ANFIS

```
>>surfview(A)
```

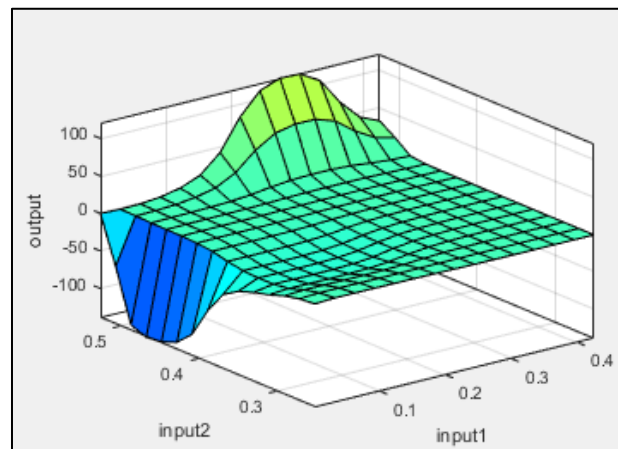


Figure F. 3. Surface plot that defines inference of ANFIS

To infer a joint angle that corresponds to the terminal end of the shank in Cartesian space say  $X=1$  and  $Y=2$ ,

```
>>theta=evalfis([1 2], A);
```

```
theta=-1.7989
```

which is the ankle angle in radians.

## APPENDIX G. Linearization of Non-Linear Model [67]

### G.1 Operating Point Selection

System linearization extracts an approximate linear model in the neighborhood of operating point. Given a non-linear dynamic system model

$$\dot{x}_i(t) = f_i(x_1, x_2, \dots, x_n, u, t)$$

To determine the operating point set  $\dot{x}_i(t) = 0$ . Let  $x_0$  be the operating point with an input signal  $u_0$ . The nonlinear system can be approximated by

$$\Delta \dot{x}_i = \sum_{j=1}^n \frac{\partial f_i(x, u)}{\partial x_j} \Big|_{x_0, u_0} \Delta x_j + \sum_{j=1}^p \frac{\partial f_i(x, u)}{\partial u_j} \Big|_{x_0, u_0} \Delta u_j$$

Using the new state variables  $z(t) = \Delta x(t)$  the linearized model is given by

$$\dot{z}(t) = A_l|_{x_0, u_0} z(t) + B_l|_{x_0, u_0} v(t)$$

Where  $v(t) = \Delta u(t)$  and

$$A_l = \begin{bmatrix} \partial f_1 / \partial x_1 & \dots & \partial f_1 / \partial x_n \\ \vdots & \ddots & \vdots \\ \partial f_n / \partial x_1 & \dots & \partial f_n / \partial x_n \end{bmatrix}, B_l = \begin{bmatrix} \partial f_1 / \partial u_1 & \dots & \partial f_1 / \partial u_p \\ \vdots & \ddots & \vdots \\ \partial f_n / \partial u_1 & \dots & \partial f_n / \partial u_p \end{bmatrix},$$

### G.2 MATLAB command

Using MATLAB command and the Simulink model file *model.slx*

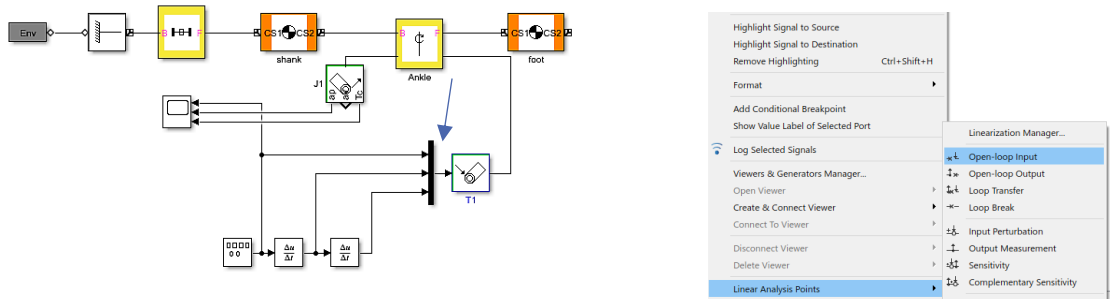
```
[x0,u0,y,dx]=trim('model')
```

the operating points can be determined and the linearized model in the vicinity of this operating point can be found using MATLAB command

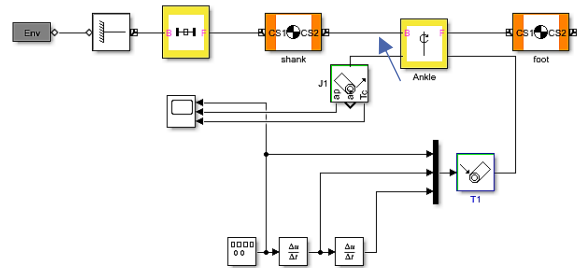
```
[A,B,C,D]=linmod2('model',x0,u0)
```

### G.3 SimMechanics Linear Analysis tool

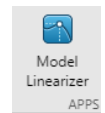
1. To linearize a model right click on the input of model.
2. Select Linear Analysis Points then Open Loop Input



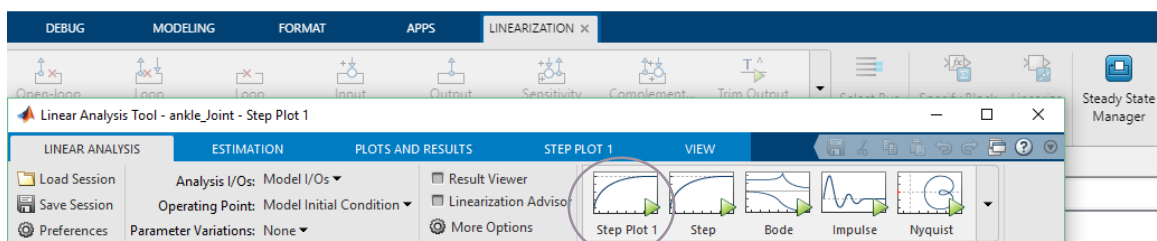
3. Right click on model output
4. Select Linear Analysis Point the select Open Loop Output
4. Then right click on output of model



5. Select Linear Analysis Point then select Model Linearizer on Linearization manager. Linear analysis tool appears



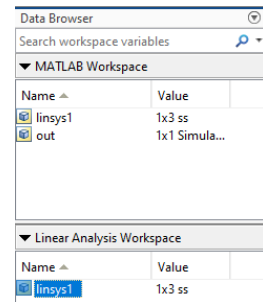
7. Select Step Plot



8. Drag and drop variable linsys1 from Linear Analysis Space into MATLAB Workspace.

9. On command line to get transfer function of linearized system

```
>>G=tf(linsys1)
```



## APPENDIX H. Force Augmentation Devices for STS

STS motion synthesis is implemented in physical settings using robotic devices, primarily for force augmentation.

### H.1 Exoskeletons for soldiers

Soldiers have to perform demanding missions to carry heavy equipment packs, walking long distances over rough terrain or running up and down stairs. The fatigue associated with these activities lowers efficiency of the individuals. A new exoskeleton from Lockheed Martin [72] offers a solution. This exoskeleton uses Dermoskeleton™ bionic augmentation technology. The FORTIS Knee Stress Release Device (K-SRD)™ is a computer-controlled exoskeleton that reduces loading and stress on the knees and legs and increases reach, endurance and load-carrying capability.



Figure H. 1. Knee exoskeleton for force augmentation of soldiers

Chapter 6 of this thesis proposes a scheme of exoskeleton customization for individual users using their BSP values and TST algorithm.

## H.2 Motion assistance and rehabilitation devices

Dynamics of STS motion have been studied by researchers in [73] to design a light-weight motion assistance device. This device helps to sit on and stand up from toilet seat safely, hence to help prevent falls in elderly and ailing individuals.

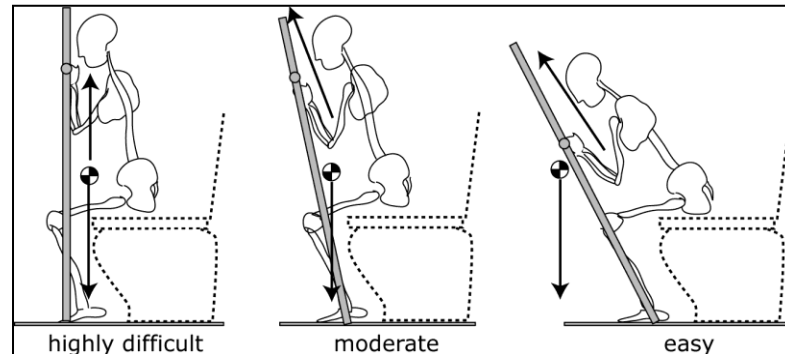


Figure H. 2. Light weight force augmentation device to prevent toilet related falls

## H.3 Physiotherapy exercises and equipment

Sit to stand has been used as a physiotherapy exercise in [74] for rehabilitation of stroke patients. Research results showed that sit to stand therapy helped regain motion and balance control in the subjects only within the duration of two weeks. Dynamics of STS are also used as design foundation of robotic physiotherapy and rehabilitation equipment.

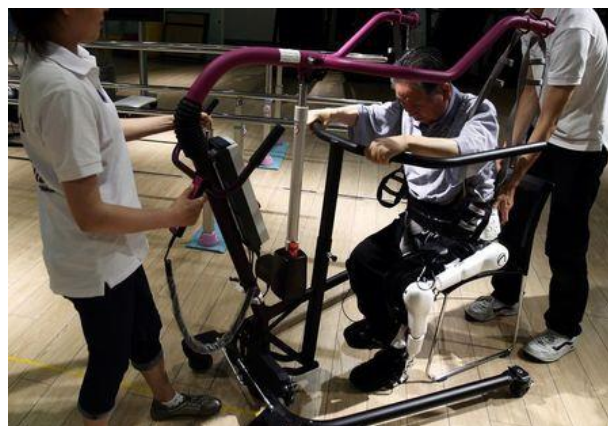


Figure H. 3. Robotic based STS physiotherapy

## **APPENDIX I: LIST OF PUBLICATIONS**

### **Journal Publications**

1. Rafique, Samina, et al. "Cartesian control of sit-to-stand motion using head position feedback." *Applied Bionics and Biomechanics* 2020 (2020). <https://doi.org/10.1155/2020/1979342>
2. Rafique, Samina, et al. "Neuro-fuzzy control of sit-to-stand motion using head position tracking." *Measurement and Control* 53.7-8 (2020): 1342-1353. <https://doi.org/10.1177/0020294020938079>
3. Rafique, Samina, Muhammad Najam-ul-Islam, and Asif Mahmood. "Sit-to-Stand Motion Control Using Head Position Feedback to CNS." *BASIC & CLINICAL PHARMACOLOGY & TOXICOLOGY*. Vol. 124. 111 RIVER ST, HOBOKEN 07030-5774, NJ USA: WILEY, 2019. (Impact Factor. 2.651) <https://onlinelibrary.wiley.com/doi/full/10.1111/bcpt.13217>

### **Conference Publications**

1. Rafique, Samina, et al. "Position driven sit-to-stand simulation using human body motion and force capture." *2019 22nd International Multitopic Conference (INMIC)*. IEEE, 2019. <https://doi.org/10.1109/INMIC48123.2019.9022738>.
2. Rafique, Samina, M. Najam-l-Islam, and A. Mahmood. "Synthesis of sit-to-stand movement using SimMechanics." *International Conference on Smart Innovation, Ergonomics and Applied Human Factors*. Springer, Cham, 2019. [https://doi.org/10.1007/978-3-030-22964-1\\_43](https://doi.org/10.1007/978-3-030-22964-1_43)
3. Rafique, Samina, A. Mahmood, and Muhammad Najam-ul-Islam. "Robust control of physiologically relevant sit-to-stand motion using reduced order measurements." *Proceedings of the Future Technologies Conference*. Springer, Cham, 2018. [https://doi.org/10.1007/978-3-030-02683-7\\_56](https://doi.org/10.1007/978-3-030-02683-7_56)